LAMINAR FLOW WITH AN AXIALLY VARYING HEAT TRANSFER COEFFICIENT

by

Robert G. Wells

Thesis submitted to the Faculty of the

Virginia Polytechnic Institute and State University

in partial fulfillment of the requirements for the degree of

Master of Science

in

Mechanical Engineering

APPROVED:

Dr. Brian Vick, Chairman

Dr. A. Moutsoglou

Dr. W. C. Thomas

February, 1986

Blacksburg, Virginia

Laminar Flow With An Axially Varying Heat Transfer Coefficient

by

Robert G. Wells

ABSTRACT

A theoretical study of convective heat transfer is presented for a laminar flow subjected to an axial variation in the external heat transfer coefficient (or dimensionless Biot number). Since conventional techniques fail for a variable boundary condition parameter, a variable eigenfunction approach is developed. An analysis is carried out for a periodic heat transfer coefficient, which serves as a model for heat transfer from a duct fitted with an array of evenly spaced fins. Three solution methods for the variable eigenfunction technique are examined: an Nth order approximation method, an iterative method and a stepwise periodic method. The stepwise periodic method provides the most convenient and accurate solution for a stepwise periodic Biot number. Graphical results match exactly to ones obtained by Charmchi and Sparrow from a finite-difference scheme. A connected region technique is also developed to provide limited exact results to test the validity of the three solution methods.

The study of a finned duct by a stepwise periodic Biot number is carried out via a parametric study, an average (constant) Biot number approximation and an assumed velocity profile analysis. Results for the parametric study show that external finning yields substantial heat transfer enhancement over an unfinned duct, especially when the Biot number of the unfinned regions is low. A decrease in the interfin

spacing causes increased enhancement. Variations of the period of the Biot number causes relatively small changes in enhancement as long as the ratio of finned to unfinned surface remains unchanged. An average (constant) Biot number approximation for a specified finned tube is compared to the stepwise periodic Biot number solution. The results show that the constant Biot number approximation provides accurate results. Finally, the results for the influence of the assumed velocity profile demonstrate that a constant velocity flow provides increased heat transfer and more effective enhancement by external finning than a laminar fully developed flow, especially at high Biot numbers.

This study provides insight into heat transfer enhancement due to finning and also develops a solution methodology for problems involving variable boundary condition parameters.

ACKNOWLEDGMENTS

I wish to thank Dr. Brian Vick for serving as Chairman of my Advisory Committee and Dr. A. Moutsoglou and Dr. W. C. Thomas for serving as Committee Members. Special gratitude is extended to Dr. Brain Vick for his tireless guidance and support which made this work possible. Additional gratitude is extended to the National Science Foundation for supporting this research through grant number MEA-8403964. I also wish to thank my parents for the love and guidance they have given me during the past 24 years. In addition, I wish to express my appreciation to my loving fiancee Mary, for her patience and understanding.

Finally, recognition is extended to Kathy, Ernie, Flip, Kelly, Harrison, Steve, Chuck, Doug, Tom, Tim, Karen and Jared, Scott, Paul, Conrad, Fritz, Jeff and a supporting cast of thousands who have enriched my experiences and made life worth living.

TABLE OF CONTENTS

TABLE OF CONTENTS (continued)

LIST OF FIGURES

LIST OF TABLES

NOMENCLATURE

a_{mp}	coefficients defined by Eq. (47b)
$A_{mp}(\xi)$	coefficients defined by Eq. (24a) or Eq. (47b)
$\underset{\sim}{A}_i$	matrix defined by Eq. (60a)
C_p	specific heat
$g(r,z)$	energy source
$h(z)$	heat transfer coefficient
$H(\xi)$	Biot number
k	thermal conductivity
$N_m(\eta)$	normalization integral
Pe	Péclét number
$Q(\xi)$	total heat transfer
$Q_w(\xi)$	wall heat transfer
r	radial variable
$R_m(\eta,\xi)$	variable eigenfunction
$S(\eta,\xi)$	dimensionless energy source
$\bar{S}_m(\xi)$	transformed energy source
$T(r,z)$	temperature
T_∞	environment temperature
$u(r)$	velocity profile
$\bar{u}$	average velocity
$v(\eta)$	dimensionless velocity
z	axial variable

Greek Symbols

α	thermal diffusivity
Γ_m^+	transforms after a jump point

NOMENCLATURE (continued)

Γ_m^-	transforms before a jump point
δ	delta function
η	dimensionless radial variable
$\theta(\eta,\xi)$	dimensionless temperature
$\theta_b(\xi)$	bulk temperature
$\bar{\theta}_m(\xi)$	transformed temperature
$\lambda_m(\xi)$	variable eigenvalue
ξ	dimensionless axial variable
ρ	density
μ	coefficient of viscosity
$\psi_m(\eta,\xi)$	variable normalized eigenfunction

Subscripts

i	high or low Biot region index
j	periodic Biot cycle index
m	summation index
p	summation index
s	geometry specifier

Superscripts

*	step jump in Biot number

I. INTRODUCTION

The objectives of this investigation are (1) to derive a solution for convective heat transfer from a conduit with a streamwise variation in the external heat transfer coefficient, and (2) to develop a methodology that can be used to solve a broad class of problems dealing with variable boundary condition parameters. At present, no standard analytical techniques are available to handle a variable boundary condition parameter.

Convective heat transfer primarily deals with heat transfer between a surface and a moving fluid at different temperatures. One method to enhance heat transfer to or from a fluid is to use extended surfaces such as fins. Figure 1a shows a schematic of an externally finned conduit. Each fin can be treated as a heat transfer device that increases the local heat transfer coefficient between the conduit base at temperature T_b and the ambient at T_∞. By application of the fin effectiveness, ε_f, defined as the ratio of heat transfer rate from the fin to that which would exist without the fin, the fin heat transfer rate is

$$q_f = \varepsilon_f \, h_1 \, A_{c,b} \, (T_b - T_\infty) \tag{1}$$

where h_1 is the external heat transfer coefficient along the unfinned portion of the conduit and $A_{c,b}$ is the fin cross sectional area at the base. Under most conditions, the value for ε_f is much greater than unity. By using $h_1 \varepsilon_f$ as the effective fin heat transfer coefficient h_2, a duct fitted with an array of fins can be modeled as an unfinned duct with a periodically alternating heat transfer coefficient, expressed as

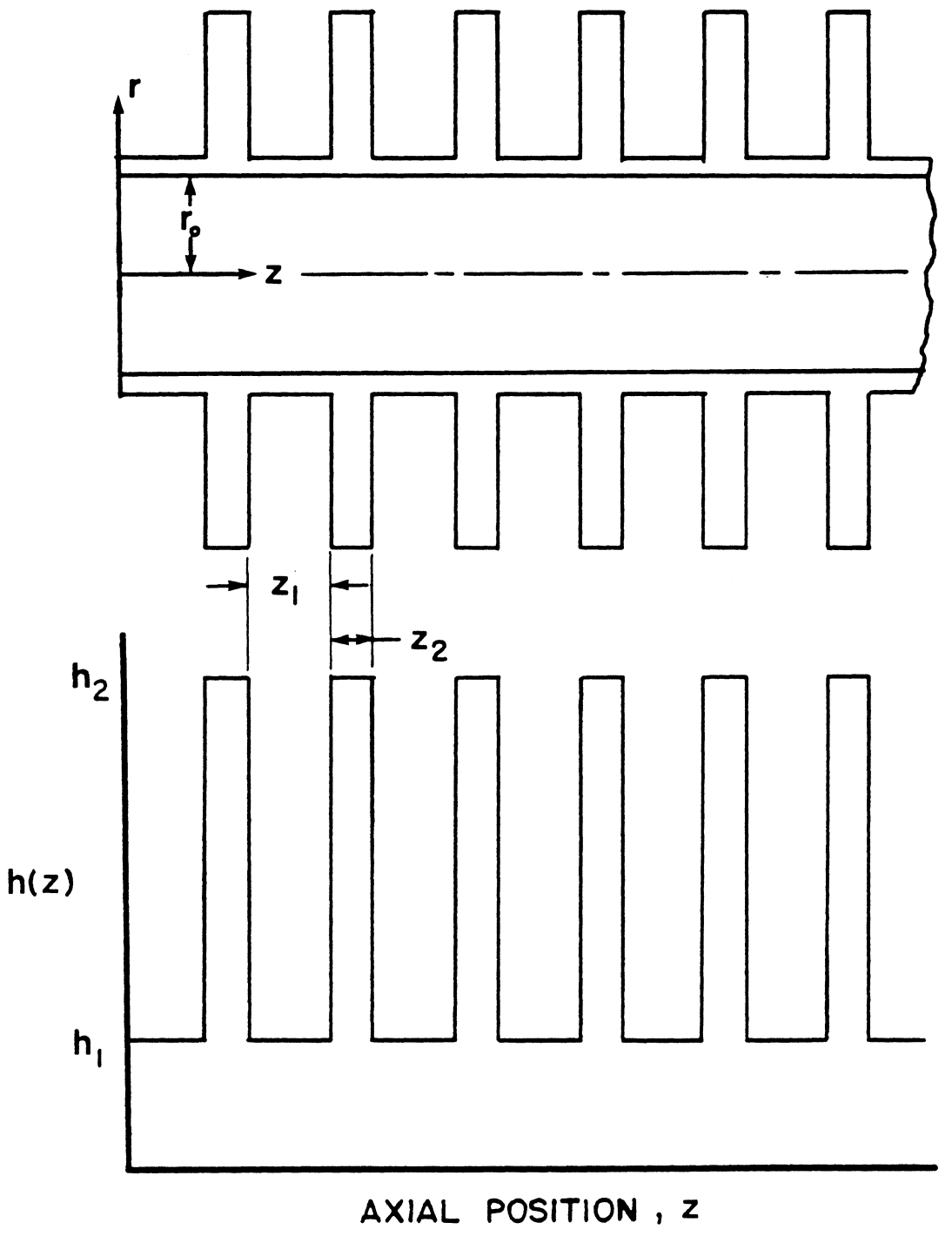

Figure 1 (a) Schematic of an externally finned conduit, and (b) model using a stepwise periodic heat transfer coefficent

$$h(z) = \begin{cases} h_2, & \text{finned regions} \\ h_1, & \text{unfinned regions} \end{cases} \tag{2}$$

This variation is displayed in Fig. 1b.

In general, by specifying the shape or distribution of the axially varying heat transfer coefficient, h(z), one can model a variety of fin geometries or conditions of the external environment. For instance, the smoothing effects caused by axial conduction in the conduit wall can be modeled as a harmonic streamwise variation whose maximum occurs at the center of the finned region and minimum at the center of the unfinned region. This study will be concerned with developing solutions for an arbitrary axial variation of the external heat transfer coefficient. The general solution will be applied to the stepwise periodic case shown in Fig. 1b.

Applications of this study for enhanced heat transfer are numerous. Finned ducts, for example, are widely used in industrial and residential heating, power plant heat exchange equipment, life support systems for aircraft and submarines, and radiators for internal combustion engines. Laminar flow applications involving periodic convective boundary conditions include the heating and cooling of viscous liquids in the chemical and food industries, the warming or cooling of blood during surgical operations, and the heating of the circulating fluid in solar collectors [1]. Design considerations for compact heat exchangers [2], cryogenic refrigeration systems [3], and shell and tube heat exchangers [4] also include an understanding of heat transfer with variable external convection coefficients.

Often the design of heat exchange systems is based upon experience,

safety factors, limited analytical studies including one dimensional models, or experiments. However, the design of heat exchangers for use in space vehicles, aircraft or nuclear reactors requires mandatory heat transfer optimization in order for the system to function properly and meet the size and weight limitations imposed. The result is a need for the synthesis of an optimal design rather than just an analysis of a particular existing design.

Despite numerous applications, until now the only solution to laminar flow with a variable convective boundary condition coefficient is the numerical solution by Charmchi and Sparrow [5] for a periodic heat transfer coefficient boundary. Due to the discontinuous nature of the boundary condition, the numerical procedure was computationally demanding and time consuming. The present analysis provides an analytical solution to problems involving a periodic heat transfer coefficient which is computationally convenient.

In general, the present work will shed light on the solution methodology for a broad class of problems with time and/or space dependent boundary condition parameters arising in different of branches of applied science. Applications include time dependent convective boundaries in the study of periodic contacting surfaces [6,7,8], thermal quenching [9], rewetting of a hot surface [10,11,12,13], temperature and stress fields in nuclear reactors [14] and transient heat conduction [15,16,17]. Another application for a variable boundary condition parameter is found in phase change problems [18] which involve a time dependent axial parameter.

II. LITERATURE REVIEW

Internal flow heat transfer and enhanced heat transfer using extended surfaces are closely interconnected in engineering applications; however, the subject areas are often treated as two separate and distinct topics. Use of a variable convective coefficient to model a finned conduit provides a convenient way to relate the two fields.

A. Internal Flow Heat Transfer

The study of internal flow heat transfer has long been the subject of numerous investigations leading back to the original Graetz problem [19]. Many extensions of this original problem have been studied. The boundary conditions normally studied at the conduit wall are as follows:

1) Boundary condition of the first kind corresponding to a specified wall temperature

$$T_{wall} = f(z)$$

2) Boundary condition of the second kind corresponding to a specified wall heat flux

$$-k\ dT/dr\big|_{wall} = f(z)$$

3) Boundary condition of the third kind corresponding to a constant external heat transfer coefficient

$$[k\ dT/dr + hT]_{wall} = f(z) \quad .$$

In addition, the flow can be classified as thermally developing, hydrodynamically developing or simultaneously developing. This study concentrates on thermally developing flows with a constant (slug) velocity profile or parabolic (laminar fully developed) velocity profile. Shah and London [20] provide an excellent review of the works in these areas

performed through 1978. To simplify the problem, a common assumption made in most papers [23-45] is that the heat conducted axially in the fluid is negligible compared to that conducted radially or convected axially. This assumption is valid for high Péclét numbers which occurs in the majority of flow situations encountered in engineering applications.

The study of heat transfer for a fluid of constant velocity and negligible axial conduction is well known for each of the three kinds of boundary conditions. Solutions for both a tube and parallel plate geometry can be found in most heat transfer texts [21]. For axially varying boundary conditions of the first or second kind, methods such as Duhamel's theorem or integral transform are commonly applied [22].

The problem of laminar fully developed flow is more difficult to solve than the constant velocity problem because the resulting Graetz functions are difficult to determine. Most of the analytical methods for laminar fully developed flow problems, used by various investigators, apply separation of variables in the energy equation, with various techniques employed for determination of the eigenvalues and constants of the resulting ordinary differential equation (O.D.E.). The solution is then in the form of an infinite series with eigenvalues, eigenfunctions and constants. The predominant boundary conditions are of the first or second kind. A general method for parallel plate geometry with boundary conditions of the third kind is reported by Javeri [23] and for tube and parallel plate geometry by Hsu [24].

The solution of the separated O.D.E. subjected to constant boundary conditions ($f(z) = c$) of the first or second kind is treated in

references [25-31]. Abramowitz [25] employed a series solution of fairly rapid convergence and calculated the first five eigenvalues and constants for a parallel plate geometry. Siegel, et al. [26] used separation of variables with Sturm-Liouville theory and calculated the first seven eigenvalues, eigenfunctions and constants for a tube geometry. Sellars, et al. [27] extended the original Graetz problem by using a WKBJ approximation to develop an asymptotic solution to calculate the first ten eigenvalues and constants for both a tube and plate geometry, and provided an asymptotic formula for higher eigenvalues and constants. The error for the asymptotic values is $O(\lambda^{-4/3})$. A more accurate solution of $O(\lambda^{-10/3})$ was provided by Lauwerier [28,29] for a tube geometry, and was summarized by Newman [30]. Lauwerier [28] expressed the Graetz eigenfunctions in terms of a confluent hypergeometric function and obtained an asymptotic solution at the wall of a tube. Both Sellar's and Lauwerier's asymptotic formulas are accurate for large eigenvalues. For small eigenvalues, Larkin [31] derived an exact solution for the Graetz eigenfunctions for both tube and parallel plate geometries by transforming them into a confluent hypergeometric series. This method allows for the first fifteen eigenfunctions to be calculated.

Boundary conditions of the first or second kind that vary with position either axially and/or radially have received considerable attention in the literature. When thermal energy sources, axial conduction and viscous dissipation are neglected, the resulting homogeneous energy equation can be solved by superposition [26,32-35]. Siegel, et al [26] used a superposition method for an arbitrary axial

heat flux distribution. Hsu [32] solved for a sinusoidal heat flux with Duhamel's theorem, and Mitchell [33] used a polynomial approximation to describe the surface temperature and then utilized Duhamel's theorem. For a variable radial heat flux, Bhattacharyya and Roy [34] used Duhamel's theorem. Other techniques used by investigators include a finite-difference technique by Grigull and Tratz [35] for a linear surface temperature distribution, an expansion in terms of a hypergeometric function by Shapovalov [36] for an arbitrary heat flux and an arbitrary initial condition, and a Laplace transform method by Zaychik [37]. Problems involving viscous dissipation and thermal energy sources have been solved by such methods as Laplace transform technique [38] and variational method [39].

A scrutiny of other methods used to solve the Graetz problem for boundary conditions of the first or second kind shows that Chandler, et al. [40] applied a Monte Carlo method, Tay and De Vahl Davis [41] used a finite-element method, and Casarella, et al. [42] used a conformal mapping method to solve for heat transfer of both constant and fully developed flows through a duct of arbitrary shape. Gottifredi, et al. [43] used a Laplace transform method applying it to non-newtonian fluids, and Whiteman and Drake [44] modified Sellar's [27] asymptotic method for general power law velocity profiles. The solution to a wide variety of heat transfer and velocity problems for thermally developing, hydrodynamically developing or simultaneously developing flows by the finite difference method was presented by Kays [45].

An interesting complication to internal flow heat transfer is the inclusion of the axial conduction term in the energy equation. The case

for no axial conduction, Pe = ∞, can be obtained as a special case. The basic mathematical difficulty in solving the energy equation with axial conduction is that the separated eigenvalue problem does not correspond to the Sturm-Liouville system. Therefore the usual orthogonal relations are not valid, thus creating a major complication to the calculation of the expansion coefficients in solutions of such problems by series expansion techniques. To overcome this difficulty various methods have been utilized [46-52].

Again, the majority of the studies including axial conduction deal with boundary conditions of the first and second kind. For the case of boundary conditions of the third kind, general methods are reported by Hsu [46], Bayazitoglu and Özisik [47] and Vick and Özisik [48].

Overall, many aspects of internal fluid flow have been studied for the three kinds of boundary conditions as well as for internal energy generation, axial conduction and viscous dissipation. However, an analytical study of a variable heat transfer coefficient was not found in the literature. Charmchi and Sparrow [5] studied a stepwise periodic heat transfer coefficient by adapting the Patankar-Spalding finite difference scheme. The solution required ten to twenty million grid points which results in very lengthy computation times. At present, no other numerical or analytical solutions for a variable heat transfer coefficient applied to convective heat transfer are found in the literature.

B. Enhanced Heat Transfer

Techniques to enhance convective heat transfer and increase the performance of heat transfer equipment are of great practical interest to the design engineer. As such, a large body of literature has been devoted to increasing and optimizing heat transfer. Various methods include extended surfaces, vortex flow, displaced promoter, vibration of the fluid or tube, electrostatic fields and fluid additives [53,54]. A summary of various works in these areas is presented by Bergles [54].

Extended surfaces are the most common and widely studied means of enhancing heat transfer [55-76], since they offer the most convenient means of achieving a larger heat transfer surface without increasing the primary surface. This augmentative technique can help reduce the overall size and weight of the heat transfer equipment. The exact analysis of extended surfaces is a complicated problem that involves considerations such as three dimensional heat flow, boundary layer inhibition at the fin-coolant interface, and natural convection for low speed flows. To simplify the analysis, a set of classical assumptions attributed to Murray [55] and Gardner [56] has been applied. These assumptions are used to create a fin model that presumably approximates reality enough to justify design decisions by providing information about different fin performances. The two most common types of extended surfaces are internal and external fins.

Many recent studies [53,57-60] deal with internal finning as a method to enhance heat transfer. The analysis, however, is complicated due to the interaction of the fin on the internal fluid flow. Thus, a simultaneous solution of the momentum equation and energy equation is

required for a study of heat transfer. As a result, the majority of results are either experimental [53,57], or numerical [58,59]. However, Hu and Chang [60] derived an analytical solution to the momentum and energy equation at discrete axial positions. The periodic variation in heat transfer coefficient used to model fins does not apply to internal fins due to the interaction of the fins on velocity profile.

The most obvious enhanced heat transfer method is external finning. The conventional method of external fin design is based upon the original work of Harper and Brown [61]. This method involves the study of heat conduction within and convection from an individual fin, entirely separate from the supporting surface. Thus, the analysis ignores the heat conduction in the supporting interface, the proximity of adjacent fins, and the heat exchange from the plain side of the supporting surface. The main advantage of studying individual fins is that a nondimensional representation of the heat transfer rate from a fin, called the fin efficiency, can be developed from a small number of fin parameters. Furthermore, the fin efficiencies for a general fin geometry can be represented by a curve which accounts for all variation of the fin parameters [55,56]. The fin efficiency charts also provide a convenient way to reduce a finned duct into a corresponding unfinned duct subjected to an overall heat transfer coefficient [80]. The overall heat transfer coefficient is derived from a one dimensional analysis of thermal resistances for the finned and unfinned sections. The heat transfer rate from a finned duct can then be approximated as the heat transfer rate from an unfinned duct subjected to the overall heat transfer coefficient.

The majority of literature on the study or optimization of individual fins [62-70] involves extensions of the concepts introduced by Harper and Brown [61]. A summary of the works in this area shows that Razelos [62] studied the optimization of a pin fin by maximizing heat transfer while minimizing fin volume, and Kovarik [63] applied a maximum heat transfer per unit cost criteria. Razelos and Imre [64] solved for the optimal dimensions of a circular fin, including the effects of variable heat transfer coefficient and variable thermal conductivity of the fin. Other optimization criteria found in the literature include a minimization of entropy generation in fins by Poulikakos and Bejan [65], a least weight circular fin by Güceri and Maday [66], and a stochastic optimization by March and Costello [67] in order to eliminate multiplication of safety factors. Li [68] optimized pin fin heat transfer both individually and in arrays under the assumption that the heat transfer coefficient along the fin is inversely proportional to the pin diameter, and Snider and Kraus [69] examined optimum variable fin shape with distributed heat sources along the fin face. An analysis of coated fins was performed by Chu, et al. [70] for the transient response of composite straight fins.

Individual fin analysis provides some ideas as to the effectiveness of a fin, which in turn can be used to model a fin as an equivalent heat transfer coefficient as mentioned in the introduction. To fully understand the interaction of adjacent fins and the supporting surface on the heat transfer rate requires the study of an array of fins. A variety of literature appears on the subject [71-76] of which a brief collection appears in the work of Manzoor [71]. By analogy with

electric circuit theory, a secondary analysis to the fin efficiency, referred to as the sum of resistances method, can be used to predict the performance of a fin assembly [71]. Manzoor, et al. [72] demonstrated that this method has a rigorous mathematical foundation assuming one-dimensional heat flow within the supporting wall and fins. Kraus and Snider [73,74] and Kraus [75] developed a technique that reduces an array of fins into a series of 2 x 2 matrices. The 2 x 2 thermal transmission matrix relates fin tip conditions to fin base conditions for each fin. Simultaneous analysis of these matrices then determines overall array performance. Mikhailov and Özisik [76] solved each fin as a finite element which reduces an array of fins to a system of algebraic equations. No mention was found in the literature of external surface problems coupled with internal flow problems.

Combined extended surfaces and internal flow are seldom studied together since this analysis requires the solution of the energy equation coupled with the heat conduction equation. Charmchi and Sparrow [5] simplified the analysis by modeling the finned surface as a series of high and low heat transfer coefficients. The equivalent heat transfer coefficient modeling of the individual fin was solved via fin efficiency charts [55,56].

C. Variable Heat Transfer Coefficient

Modeling a finned conduit as a series of high and low heat transfer coefficients raises the question of analogous works in other subject areas dealing with variable boundary condition parameters. Studies containing variable boundary condition parameters include periodic

contact analysis [6,7,8], rewetting analysis [10,11,12,13], transient heat conduction analysis [14,15,16,17] and phase change analysis [18].

The study of heat transfer in two periodically contacting surfaces that make and break contact according to a regular cycle involves a time dependent thermal contact conductance. Reed and Mullineux [6] and Mikhailov [7] each defined the contact conductance to be zero across the contacting surfaces during separation and finite during contact. Reed and Mullineux [6] examined the quasi-steady state temperature distribution within a cylinder in periodic contact with a surface. They applied an approximate semi-numerical procedure by dividing up the cylinder into equal intervals and using a trapezoidal approximation to obtain a system of simultaneous equations that describe the temperature distribution at any specified point during the instant of closure and separation. The solution, as pointed out by the authors, is not a simple one with which to obtain results. Mikhailov [7] applied an integral transform technique to the same problem. He reduced the analysis to an exact solution of a system of simultaneous algebraic equations for the temperature transform. Vick and Özisik [8] examined quasi-steady state conditions for periodic contact between two regions and included the effect of convection during separation. An integral transform technique reduced the problem to a system of simultaneous algebraic equations for the temperature transform.

Rewetting analysis involves the study of heat transfer as a moving liquid fluid front passes over a heated surface. As the fluid front advances, the heat transfer coefficient jumps from zero for the dry heated surface to a finite value as the surface becomes wetted.

Salcudean, et al. [10] solved the rewetting process in a horizontal channel using finite differences. Blair [11] used separation of variables to construct an infinite series expansion on each side of the fluid front for the temperature distribution in the surface. The expansion coefficients for each side were found by applying Galerkin's method at the fluid front. Lemmon [12] studied the effects of rewetting using a two dimensional moving finite element transient conduction algorithm. To better model the rewetting phenomenon, Salcudean, et al. [13] added a third precooled region of intermediate heat transfer coefficient between the dry and wet regions. Each heat transfer coefficient region was solved separately using separation of variables, the solutions were then coupled together at the region boundaries to find the unknown constants. The methods applied for rewetting analysis work well only for a limited number of step changes in convection coefficient.

A similar problem to rewetting is the quenching of a heated object in a low temperature coolant. The subsequent boiling of the liquid at the surface as heat is transferred effectively creates a continuous time varying heat transfer coefficient. Such a problem is difficult to solve since the variables are nonseparable due to the time dependent convection coefficient appearing in the boundary condition. Thompson and Holy [9] examined the quenching of a sphere by separating the heat transfer coefficient into a constant and time dependent part. The method of eigenfunction expansion was applied to transform the problem into a Volterra-type integral equation for the boundary surface temperature. The solution of this integral, however, is difficult.

The study of heat conduction with time or space dependent heat transfer coefficient again creates a nonseparable problem. Holy [14] extended the work of Thompson and Holy [9] to model heat conduction within nuclear fuel elements subjected to both time and space dependent boundary conditions of the third kind. Another approach to the solution of variable convective coefficient proposed by Ivanov and Salomotov [15] involves using a change of the dependent variable. This simplifies the boundary condition but introduces a nonlinear term into the heat conduction equation. To overcome the nonseparable variable condition, Özisik and Murray [16] applied a variable eigenvalue approach using the finite integral transform technique for transient heat conduction with both time and space dependent convection coefficient. The problem was then reduced to an infinite series of simultaneous first-order differential equations with variable coefficients. An Nth order approximation method was presented and explicit relationships were provided for the zero order solution (N = 0) and first order solution (N = 1). Yener and Özisik [17] extended the analysis of Özisik and Murray [16] for a multiregion medium with time and space dependent thermal conductivity and heat transfer coefficient.

For phase change problems, the position coordinate of the phase front varies with time thus creating a nonseparable problem which is similar to the variable heat transfer coefficient problem of reference [16]. Özisik and Guceri [18] modified the variable eigenvalue approach of Özisik and Murray [16] for a variable position coordinate and provided a zero order approximate solution.

From the review of the literature, the analytical solution of

variable heat transfer coefficient applied to convective flows has not been attempted. The variable eigenvalue method developed by Özisik and Murray [16] applied to convective heat transfer with space dependent heat transfer coefficient appears to be the most promising analytical method. Results of the analysis for a laminar flow in a tube subjected to a stepwise periodic heat transfer coefficient can be compared to the numerical results presented by Charmchi and Sparrow [5].

III. GENERAL FORMULATION

The physical system under investigation concerns heat transfer from a constant property, incompressible, Newtonian fluid inside a conduit of either a circular or channel geometry. The flow enters the conduit at z = 0 fully mixed so that the temperature is constant, with either a laminar fully developed or constant velocity profile, as shown in Fig. 2. The flow then exchanges heat with an ambient environment at temperature T_∞ by virtue of an axially varying heat transfer coefficient, h(z). The effects of axial diffusion in the flow are considered negligible. Furthermore, the conduit wall thickness is assumed negligible, having no other effect than to contain the fluid.

A. Governing Equations

The energy equation for the previously outlined physical system is given below:

$$\rho C_p u(r) \frac{\partial T}{\partial z} = k \frac{1}{r^s} \frac{\partial}{\partial r} \left(r^s \frac{\partial T}{\partial r}\right) + g(r,z) + \mu\left(\frac{du}{dr}\right)^2 \quad , \qquad 0 < r < r_o \quad , \quad z > 0 \tag{3a}$$

The required boundary conditions are taken as

$$\frac{\partial T}{\partial r} = 0 \quad , \quad r = 0 \tag{3b}$$

$$-k \frac{\partial T}{\partial r} = h(z) (T - T_\infty) \quad , \quad r = r_o \tag{3c}$$

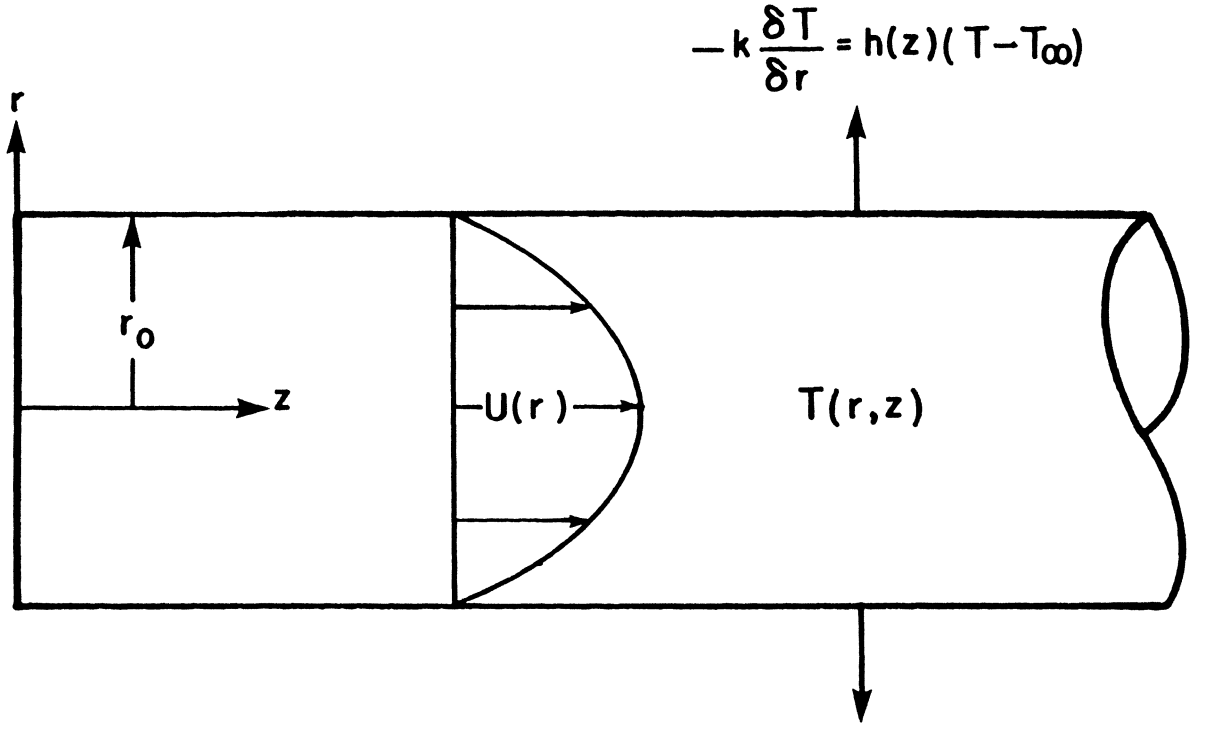

Figure 2 Geometry and coordinates

The inlet condition is

$$T = T_o \quad , \quad z = 0 \tag{3d}$$

and the geometry specifier, s, is defined by

$$s = \begin{cases} 0, \text{ parallel plate} \\ 1, \text{ circular tube} \end{cases} \tag{4}$$

The velocity profile u(r) is given as

$$u(r) = \begin{cases} \bar{u} & , \text{ slug flow} \\ 2\bar{u}[1-(r/r_o)^2] & , \text{ laminar fully developed flow in tube} \\ \frac{3}{2}\bar{u}[1-(r/r_o)^2] & , \text{ laminar fully developed flow in channel} \end{cases} \tag{5}$$

B. Dimensionless Equations

The system of Eqs. (3) through (5) is more conveniently written in dimensionless form using the following quantities:

$$\theta(\eta,\xi) = \frac{T(r,z) - T_\infty}{T_o - T_\infty} \tag{6a}$$

$$\eta = r/r_o \ , \ \xi = \frac{z/r_o}{Pe} \ , \ Pe = \frac{2r_o\bar{u}}{\alpha} \tag{6b}$$

$$v(\eta) = \frac{u(r)}{\bar{u}} \tag{6c}$$

$$H(\xi) = \frac{h(z)r_o}{k} \tag{6d}$$

$$S(\eta,\xi) = \frac{\left[g(r,z) + \mu \left(\frac{\partial u}{\partial r}\right)^2\right] r_o^2}{k(T_o - T_\infty)} \tag{6e}$$

Writing the system of Eqs. (3) through (5) in terms of dimensionless quantities (6a-e), one obtains the following

$$\frac{v(\eta)}{2} \frac{\partial \theta}{\partial \xi} = \frac{1}{\eta^s} \frac{\partial}{\partial \eta} \left(\eta^s \frac{\partial \theta}{\partial \eta}\right) + S(\eta,\xi), \quad 0 < \eta < 1, \quad \xi > 0 \tag{7a}$$

with

$$\frac{\partial \theta}{\partial \eta} = 0 \quad , \quad \eta = 0 \tag{7b}$$

$$\frac{\partial \theta}{\partial \eta} + H(\xi)\theta = 0 \quad , \quad \eta = 1 \tag{7c}$$

$$\theta = 1 \quad , \quad \xi = 0 \tag{7d}$$

The dimensionless energy Eq. (7a) includes a choice of both duct geometry, via the specifier s defined in (4), and dimensionless velocity profile, $v(\eta)$, defined as

$$v(\eta) = \begin{cases} 1 & \text{, slug flow} \\ \frac{3}{2}[1 - (\eta)^2] & \text{, fully developed flow, parallel plates} \\ 2[1 - (\eta)^2] & \text{, fully developed flow, circular tube} \end{cases} \tag{8}$$

Other velocity profiles may also be specified for applications such as a flow of a non-newtonian fluid. The dimensionless source term, $S(\eta,\xi)$, contains both viscous dissipation effects and internal heat generation, and the dimensionless Biot number, $H(\xi)$, contains the variable heat transfer coefficient.

The analysis is now concerned with the solution of Eq. (7a) subjected to boundary conditions (7b,c) and inlet condition (7d). Many special cases of engineering interest can be obtained from the system of Eqs. (7) by merely specifying the functional form of the heat transfer coefficient, $H(\xi)$. However, this flexibility in modeling is accompanied by mathematical difficulties when an analytical solution is attempted. Although the problem given by the system of Eqs. (7) is relatively easy to describe and is solvable when $H(\xi)$ is constant [21], solutions for a variable Biot number become surprisingly difficult as all standard analytical procedures fail.

In the following subsections, two solution techniques will be employed. The first method is a variable eigenfunction technique developed from the general integral transform technique which will handle variable boundary condition parameters. The second method is a connected region technique which is a limited exact solution for the case of a stepwise periodic heat transfer coefficient. This technique is limited by its computational difficulty, but can be used as a solution benchmark for the variable eigenfunction technique.

IV. SOLUTION USING VARIABLE EIGENFUNCTION TECHNIQUE

A. General Method

When dealing with linear partial differential equations, a variety of analytical methods are available including separation of variables, Green's functions, Laplace transforms, and Duhamel's method. The most powerful technique is the integral transform technique. However, when a variable convective boundary coefficient is involved, all standard analytical techniques fail since the boundary condition (7c) does not satisfy the criteria for a Sturm-Liouville problem, and is nonseparable.

In order to solve the system of Eqs. (7), we adopt a variable eigenfunction technique originally applied to transient heat conduction by Özisik and Murray [16]. This technique is a generalization of the integral transform technique. In this method, we apply an integral transform and inversion, derived from a variable eigenvalue problem for Eq. (7a) in order to remove the second order partial differential from the differentional equation (7a). The resultant first order equation is solved using the transformed boundary conditions and a back substitution of the integral inversion. The inversion formula is then applied to recover the temperature distribution $\theta(\eta,\xi)$.

The system of Eqs. (7) does not correspond to a Sturm-Liouville system and so cannot be solved by separating variables. The variable eigenfunction technique is based on assuming a variable eigenvalue problem not directly derivable, but rather suggested by the Sturm-Liouville problem for $H(\xi)$ = constant. The variable eigenvalue problem is taken as

$$\frac{\partial}{\partial \eta}\left(\eta^s \frac{\partial \psi_m}{\partial \eta}\right) + \lambda_m^2(\xi)\eta^s \frac{v(\eta)}{2} \psi_m(\eta,\xi) = 0 \ , \ 0 < \eta < 1, \ \xi > 0 \qquad (9a)$$

$$\frac{\partial \psi_m}{\partial \eta} = 0 \quad , \quad \eta = 0 \qquad (9b)$$

$$\frac{\partial \psi_m}{\partial \eta} + H(\xi) \ \psi_m = 0 \quad , \quad \eta = 1 \qquad (9c)$$

Here, the axial variable ξ, is treated as a parameter. At any given location ξ, the Biot number, $H(\xi)$, has a definite value and a corresponding set of eigenvalues, $\lambda_m(\xi)$, and normalized eigenfunctions, $\psi_m(\eta,\xi)$. The eigenfunctions, $\psi_m(\eta,\xi)$, obey the following normalized orthogonality relation at any given ξ location

$$\int_{\eta=0}^{1} \eta^s \frac{v(\eta)}{2} \psi_m(\eta,\xi) \ \psi_p(\eta,\xi)d\eta = \begin{cases} 0, & m \neq p \\ 1, & m = p \end{cases} \qquad (10)$$

The proof of this and other eigenfunction relations used later are presented in Appendix A.

For convenience, the eigenfunction has been normalized as

$$\psi_m(\eta,\xi) = R_m(\eta,\xi)/[N_m(\xi)]^{1/2} \qquad (11)$$

using the normalization integral defined as,

$$N_m(\xi) = \int_{\eta=0}^{1} \eta^s \frac{v(\eta)}{2} R_m^2(\eta,\xi)d\eta \qquad (12)$$

where $R_m(\eta,\xi)$ satisfies Eqs. (9) but has not been normalized.

The first step in using the integral transform technique is to derive the integral transform pair. One can define the temperature $\theta(\eta,\xi)$ in the region $0 < \eta < 1$, in terms of the linear combination of normalized eigenfunctions $\psi_m(\eta,\xi)$ in the form

$$\theta(\eta,\xi) = \sum_{m=1}^{\infty} C_m(\xi)\ \psi_m(\eta,\xi) \tag{13}$$

To determine the coefficients $C_m(\xi)$, operate on both sides of Eq. (13) with the operator

$$\int_{\eta=0}^{1} \eta^s\ \frac{v(\eta)}{2}\ \psi_m(\eta,\xi)d\eta \tag{14}$$

and apply the orthogonality relation (10) to find the coefficients $C_m(\xi)$, as

$$C_m(\xi) = \int_{\eta=0}^{1} \eta^s\ \frac{v(\eta)}{2}\ \psi_m(\eta,\xi)\ \theta(\eta,\xi)d\eta \tag{15}$$

By introducing expression (15) into the temperature function (13), one can construct the integral transform pair

$$\text{Transform:}\quad \bar{\theta}_m(\xi) = \int_{\eta=0}^{1} \eta^s\ \frac{v(\eta)}{2}\ \psi_m(\eta,\xi)\theta(\eta,\xi)d\eta \tag{16a}$$

$$\text{Inversion:}\quad \theta(\eta,\xi) = \sum_{m=1}^{\infty} \psi_m(\eta,\xi)\ \bar{\theta}_m(\xi) \tag{16b}$$

Having defined the transform pair, the next step is to remove the radial variable η, from the partial derivatives of Eq. (7a) by applying

transform (16a). Operate on energy Eq. (7a) with

$$\int_{\eta=0}^{1} \eta^s \, \psi_m(\eta,\xi) d\eta \tag{17}$$

to obtain the relation

$$\int_{\eta=0}^{1} \eta^s \, \frac{v(\eta)}{2} \, \psi_m(\eta,\xi) \, \frac{\partial\theta}{\partial\xi} \, d\eta = \int_{\eta=0}^{1} \psi_m(\eta,\xi) \, \frac{\partial}{\partial\eta} \, (\eta^s \, \frac{\partial\theta}{\partial\eta}) d\eta + \bar{S}_m(\xi) \tag{18a}$$

where $\bar{S}_m(\xi)$ is the integral transform of the dimensionless source function $S(\eta,\xi)$, defined as

$$\bar{S}_m(\xi) = \int_{\eta=0}^{1} \eta^s \, \psi_m(\eta,\xi) \, S(\eta,\xi) d\eta \tag{18b}$$

In Eq. (18a) integrate the first term of the RHS by parts twice to get

$$\begin{aligned} \int_{\eta=0}^{1} \psi_m(\eta,\xi) \, \frac{\partial}{\partial\eta} \, (\eta^s \, \frac{\partial\theta}{\partial\eta}) d\eta &= \psi_m(\eta,\xi) \, \eta^s \, \frac{\partial\theta}{\partial\eta}\Big|_{\eta=0}^{1} \\ - \eta^s \, \frac{\partial\psi_m}{\partial\eta} \, \theta(\eta,\xi)\Big|_{\eta=0}^{1} &+ \int_{\eta=0}^{1} \theta(\eta,\xi) \, \frac{\partial}{\partial\eta} \, (\eta^s \, \frac{\partial\psi_m}{\partial\eta}) d\eta \end{aligned} \tag{19}$$

Utilize boundary conditions (7b,c) and (9b,c), and Eqs. (9a) and (16a) to simplify (19) into the form

$$\begin{aligned} \int_{\eta=0}^{1} \psi_m(\eta,\xi) \, \frac{\partial}{\partial\eta} \, (\eta^s \, \frac{\partial\theta}{\partial\eta}) d\eta &= \int_{\eta=0}^{1} \theta(\eta,\xi)[-\lambda_m^2(\xi) \, \eta^s \, \frac{v(\eta)}{2} \, \psi_m(\eta,\xi)] d\eta \\ &= - \lambda_m^2(\xi) \, \bar{\theta}_m(\xi) \end{aligned} \tag{20}$$

Since the eigenfunctions, $\psi_m(\eta,\xi)$, depend on ξ, the partial derivative in the LHS of Eq. (18a) cannot be brought outside of the integral. However, to overcome this difficulty, one can resort to the eventual solution given by the inversion formula (16b). Substitution of Eq. (16b) for $\theta(\eta,\xi)$ in the partial derivative yields,

$$\int_{\eta=0}^{1} \eta^s \frac{v(\eta)}{2} \psi_m(\eta,\xi) \frac{\partial\theta}{\partial\xi} d\eta = \int_{\eta=0}^{1} \eta^s \frac{v(\eta)}{2} \psi_m(\eta,\xi) \cdot \frac{\partial}{\partial\xi} \left[\sum_{p=1}^{\infty} \psi_p(\eta,\xi) \bar{\theta}_p(\xi) \right] d\eta \tag{21}$$

Then, use the product rule on the differential in the RHS of Eq. (21) and exchange the order of integration to get

$$\int_{\eta=0}^{1} \eta^s \frac{v(\eta)}{2} \psi_m(\eta,\xi) \frac{\partial\theta}{\partial\eta} d\eta = \sum_{p=1}^{\infty} \bar{\theta}_p(\xi) \int_{\eta=0}^{1} \eta^s \frac{v(\eta)}{2} \psi_m(\eta,\xi) \frac{\partial\psi_p}{\partial\xi} d\eta + \sum_{p=1}^{\infty} \frac{d\bar{\theta}_p}{d\xi} \int_{\eta=0}^{1} \eta^s \frac{v(\eta)}{2} \psi_m(\eta,\xi) \psi_p(\eta,\xi) d\eta \tag{22}$$

Equation (22) can further be simplified by using the orthogonality condition (10) to find

$$\int_{\eta=0}^{1} \eta^s \frac{v(\eta)}{2} \psi_m(\eta,\xi) \frac{\partial\theta}{\partial\eta} d\eta = \sum_{p=1}^{\infty} \bar{\theta}_p(\xi) A_{mp}(\xi) + \frac{d\bar{\theta}_m}{d\xi} \tag{23}$$

where

$$A_{mp}(\xi) = \int_{\eta=0}^{1} \eta^s \frac{v(\eta)}{2} \psi_m(\eta,\xi) \frac{\partial\psi_p}{\partial\xi} d\eta \tag{24a}$$

The $A_{mp}(\xi)$ function can further be manipulated to the form

$$A_{mp}(\xi) = \frac{dH(\xi)}{d\xi} \left[\frac{\psi_m(1,\xi)\ \psi_p(1,\xi)}{\lambda_p^2(\xi) - \lambda_m^2(\xi)}\right] \tag{24b}$$

as developed in Appendix B.

Finally, substituting Eqs. (20) and (23) into Eq. (18a) gives the desired transformed differential equation of (7a)

$$\frac{d\bar{\theta}_m}{d\xi} + \lambda_m^2(\xi)\ \bar{\theta}_m(\xi) + \sum_{p=1}^{\infty} \bar{\theta}_p(\xi)\ A_{mp}(\xi) = \bar{S}_m(\xi) \quad ,$$

$$m = 1,2,3,\ldots,\ \xi > 0 \tag{25}$$

where $\bar{S}_m(\xi)$ is defined in Eq. (18b) and $A_{mp}(\xi)$ is defined in Eq. (24b). The initial conditions are obtained by taking the transform of Eq. (7d) to get

$$\bar{\theta}_m = \frac{H(0)\ \psi_m(1,0)}{\lambda_m^2(0)} = B_m \quad ,$$

$$m = 1,2,3,\ldots,\ \xi = 0 \tag{26}$$

The system of Eqs. (25) subjected to initial conditions (26) provides an infinite set of coupled ordinary differential equations with variable coefficients for the integral transform $\theta_m(\xi)$. Once the transforms are determined, the inversion formula (16b) is used to determine the dimensionless temperature $\theta(\eta,\xi)$.

After the temperature distribution is known, the bulk temperature for the region $\xi > 0$ can be determined from

$$\theta_b(\xi) = 2^s \int_{\eta=0}^{1} \eta^s \, v(\eta) \, \theta(\eta,\xi) d\eta \tag{27a}$$

Using the inversion formula (16b) and the eigenvalue problem (9a), Eq. (27a) can be manipulated into the form

$$\theta_b(\xi) = 2^{s+1} \, H(\xi) \sum_{m=1}^{\infty} \frac{\psi_m(1,\xi)}{\lambda_m^2(\xi)} \bar{\theta}_m(\xi) \tag{27b}$$

The local heat transfer rate at the wall, $Q_w(\xi)$, is available as

$$Q_w(\xi) = - \left.\frac{\partial\theta}{\partial\eta}\right|_{\eta=1} = \sum_{m=1}^{\infty} \bar{\theta}_m(\xi) \, H(\xi) \, \psi_m(\eta,\xi) \tag{28}$$

The total heat transfer rate can be found from an energy balance from 0 to ξ as

$$Q(\xi) = 1 - \theta_b(\xi) \tag{29}$$

where viscous dissipation and energy sources are neglected.

The solution of an infinite set of ordinary first order differential equations with variable coefficients such as the system of Eqs. (25) is mathematically and computationally difficult. Some approximate techniques and an exact solution for the stepwise periodic case are presented in the following section.

B. Solution for Transforms

Presented here are three solution techniques to resolve the system

of Eqs. (25). These are the Nth order approximation method, the iterative method and the stepwise periodic solution method.

1) Nth Order Approximation Method

The calculation of the transforms in the system of Eqs. (25) is difficult because of the coupling of the equations. However, in many applications an approximate solution will suffice. By truncating the various orders of the summation, the solution can be greatly simplified. The Nth order approximation is obtained by truncating the series in Eq. (25) at N terms. The first N equations are then coupled and must be solved simultaneously while the remaining equations for m = N + 1, N + 2, ..., are uncoupled. In general, one has

$$\frac{d\bar{\theta}_m}{d\xi} + \lambda_m^2(\xi)\,\bar{\theta}_m(\xi) + \sum_{p=1}^{N} \bar{\theta}_p(\xi)\,A_{mp}(\xi) = \bar{S}_m(\xi) \quad , \quad \xi > 0 \quad , \tag{30a}$$

$$\bar{\theta}_m(0) = \frac{H(0)\,\psi_m(1,0)}{\lambda_m^2(0)} = B_m \quad , \quad \xi = 0 \quad , \tag{30b}$$

$$m = 1,2,\ldots$$

The lowest order analysis is the zero order approximation where N = 0 and the summation is neglected entirely. Equation (30a) becomes

$$\frac{d\bar{\theta}_m}{d\xi} + \lambda_m^2(\xi)\,\bar{\theta}_m(\xi) = \bar{S}_m(\xi) \tag{31}$$

The advantage of the zero order solution is that the equations are

uncoupled and the coefficients $A_{mp}(\xi)$ do not enter the analysis. The solution of Eq. (31) is immediately available as

$$\bar{\theta}_m(\xi) = \exp\Big(-\int_{\xi'=0}^{\xi} \lambda_m^2(\xi')d\xi'\Big)\Big[B_m + \int_{\xi'=0}^{\xi} \bar{S}_m(\xi') \cdot \exp\Big(\int_{\xi''=0}^{\xi'} \lambda_m^2(\xi'')d\xi''\Big)d\xi'\Big] , \tag{32}$$

$$m = 1,2,\ldots, \quad \xi > 0$$

The error of Eq. (32) is on the order of the size of the summation, $\sum_{p=1}^{N} \bar{\theta}_p(\xi)\, A_{mp}(\xi)$.

To hopefully increase the accuracy, the first term in the summation is retained to give the first order solution. The first order equations become

$$\frac{d\bar{\theta}_m}{d\xi} + \lambda_m^2(\xi)\, \bar{\theta}_m(\xi) + \bar{\theta}_1(\xi)\, A_{m1}(\xi) = \bar{S}_m(\xi) \quad , \tag{33}$$

$$m = 1,2,\ldots, \quad \xi > 0$$

with Eq. (30b) as the inital condition.

The solution to Eq. (33) is found by first solving for $\bar{\theta}_1(\xi)$ where $A_{11}(\xi) = 0$ by $A_{mp}(\xi)$ relation (89b), and then using $\bar{\theta}_1(\xi)$ as a non-homogeneous contribution to solve for $\bar{\theta}_m(\xi)$, $m = 2,3,\ldots$. The result is readily obtained as

$$\bar{\theta}_1(\xi) = \exp\Big(-\int_{\xi'=0}^{\xi} \lambda_1^2(\xi')d\xi'\Big)\Big[B_1 + \int_{\xi'=0}^{\xi} \bar{S}_1(\xi') \cdot \exp\Big(-\int_{\xi''=0}^{\xi'} \lambda_1^2(\xi'')d\xi''\Big)d\xi'\Big] \tag{34a}$$

$$\bar{\theta}_m(\xi) = \exp\Big(-\int_{\xi'=0}^{\xi} \lambda_m^2(\xi')d\xi'\Big)\Big[B_m - \int_{\xi'=0}^{\xi} \exp\Big(-\int_{\xi''=0}^{\xi'} \lambda_m^2(\xi'')d\xi''\Big) \cdot \bar{\theta}_1(\xi')\, A_{m1}(\xi')d\xi' + \int_{\xi'=0}^{\xi} \bar{S}_m(\xi') \exp\Big(-\int_{\xi''=0}^{\xi'} \lambda_m^2(\xi'')d\xi''\Big)d\xi'\Big] , \tag{34b}$$

$$m = 2,3,4,\ldots,\ \xi > 0$$

Computationally, the system (34a,b) is more demanding than Eq. (32) but hopefully provides greater accuracy. Increasing the order N makes the solution increasingly more accurate at the expense of greater complexity. For higher orders, the first m = N coupled equations must be solved simultaneously, the remaining equations for m = N + 1, N + 2, ... are solved with the summation as a non-homogeneous solution. For example, the second order approximation would be written

$$\frac{d\bar{\theta}_1}{d\xi} + \lambda_1^2(\xi)\,\bar{\theta}_1(\xi) + \bar{\theta}_2(\xi)\,A_{12}(\xi) = \bar{S}_1(\xi) \tag{35a}$$

$$\frac{d\bar{\theta}_2}{d\xi} + \lambda_2^2(\xi)\,\bar{\theta}_2(\xi) + \bar{\theta}_1(\xi)\,A_{21}(\xi) = \bar{S}_2(\xi) \tag{35b}$$

$$\frac{d\bar{\theta}_m}{d\xi} + \lambda_m^2(\xi)\,\bar{\theta}_m(\xi) + \bar{\theta}_1(\xi)\,A_{m1}(\xi) + \bar{\theta}_2(\xi)\,A_{m2}(\xi) = \bar{S}_m(\xi) , \tag{35c}$$

$$m = 3,4,5,\ldots,\ \xi > 0$$

Equations (35a) and (35b) must be solved simultaneously. Then Eq. (35c)

can be solved using the solution of (35a) and (35b) as a nonhomogeneous contribution. For a continuously variable heat transfer coefficient, the second and higher order approximations can conveniently be solved simultaneously [16]. However, when a discontinuous or stepwise periodic heat transfer coefficient is applied, the numerical solution becomes quite difficult.

For the study of a stepwise periodic heat transfer coefficient, the zero and first order approximations are tested. A second order approximation was derived and found to be computationally extravagant.

2) Iterative Method

One can arrange the system of Eqs. (25) as

$$\frac{d\bar{\theta}_m}{d\xi} + \lambda_m^2(\xi)\ \bar{\theta}_m(\xi) = F_m(\xi) \tag{36a}$$

$$\bar{\theta}_m(0) = \frac{H(0)\ \psi_m(0,1)}{\lambda_m^2(0)} = B_m \quad , \quad \xi = 0 \quad , \tag{36b}$$

$$m = 1,2,\ldots$$

where

$$F_m(\xi) = \bar{S}_m(\xi) - \sum_{p=1}^{\infty} \bar{\theta}_p(\xi)\ A_{mp}(\xi) \tag{36c}$$

Treating $F_m(\xi)$ as a nonhomogeneous contribution, Eqs. (36a,b) can be formally solved as

$$\bar{\theta}_m(\xi) = \exp\left(-\int_{\xi'=0}^{\xi} \lambda_m^2(\xi')d\xi'\right)\left[B_m + \int_{\xi'=0}^{\xi} F_m(\xi')\exp\left(-\int_{\xi''=0}^{\xi'} \lambda_m^2(\xi'')d\xi''\right)d\xi'\right] \tag{37}$$

Equation (37) constitutes an infinite set of complete integral equations for the function $\bar{\theta}_m(\xi)$. One might solve Eq. (37) by guessing an initial value for $F_m(\xi)$ and iteratively updating $\bar{\theta}_m(\xi)$. In mathematical notation, this results in the expression

$$\bar{\theta}_m^{(\alpha+1)} = \exp\left(-\int_{\xi'=0}^{\xi} \lambda_m^2(\xi')d\xi'\right)\left[B_m + \int_{\xi'=0}^{\xi} F_m^{(\alpha)}(\xi')\cdot\exp\left(-\int_{\xi''=0}^{\xi'} \lambda_m^2(\xi'')d\xi''\right)d\xi'\right] , \tag{38a}$$

$$m = 1,2,\ldots \quad , \quad \alpha = 0,1,2,\ldots$$

where

$$F_m^{(\alpha)}(\xi') = \bar{S}_m(\xi') - \sum_{p=1}^{\infty} \bar{\theta}_p^{(\alpha)}(\xi')\, A_{mp}(\xi') \tag{38b}$$

The value α is the present iterated value (or guessed value for $\alpha = 0$), and $\alpha + 1$ is the updated value. The new value for $\bar{\theta}_m^{(\alpha+1)}(\xi)$ can be substituted into the series summation to find $F_m^{(\alpha+1)}(\xi)$ in order to iterate for $\bar{\theta}_m^{(\alpha+2)}(\xi)$ and so forth until some desired accuracy is achieved.

To begin the iteration with $\alpha = 0$, use as the initial guess $F_m^{(0)}(\xi) = 0$. Equation (38a) becomes

$$\bar{\theta}_m^{(1)}(\xi) = \exp\left(-\int_{\xi'=0}^{\xi} \lambda_m^2(\xi')d\xi'\right)\left[B_m + \int_{\xi'=0}^{\xi} \bar{S}_m(\xi')\right.$$

$$\left.\cdot \exp\left(-\int_{\xi''=0}^{\xi} \lambda_m^2(\xi'')d\xi''\right)d\xi'\right] \quad , \quad m = 1,2,\ldots, \ \xi > 0 \tag{39}$$

which is equivalent to the zero order approximation (32). Substituting Eq. (39) into (38b) yields the next iterative value

$$F_m^{(1)}(\xi) = \bar{S}_m(\xi) - \sum_{p=1}^{\infty} \exp\left(-\int_{\xi'=0}^{\xi} \lambda_p^2(\xi')d\xi'\right)\left[B_p + \int_{\xi'=0}^{\xi} \bar{S}_p(\xi')\right.$$

$$\left.\cdot \exp\left(-\int_{\xi''=0}^{\xi'} \lambda_p^2(\xi'')d\xi''\right)d\xi'\right] A_{mp}(\xi) \tag{40}$$

Using Eq. (40) in Eq. (38a), we obtain the second iteration for the transformed dimensionless temperature as

$$\bar{\theta}_m^{(2)}(\xi) = \exp\left(-\int_{\xi'=0}^{\xi} \lambda_m^2(\xi')d\xi'\right)\left\{B_m + \int_{\xi'=0}^{\xi}\left[\bar{S}_m(\xi') - \right.\right.$$

$$\sum_{p=1}^{\infty} \exp\left(-\int_{\xi''=0}^{\xi'} \lambda_p^2(\xi'')d\xi''\right)$$

$$\cdot\left(B_p + \int_{\xi''=0}^{\xi'} \bar{S}_p(\xi'')\exp\left(-\int_{\xi'''=0}^{\xi''} \lambda_p^2(\xi''')d\xi'''\right)d\xi''\right)A_{mp}(\xi')d\xi'\Big] \tag{41}$$

$$\left.\cdot \exp\left(-\int_{\xi''=0}^{\xi'} \lambda_m^2(\xi'')d\xi''\right)\right\}d\xi' \quad ,$$

$$m = 1,2,\ldots, \ \xi > 0$$

This process can be carried out indefinitely with each value of $F_m(\xi)$ becoming increasingly more involved. The accuracy of the solution is

dependent on the number of iterations taken, yet after the first two iterations the solution becomes computationally impractical. The solution method has merit if the first two iterations are enough to provide an acceptable approximation. For this study, the second iterative approximation of Eq. (41) is evaluated.

3) Stepwise Periodic Method

The two previous solution methods for the system of coupled differential Eqs. (25) applys to any functional form of $H(\xi)$. The stepwise periodic method, however, can only be applied to a stepwise periodic variation in $H(\xi)$ such as the periodic variation of the heat transfer coefficient used to model fins. This method is derived as a formally exact solution whereas the first two solution methods are approximate.

For the case of a stepwise periodic Biot number, representing the system of Fig. 1, $H(\xi)$ can be expressed as,

$$H(\xi) = \begin{cases} H_1, & \xi^*_{1j} < \xi < \xi^*_{2j} \\ H_2, & \xi^*_{2j} < \xi < \xi^*_{1,j+1} \end{cases} , \qquad j = 0,1,2... \tag{42}$$

where the jump points are designated by the notation

$$\xi^*_{1j} = j(\xi_1 + \xi_2) \quad , \text{ start of unfinned region in cycle } j \tag{43a}$$

$$\xi^*_{2j} = j(\xi_1 + \xi_2) + \xi_1 \quad , \text{ start of finned region in cycle } j \tag{43b}$$

where ξ_1 is the dimensionless representation of the interfin spacing z_1 and ξ_2 is the dimensionless representation of the fin thickness z_2 in Fig 1. With a discontinuous Biot number, the eigenvalues and eigenfunctions resulting from the system of Eqs. (9) must also be discontinuous and are designated as

$$\lambda_m(\xi) = \begin{cases} \lambda_{1m}, & \xi^*_{1j} < \xi < \xi^*_{2j} \\ \lambda_{2m}, & \xi^*_{2j} < \xi < \xi^*_{1,j+1} \end{cases} \tag{44}$$

and

$$\psi_m(\eta,\xi) = \begin{cases} \psi_{1m}(\eta), & \xi^*_{1j} < \xi < \xi^*_{2j} \\ \psi_{2m}(\eta), & \xi^*_{2j} < \xi < \xi^*_{1,j+1} \end{cases} \tag{45}$$

The nature of the transforms (16a) resulting from the system of Eqs. (25) and (26) also involves discontinuities at each jump point. By recognizing this discontinuous behavior, one can adopt the following notation for the integral transforms (16a) on either side of a jump point

$$\Gamma^-_m(\xi^*_{ij}) = \lim_{\varepsilon\to 0} \bar{\theta}_m(\xi^*_{ij} - \varepsilon) \tag{46a}$$

$$\Gamma^+_m(\xi^*_{ij}) = \lim_{\varepsilon\to 0} \bar{\theta}_m(\xi^*_{ij} + \varepsilon) \quad , \tag{46b}$$

$$i = 1 \text{ or } 2, \; j = 0,1,2,\ldots$$

as pictured in Fig. 3 for the first jump point, i = 2 and j = 0.

The $A_{mp}(\xi)$ function (24a) for this special discontinuous case is manipulated as detailed in Appendix B as

$$A_{mp}(\xi) = a_{mp} \sum_{j=0}^{\infty} [\delta(\xi - \xi^*_{2j}) - \delta(\xi - \xi^*_{1,j+1})] \tag{47a}$$

where

$$a_{mp} = \frac{H_2 - H_1}{2} \left[\frac{\psi_{1m}(1)\ \psi_{2p}(1)}{\lambda^2_{2p} - \lambda^2_{1m}} - \frac{\psi_{2m}(1)\ \psi_{1p}(1)}{\lambda^2_{2m} - \lambda^2_{1p}}\right] \tag{47b}$$

Equations (47a,b) show that the coefficients $A_{mp}(\xi)$, contribute to the system of Eqs. (25) only at a jump point, where they contribute an impulse, or delta function as seen in Fig. 3. With this behavior in mind, formally integrate Eq. (25) from the beginning of a constant Biot number region, $\xi = \xi^*_{ij}$, where $\bar{\theta}_m(\xi^*_{ij}) = \Gamma^+_m(\xi^*_{ij})$, up to an arbitrary location before the next jump point. The result is expressed as

$$\begin{aligned} \bar{\theta}_m(\xi) &= \Gamma^+_m(\xi^*_{ij}) \exp\left[-\lambda^2_{im}\ (\xi - \xi^*_{ij})\right] \\ &+ \int_{\xi'=\xi^*_{ij}}^{\xi} \exp[-\lambda^2_{im}\ (\xi - \xi')]\ \bar{S}_m(\xi')d\xi' \end{aligned} \tag{48}$$

which is valid for

$$\xi^*_{1j} < \xi < \xi^*_{2j} \qquad , \qquad \text{when } i = 1$$

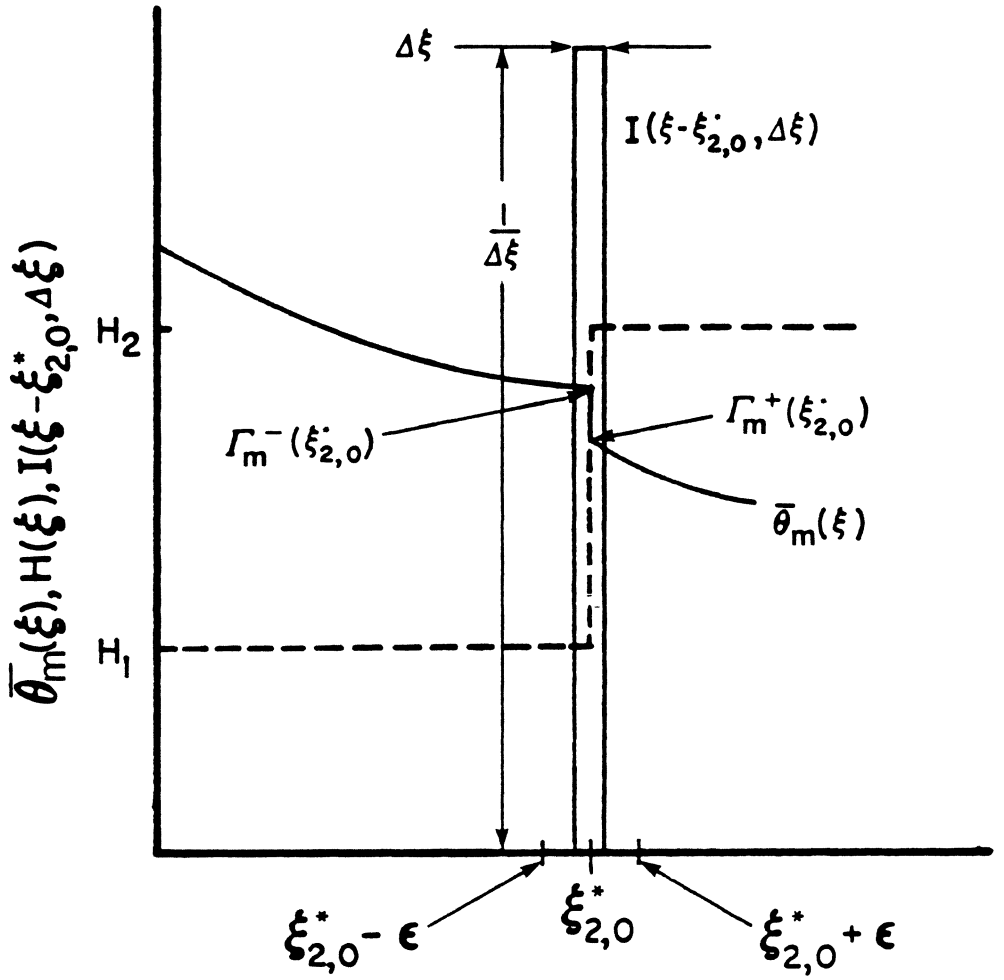

Figure 3 Notation for stepwise periodic method with impulse function

$$\xi^*_{2j} < \xi < \xi^*_{1,j+1} \quad , \quad \text{when } i = 2 \quad ,$$

$$j = 0,1,2,\ldots \quad , \quad m = 1,2,3,\ldots$$

The problem is now reduced to finding the values $\Gamma^+_m(\xi^*_{ij})$. The derivation of the solution for $\Gamma^+_m(\xi^*_{ij})$ is solved explicitly for the first low Biot number or unfinned region and the first high Biot number or finned region. A general form for any axial location is then obtained by induction.

FIRST UNFINNED REGION: $0 = \xi^*_{1,0} < \xi < \xi^*_{2,0}$.

This region does not include a discontinuity and as a result the $A_{mp}(\xi)$ function makes no contribution. Therefore, the summation term in Eq. (25) is zero, thus uncoupling the equations which can then be integrated directly as

$$\bar{\theta}_m(\xi) = \exp(-\lambda^2_{1m}\xi) \left[B_m + \int_{\xi'=0}^{\xi} \bar{S}_m(\xi') \exp(\lambda^2_{1m}\xi')\, d\xi'\right] \tag{49}$$

where B_m is defined in Eq. (26). Equation (49) is also obtainable directly from expression (48) by recognizing that $\Gamma^+_m(\xi^*_{1,0}) = B_m$, and $\xi^*_{ij} = \xi^*_{1,0} = 0$ in the first unfinned region.

FIRST FINNED REGION: $\xi^*_{2,0} < \xi < \xi^*_{1,1}$.

Rewrite Eq. (25) with the integrating factor

$$\exp \int^{\xi} \lambda^2_m(\xi')d\xi' \tag{50}$$

and integrate across the discontinuity $\xi = \xi^*_{2,0} - \varepsilon$ to $\xi = \xi^*_{2,0} + \varepsilon$ to obtain

$$\int_{\xi^*_{2,0}-\varepsilon}^{\xi^*_{2,0}+\varepsilon} \frac{d}{d\xi}\left[\exp\left(\int^{\xi} \lambda_m^2(\xi')d\xi'\right)\ \bar{\theta}_m(\xi)\right]d\xi$$

$$= -\int_{\xi^*_{2,0}-\varepsilon}^{\xi^*_{2,0}+\varepsilon} \exp\left(\int^{\xi} \lambda_m^2(\xi')d\xi'\right) \sum_{p=1}^{\infty} \bar{\theta}_p(\xi)\ A_{mp}(\xi)d\xi \qquad (51)$$

$$+\int_{\xi^*_{2,0}-\varepsilon}^{\xi^*_{2,0}+\varepsilon} \exp\left(\int^{\xi} \lambda_m^2(\xi')d\xi'\right)\ \bar{S}_m(\xi)d\xi$$

Each part of the Eq. (51) must be evaluated carefully.

For the LHS, take the limit as $\varepsilon \to 0$, integrate and use definition (46a) and (46b) to find

$$\lim_{\varepsilon\to 0}\left[\int_{\xi^*_{2,0}-\varepsilon}^{\xi^*_{2,0}+\varepsilon} \frac{d}{d\xi}\left[\exp\left(\int^{\xi} \lambda_m^2(\xi')d\xi'\right)\ \bar{\theta}_m(\xi)d\xi\right)\right] \qquad (52)$$

$$= \exp\left(\int^{\xi^*_{2,0}} \lambda_m^2(\xi')d\xi'\right)\left[\Gamma_m^+(\xi^*_{2,0}) - \Gamma_m^-(\xi^*_{2,0})\right]$$

To the first term on the RHS, substitute the $A_{mp}(\xi)$ function Eq.

(47), and integrate across the Dirac delta function to get

$$\int_{\xi^*_{2,0}-\varepsilon}^{\xi^*_{2,0}+\varepsilon} \exp\left(\int^{\xi} \lambda_m^2(\xi')d\xi'\right) \sum_{p=1}^{\infty} \bar{\theta}_p(\xi) A_{mp}(\xi)d\xi$$

$$= - \sum_{p=1}^{\infty} a_{mp} \exp\left(\int^{\xi_{2,0}} \lambda_m^2(\xi')d\xi'\right) \bar{\theta}_p(\xi^*_{2,0}) \tag{53a}$$

Note that at the jump point $\xi^*_{2,0}$, the temperature transform $\bar{\theta}_p(\xi^*_{2,0})$ is also discontinuous. By applying the Fourier convergence criteria at a discontinuity as the average value and utilizing Eqs. (46a,b) yields

$$\bar{\theta}_p(\xi^*_{2,0}) = \left(\frac{\Gamma_p^+(\xi^*_{2,0}) + \Gamma_p^-(\xi^*_{2,0})}{2}\right) \tag{53b}$$

Finally, integrate the second term on the RHS of Eq. (51)

$$\int_{\xi^*_{2,0}-\varepsilon}^{\xi^*_{2,0}+\varepsilon} \exp\left(\int^{\xi} \lambda_m^2(\xi')d\xi'\right) \bar{S}_m(\xi)d\xi = 0 \tag{54}$$

since $\bar{S}_m(\xi)$ is a continuous function not affected by a step change in Biot. Substitution of relations (52), (53a,b) and (54) into Eq. (51) and simplifying yields

$$\Gamma_m^+(\xi^*_{2,0}) - \Gamma_m^-(\xi^*_{2,0}) = - \sum_{p=1}^{\infty} A_{mp}\left(\frac{\Gamma_p^+(\xi^*_{2,0}) + \Gamma_p^-(\xi^*_{2,0})}{2}\right) \tag{55}$$

Note that Eq. (55) is the form of an infinite set of algebraic equations with $\Gamma_m^-(\xi_{2,0}^*)$ and $A_{mp}(\xi)$ coefficients known. Finally, truncate the set to N terms, and rearrange in matrix form as

$$\underset{\sim}{A}_2 \; \underset{\sim}{\Gamma}^+(\xi_{2,0}^*) = \underset{\sim}{\Gamma}^-(\xi_{2,0}^*) \tag{56}$$

where the various matrices and vectors are defined as follows:

$$\underset{\sim}{A}_2 = \begin{bmatrix} 2 & a_{12} & a_{13} & \cdots & a_{1N} \\ a_{21} & 2 & a_{23} & \cdots & a_{2N} \\ & \vdots & & & \vdots \\ a_{N1} & & \cdots & & 2 \end{bmatrix} \tag{57a}$$

$$\underset{\sim}{\Gamma}^+(\xi_{2,0}^*) = \begin{bmatrix} \Gamma_1^+(\xi_{2,0}^*) \\ \Gamma_2^+(\xi_{2,0}^*) \\ \vdots \\ \Gamma_N^+(\xi_{2,0}^*) \end{bmatrix} \tag{57b}$$

$$\underset{\sim}{\Gamma}^{-}(\xi^{*}_{2,0}) = \begin{bmatrix} 2\Gamma^{-}_{1}(\xi^{*}_{2,0}) - \sum_{p=1}^{N} a_{1p}\ \Gamma^{-}_{p}(\xi^{*}_{2,0}) \\ 2\Gamma^{-}_{2}(\xi^{*}_{2,0}) - \sum_{p=1}^{N} a_{2p}\ \Gamma^{-}_{p}(\xi^{*}_{2,0}) \\ \vdots \\ 2\Gamma^{-}_{N}(\xi^{*}_{2,0}) - \sum_{p=1}^{N} a_{Np}\ \Gamma^{-}_{p}(\xi^{*}_{2,0}) \end{bmatrix} \quad , \qquad (57c)$$

$$p = 1,2,3,\ldots N \quad , \quad \xi > 0$$

At this point the values for $\Gamma^{-}_{m}(\xi^{*}_{2,0})$ are known from the solution in the previous region Eq. (49), and the values needed in matrix $\underset{\sim}{A}_{2}$ can be calculated from Eq. (47). The coefficients $\Gamma^{+}_{m}(\xi^{*}_{2,0})$ are now available by solving matrix Eq. (56) to get

$$\underset{\sim}{\Gamma}^{+}(\xi^{*}_{2,0}) = (\underset{\sim}{A}_{2})^{-1}\ \underset{\sim}{\Gamma}^{-}(\xi^{*}_{2,0}) \qquad (58)$$

Substitution of the coefficients $\Gamma^{+}_{m}(\xi^{*}_{2,0})$ from Eq. (58) into Eq. (48) provides the temperature transform which can be used to find the dimensionless temperature distribution from inversion formula (16b).

By induction, the general form of the $\Gamma^{+}_{m}(\xi^{*}_{ij})$ coefficients for Eq. (48) for any axial region becomes

$$\underset{\sim}{\Gamma}\ (\xi^{+}_{ij})^{*} = (\underset{\sim}{A}_{i})^{-1}\ \underset{\sim}{\bar{\Gamma}}\ (\xi^{*}_{ij}) \qquad (59a)$$

with

$$\Gamma_m^+(\xi_{1,0}^*) = B_m \quad , \quad \xi = \xi_{1,0}^* = 0 \quad , \quad m = 1,2,... \tag{59b}$$

with the various matrices and vectors defined as

$$\underset{\sim}{A}_i = \begin{bmatrix} 2 & (-1)^i a_{12} & (-1)^i a_{13} & \cdots & (-1)^i a_{1N} \\ (-1)^i a_{21} & 2 & (-1)^i a_{23} & \cdots & (-1)^i a_{2N} \\ \vdots & & & & \vdots \\ (-1)^i a_{N1} & & \cdots & & 2 \end{bmatrix} \tag{60a}$$

$$\underset{\sim}{\Gamma}^+(\xi_{ij}^*) = \begin{bmatrix} \Gamma_1^+(\xi_{ij}^*) \\ \Gamma_2^+(\xi_{ij}^*) \\ \vdots \\ \Gamma_N^+(\xi_{ij}^*) \end{bmatrix} \tag{60b}$$

$$\underset{\sim}{\Gamma}^{-}(\xi^{*}_{ij}) = \begin{bmatrix} 2\Gamma^{-}_{1}(\xi^{*}_{ij}) - (-1)^{i} \sum_{p=1}^{N} a_{1p}\Gamma^{-}_{p}(\xi^{*}_{ij}) \\ 2\Gamma^{-}_{2}(\xi^{*}_{ij}) - (-1)^{i} \sum_{p=1}^{N} a_{2p}\Gamma^{-}_{p}(\xi^{*}_{ij}) \\ \vdots \\ 2\Gamma^{-}_{N}(\xi^{*}_{ij}) - (-1)^{i} \sum_{p=1}^{N} a_{Np}\Gamma^{-}_{p}(\xi^{*}_{ij}) \end{bmatrix} , \qquad (60c)$$

$$p = 1,2,3...N \quad , \quad i = 1 \text{ or } 2 \quad , \quad j = 0,1,2,...$$

Note that the alternating signs of the Dirac delta functions in Eq. (47a) give rise to the factor $(-1)^{i}$ in matrices (60a,c). Since the solution for $\Gamma^{+}_{m}(\xi^{*}_{ij})$ depends on the values $\Gamma^{-}_{m}(\xi^{*}_{ij})$ obtained from the previous region, computations must start from the duct entrance and proceed downstream. The numerical accuracy of this method is dependent on the number of terms N used in matrices (60).

To test the various methods presented in this section a limited exact solution, called the connected region technique, is derived. This technique is used to calculate the temperature and heat transfer results for the first six variations in the stepwise periodic heat transfer coefficient shown in Fig. 1b. This technique is presented in the next section.

V. SOLUTION USING CONNECTED REGION TECHNIQUE

An exact solution to system (7) for $S(\eta,\xi) = 0$, using a connected region technique is now presented for the stepwise periodic heat transfer coefficient. Note that for this study, each individual variation of the external heat transfer coefficient (Biot number), as represented in Fig. 1b, will be referred to as a region. Sequentially, the first region corresponds to the first unfinned region at the duct entrance, the second region corresponds to the first finned region, and so forth. This point is illustrated in Fig. 4. The essence of the connected region technique is to consider the temperature distribution at the exit of each constant Biot number region as the inlet condition for the adjoining downstream region. This method proves to be computationally time consuming beyond the first few regions and is used as a benchmark solution to test the accuracy of the various other schemes.

Energy Eq. (7a) with $S(\eta,\xi) = 0$ is valid in each region with the solutions designated by

$$\theta(\eta,\xi) = \begin{cases} \theta_1(\eta,\xi) & , \quad \xi^*_{1j} < \xi < \xi^*_{2j} \\ \theta_2(\eta,\xi) & , \quad \xi^*_{2j} < \xi < \xi^*_{1,j+1} \end{cases} \tag{61}$$

where ξ^*_{ij} is defined by Eqs. (43). Boundary conditions (7b,c) are also valid in each region with $H(\xi)$ specified by Eq. (42). However, since this solution technique considers each region of constant Biot number connected or matched to the adjoining regions, initial conditions (7d) must be replaced by the following conditions:

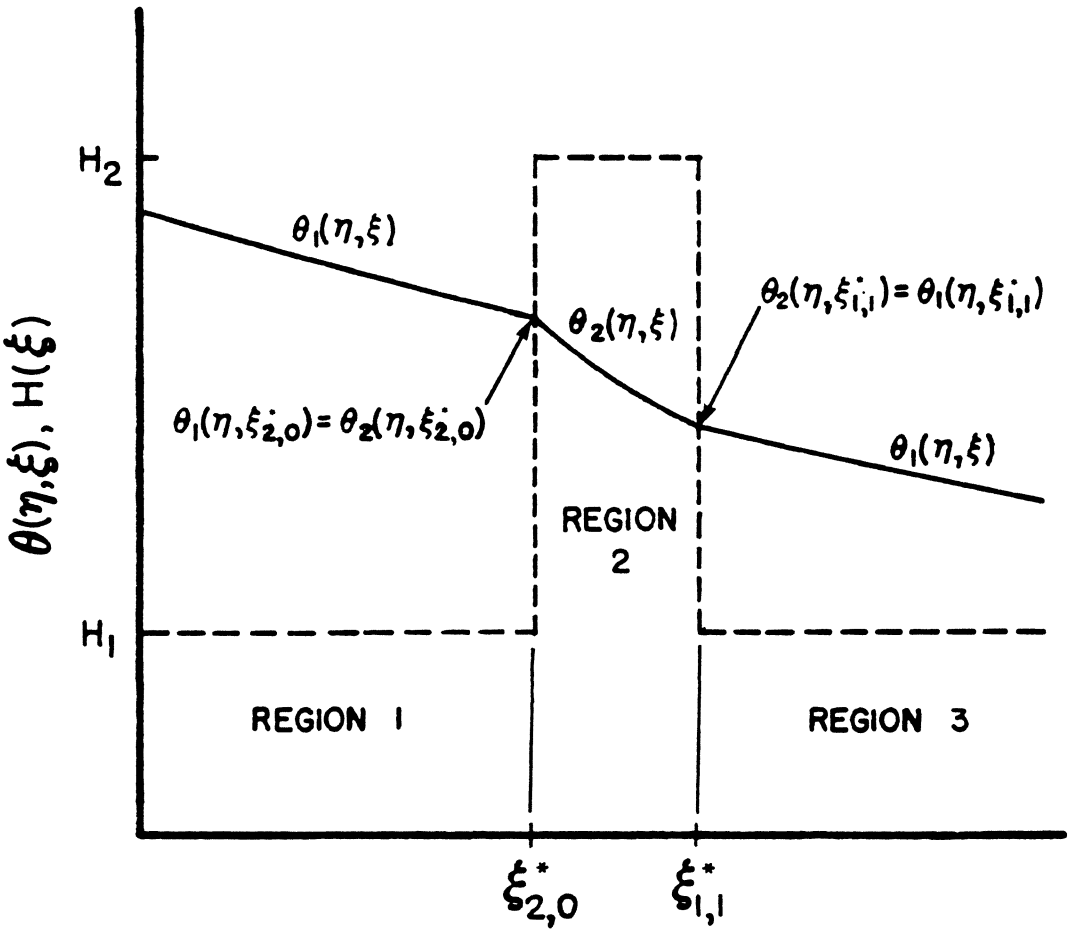

Figure 4 Notation for connected region technique

$$\theta_1(\eta,0) = 1 \quad , \quad \xi = 0 \tag{62a}$$

$$\theta_i(\eta,\xi^*_{ij}) = \theta_{3-i}(\eta,\xi^*_{ij}) \quad , \tag{62b}$$

$$i = 1 \text{ or } 2 \quad , \quad j = 0,1,2,\ldots$$

This relationship is demonstrated in Fig. 4 for the first three regions.

Since each region is considered individually with a constant Biot number, one can construct the following integral transform pairs using the notation of Eqs. (42-45)

$$\text{Transform:} \quad \bar{\theta}_{im}(\xi) = \int_{\eta=0}^{1} \eta^s \frac{v(\eta)}{2} \psi_{im}(\eta)\, \theta_i(\eta,\xi)d\eta \tag{63a}$$

$$\text{Inversion:} \quad \theta_i(\eta,\xi) = \sum_{m=1}^{\infty} \psi_{im}(\eta)\, \bar{\theta}_{im}(\xi) \quad , \tag{63b}$$

$$i = 1 \text{ or } 2 \quad , \quad m = 1,2,\ldots$$

valid for

$$\xi^*_{1j} < \xi < \xi^*_{2j} \quad , \quad \text{when } i = 1$$

$$\xi^*_{2j} < \xi < \xi^*_{1,j+1} \quad , \quad \text{when } i = 2$$

Next, operate on (7a) with

$$\int_{\eta=0}^{1} \eta^s \, \psi_{im}(\eta) d\eta \tag{64}$$

and incorporate the notation in Eq. (61) to obtain

$$\int_{\eta=0}^{1} \eta^s \frac{v(\eta)}{2} \psi_{im}(\eta) \frac{\partial \theta_i}{\partial \xi} d\eta = \int_{\eta=0}^{1} \psi_{im}(\eta) \frac{\partial}{\partial \eta} \eta^s \frac{\partial \theta_i}{\partial \eta} d\eta \ , \tag{65}$$

$$i = 1 \text{ or } 2 \ , \quad m = 1,2,\ldots \ , \quad \xi > 0$$

In contrast to the variable eigenfunction technique presented in the previous section, the eigenfunctions are independent of the axial coordinate ξ and the partial derivative on the LHS of this expression may be brought outside the integral. The RHS of Eq. (65) can be evaluated in the usual manner by integrating by parts twice and utilizing boundary conditions (7b,c) and (9b,c), and Eqs. (9a) and (63a). The result is expressed as

$$\frac{d\bar{\theta}_{im}}{d\xi} + \lambda_{im}^2 \bar{\theta}_{im}(\xi) = 0 \tag{66}$$

The initial conditions required for Eq. (66) comes from transforming the inlet conditions (62a,b) to get

$$\bar{\theta}_{1m}(0) = \frac{H_1 \psi_{1m}(1)}{\lambda_{1m}^2} = B_m \ , \quad \xi = 0 \tag{67a}$$

$$\bar{\theta}_{im}(\xi_{ij}^*) = \int_{\eta=0}^{1} \eta^s \frac{v(\eta)}{2} \psi_{im}(\eta) \theta_{3-i}(\eta, \xi_{ij}^*) d\eta \ , \quad \xi > 0 \ , \tag{67b}$$

$$i = 1 \text{ or } 2 \quad , \quad m = 1,2,\ldots$$

Since the integral on the RHS of condition (67b) has the eigenfunction of one region with a temperature distribution from the previous region, it does not match the definition of the integral transform, Eq. (63a)

Equations (66) and (67) make up a set of ordinary uncoupled differential equations which can readily be solved to get

$$\bar{\theta}_{im}(\xi) = \bar{\theta}_{im}(\xi^*_{ij}) \exp(-\lambda^2_{im}\xi) \tag{68}$$

Application of the inversion formula (63b) provides the temperature distributions

$$\theta_i(\eta,\xi) = \sum_{m=1}^{\infty} \psi_{im}(\eta) \bar{\theta}_{im}(\xi^*_{ij}) \exp(-\lambda^2_{im}\xi) \quad , \tag{69}$$

$$i = 1, 2 \quad , \quad j = 0,1,2$$

Using the transformed inlet condition (67a) in the general solution given by Eq. (69), the temperature distribution in the first unfinned region simply becomes

$$\theta_1(\eta,\xi) = H_1 \sum_{m=1}^{\infty} \frac{\psi_{1m}(1)\ \psi_{1m}(\eta)}{\lambda^2_{1m}} \exp(-\lambda^2_{1m}\xi) \quad , \tag{70}$$

$$\xi^*_{1,0} < \xi < \xi^*_{2,0}$$

The solution for the second region (first finned region) is obtained by using temperature distribution (70) in condition (67b) with

i = 2, j = 0 and substituting the result into Eq. (69). The result is expressed as

$$\theta_2(\eta,\xi) = H_1 \sum_{p=1}^{\infty} \sum_{m=1}^{\infty} \frac{\psi_{1m}(1)}{\lambda_{1m}^2} \exp(-\lambda_{1m}^2 \xi) \int_{\eta=0}^{1} \eta \frac{v(\eta)}{2} \psi_{2p}(\eta)\, \psi_{1m}(\eta) d\eta \tag{71}$$

The following integral relation is now utilized to relate the set of normalized eigenfunctions $\psi_{2p}(\eta)$ and $\psi_{1m}(\eta)$

$$\int_{\eta=0}^{1} \eta^2 \frac{v(\eta)}{2} \psi_{2p}(\eta)\, \psi_{1m}(\eta) d\eta = \frac{H_1 - H_2}{\lambda_{1m}^2 - \lambda_{2p}^2} [\psi_{1m}(1)\, \psi_{2p}(1)] \tag{72}$$

which is valid for all m and p. The proof of this relation is provided in Appendix A.

Using integral relation (72), the dimensionless temperature distribution for the second region becomes

$$\theta_2(\eta,\xi) = H_1(H_1 - H_2) \sum_{p=1}^{\infty} \sum_{m=1}^{\infty} \frac{\psi_{1m}^2(1)}{\lambda_{1m}^2} \frac{\psi_{2p}(1)}{(\lambda_{1m}^2 - \lambda_{2p}^2)} \psi_{2p}(\eta) \cdot \exp[-\lambda_{2p}^2(\xi - \xi_{2,0}^*) - \lambda_{1m}^2 \xi_1] \quad , \quad \xi_{2,0}^* < \xi < \xi_{1,1}^* \tag{73}$$

This temperature distribution contains nested sums, an added complexity over the first region solution of Eq. (70) that contains only one summation. This pattern continues with each new region contributing an additional nested summation; the third region contains three nested summations and so forth. The general equation for the connected region

technique is then

$$\theta_1(\eta,\xi) = H_1(H_1 - H_2)^{N-1} \sum_{m_N=1}^{\infty} \sum_{p_{N-1}=1}^{\infty} \cdots \sum_{p_1=1}^{\infty} \sum_{m_1=1}^{\infty} \frac{\psi_{1m}^2(1)}{\lambda_{1m_1}^2} \frac{\psi_{2p}^2(1)}{(\lambda_{1m_1}^2 - \lambda_{2p_1}^2)}$$

$$\cdots \frac{\psi_{1m_N}(1)\,\psi_{1m_N}(\eta)}{(\lambda_{1m_N}^2 - \lambda_{2p_{N-1}}^2)} \exp[-\lambda_{1m_N}^2(\xi-\xi_{1,N-1}^*) - \cdots - \lambda_{2p_1}^2(\xi_2) - \lambda_{1m_1}^2(\xi_1)] \quad , \tag{74a}$$

$$\xi_{1,N-1}^* < \xi < \xi_{2,N-1}^* \quad , \quad N = 2,3,4,\ldots$$

and

$$\theta_2(\eta,\xi) = H_1(H_1 - H_2)^N \sum_{p_N=1}^{\infty} \sum_{m_N=1}^{\infty} \cdots \sum_{p_1=1}^{\infty} \sum_{m_1=1}^{\infty} \frac{\psi_{1m_1}^2(1)}{\lambda_{1m_1}^2} \cdot \frac{\psi_{2p}^2(1)}{(\lambda_{1m}^2 - \lambda_{2p_1}^2)} \cdots$$

$$\frac{\psi_{2p_N}(1)\,\psi_{2p_N}(\eta)}{(\lambda_{1m_N}^2 - \lambda_{2p_N}^2)} \exp[-\lambda_{2p_N}^2(\xi - \xi_{2,N-1}^*) - \lambda_{1m_N}^2(\xi_1) - \cdots$$

$$- \lambda_{2p_1}^2(\xi_2) - \lambda_{1m_1}^2(\xi_1)] \quad , \tag{74b}$$

$$\xi_{2,N-1}^* < \xi < \xi_{1,N}^* \quad , \quad N = 2,3,4,\ldots$$

where again, ξ_1 represents the interfin spacing and ξ_2 represents the fin thickness.

The summations of Eqs. (74) represent a geometric growth and when the region lengths are small, the decaying exponential terms are not able to make the series converge in a reasonable number of terms. For

purposes of benchmarking the solution methods of the previous section, a program was written to calculate the exact dimensionless wall and bulk temperature distributions, and heat transfer rates for the first six regions at the duct entrance.

VI. RESULTS AND DISCUSSION

Heat transfer results for the stepwise periodic Biot number are now presented. Although the variable eigenfunction technique was developed for an arbitrary variation of the external heat transfer coefficient, the stepwise periodic variation is the most computationally demanding. In addition, the stepwise periodic variation serves as a model for a duct fitted with an array of regularly spaced fins as depicted in Fig. 1.

In the following results, viscous energy dissipation and internal heat sources are neglected by setting $S(\eta,\xi) = 0$ in energy Eq. (7a). Three combinations of conduit geometry and velocity profile are considered: (1) slug flow between parallel plates (slug-plate problem $s = 1$, $v(\eta) = 1$), (2) slug flow inside a tube (Bessel problem $s = 1$, $v(\eta) = 1$) and (3) laminar fully developed flow inside a tube (Graetz problem $s = 1$, $v(\eta) = 2\,(1 - \eta^2)$). The constant velocity profile is useful for low Prandtl number flows where the velocity profile develops much slower than the temperature profile in the entrance region. The laminar velocity profile is more commonly seen in low velocity internal flows where the velocity profile has developed faster than the temperature profile. In general, the solution for the heat transfer results of these three cases is different only in the specific functions generated from the eigenvalue problem (9). These functions are summarized in Table D1. Although the numerical results differ somewhat, the essential features and heat transfer characteristics for all of these cases are similar. Thus, a numerical study of any one of the cases will reveal characteristics displayed by all three. Also, the

case of laminar fully developed flow between parallel plates ($s = 0$, $v(\eta) = 3/2(1 - \eta^2)$) is available from the general analysis, but numerical results are not presented for this case.

The body of the results and discussion is divided into four main parts: (1) an evaluation of the solution methods of Chapters IV and V, (2) a parameter study using the slug plate problem, (3) an evaluation of the influence of the assumed velocity profile on heat transfer, and (4) a comparison of the stepwise periodic Biot number to an approximation using an average Biot number for a specified finned duct.

A. Evaluation of Solution Methods

The solution for each combination of conduit geometry and velocity profile requires the specification of four independent dimensionless parameters ξ_1, ξ_2, H_1 and H_2. For a finned duct, the length ξ_1 represents the interfin spacing, while ξ_2 represents the fin thickness. The low Biot number H_1 represents the external dimensionless heat transfer coefficient for the unfinned areas, while H_2 represents the effective Biot number in finned areas as seen from Eq. (1). These four dimensionless parameters represent a great simplification over the ten independent parameters of the physical system corresponding to the conduit and fin geometry, and the conduit and fluid properties.

A study of tube and fin geometries [79], along with a study of engineering fluids typically used for heat exchange applications suggests that the axial spacings ξ_1 and ξ_2 be of the order $(10)^{-4}$ to $(10)^{-5}$ with ξ_1 from three to seven times larger than ξ_2. For external air flows, the Biot number H_1 can range from 1 to 30+ and H_2 can range

from 10 to 250+ for the cases under study. The results presented in the following sections are based upon numbers from these ranges. For convenience, the evaluation of the solution methods of Chapters IV and V is presented for the slug plate problem since eigenvalue problem Eq. (9) yields trigonometric functions as shown in Table D1.

First, examine the connected region technique, in Eqs. (74), which is an exact solution to the stepwise periodic heat transfer problem as shown in Fig. 1b. Table 1 shows the approximate number of terms needed for Eqs. (74) to converge to four significant figures. The results shown in Table 1 are for $\xi_1 = 0.0003$, $\xi_2 = 0.0001$ and $H_1 = 1$ with $H_2 = 5$ and 50. In each successive region, the overall number of terms required for convergence increases. This is due to the nesting of summation loops in Eqs. (74), which causes a geometric growth in terms for solution convergence for each region. The largest number of terms required in each region is found immediately after a jump in Biot number. This value then decreases downstream until the next Biot number jump, due to the decaying exponential term in Eqs. (74). Thus, as the axial lengths ξ_1 and ξ_2 decrease, the decaying exponential becomes less important and the number of terms for convergence increases. For the case of $H_2 = 50$, the number of terms required for convergence becomes overwhelming in order to accommodate the large jump in the Biot number. In fact, only the first five regions are calculated. The limitations of this method are thus apparent, particularly for small axial lengths and large Biot ratios, since millions of terms are required to provide a solution that covers only a very small portion of the thermally developing section. The connected region technique is

TABLE 1. Number of Terms for Connected Region Technique to Converge Four Significant Figures - Slug Plate Problem.

		Number of Terms	
	Axial Position, ξ	$H_1 = 1$ $H_2 = 5$	$H_1 = 1$, $H_2 = 50$
Region 1	.00005	78	78
	.00015	49	49
	.0003	37	37
Region 2	.00035	1036	1481
	.0004	815	1111
Region 3	.00055	5846	16,625
	.0007	4737	12,477
Region 4	.00075	142,388	635,004
	.0008	118,191	487,925
Region 5	.00095	1,244,981	10,549,781
	.0011	989,374	7,805,263
Region 6	.00115	5,686,545	---
	.0012	4,905,204	---

much more practical for large values of the axial lengths ξ_1 and ξ_2 since the decaying exponential in Eqs. (74) becomes more significant. Despite the extravagant number of computations shown in Table 1, the connected region technique is exact and is used as a benchmark for comparing the other solution methods. Since the number of terms for convergence increases for each new region due to the nesting of summation loops in Eqs. (74), comparisons are made only in the first few regions. Appendix E contains the general computer program implementing the connected region technique for all combinations of velocity profile and duct geometry.

Tables 2 and 3 present the errors associated with the zero and first order approximation, the second iterative approximation, and the stepwise solution, as compared to the exact results from the connected region technique. The results shown in Tables 2 and 3 are for ξ_1 = .0003, ξ_2 = .0001, H_1 = 1 and H_2 = 5 or 50. The numerical results for the evaluation of the various solution methods are presented for the bulk or mixing cup temperature $\theta_b(\xi)$, given by Eq. (27b). As energy is transferred from the fluid to the surroundings, the dimensionless bulk temperature falls from the initial value of 1.0 at the duct inlet to 0 once thermal saturation is reached. The bulk temperature is a relevant quantity and provides a convenient means to evaluate relative error of the solution methods. To maintain a consistent error analysis, all errors presented in Tables 2 and 3 are relative to the inlet bulk temperature of 1.0.

Table 2 shows the case for H_2 = 5. Notice that in the first region the error is zero since all solutions reduce to the exact case. Beyond

TABLE 2. Evaluation of Relative Errors Using Various Solutions for the Slug Plate Problem with Parameters $\xi_1 = .0003$, $\xi_2 = .0001$, $H_1 = 1$ and $H_2 = 5$.

		Connected Region Technique	Zero Order Approximation		First Order Approximation		Second Iterative Approximation		Stepwise Solution	
	Axial Position, ξ	$\theta_b(\xi)$	$\theta_b(\xi)$	Relative Error, %	$\theta_b(\xi)$	Relative Error, %	$\theta_b(\xi)$	Relative Error, %	$\theta_b(\xi)$	Relative Error, %
Region	.0	1.0000	1.0000	0	1.0000	0	1.0000	0	1.0000	0
1	.00015	.9997	.9997	0	.9997	0	.9997	0	.9997	0
H_1=1	.0003	.9994	.9994	0	.9994	0	.9994	0	.9994	0
Region	.0003	.9994	.9822	1.72	1.0344	3.50	1.0378	3.84	.9994	0
2	.00035	.9989	.9819	1.70	1.0339	3.50	1.0375	3.86	.9989	0
H_2=5	.0004	.9985	.9817	1.68	1.0335	3.50	1.0370	3.85	.9985	0
Region	.0004	.9985	.9992	.07	.9989	.04	.9988	.03	.9985	0
3	.00055	.9982	.9987	.05	.9986	.04	.9986	.04	.9982	0
H_1=1	.0007	.9979	.9984	.05	.9983	.04	.9983	.04	.9979	0
Region	.0007	.9979	.9809	1.70	1.0327	3.48	1.0363	3.84	.9979	0
4	.00075	.9975	.9806	1.69	1.0323	3.48	1.0359	3.84	.9975	0
H_2=5	.0008	.9970	.9804	1.66	1.0312	3.42	1.0354	3.84	.9970	0
Region	.0008	.9970	.9982	.12	.9979	.09	.9979	.09	.9970	0
5	.00095	.9967	.9978	.11	.9976	.09	.9977	.10	.9968	.01
H_1=1	.0011	.9965	.9975	.10	.9973	.08	.9974	.09	.9965	0
Region	.0011	.9965	.9795	1.70	1.0311	3.46	1.0349	3.84	.9965	0
6	.00115	.9960	.9793	1.67	1.0307	3.47	1.0345	3.85	.9960	0
H_2=5	.0012	.9956	.9791	1.65	1.0303	3.47	1.0341	3.85	.9956	0

TABLE 3. Evaluation of Relative Errors Using Various Solutions for the Slug Plate Problem with Parameters $\xi_1 = .0003$, $\xi_2 = .0001$, $H_1 = 1$ and $H_2 = 50$

		Connected Region Technique	Zero Order Approximation		First Order Approximation		Second Iterative Approximation		Stepwise Solution	
	Axial Position, ξ	$\theta_b(\xi)$	$\theta_b(\xi)$	Relative Error, %	$\theta_b(\xi)$	Relative Error, %	$\theta_b(\xi)$	Relative Error, %	$\theta_b(\xi)$	Relative Error, %
Region	0	1.0000	1.0000	0	1.0000	0	1.0000	0	1.0000	0
1	.00015	.9997	.9997	0	.9997	0	.9997	0	.9997	0
H_1=1	.0003	.9994	.9994	0	.9994	0	.9994	0	.9994	0
Region	.0003	.9994	.9449	5.45	1.0637	6.43	1.0812	8.18	.9988	.06
2	.00035	.9959	.9445	5.14	1.0618	6.59	1.0788	8.29	.9954	.05
H_2=50	.0004	.9931	.9441	4.90	1.0602	6.71	1.0767	8.36	.9927	.04
Region	.0004	.9931	.9992	.61	.9986	.55	.9986	.55	.9936	.05
3	.00055	.9929	.9986	.57	.9984	.55	.9984	.55	.9933	.04
H_1=1	.0007	.9927	.9983	.56	.9981	.54	.9980	.55	.9931	.04
Region	.0007	.9927	.9430	4.97	1.0601	6.74	1.0777	8.50	.9920	.07
4	.00075	.9896	.9426	4.70	1.0583	6.87	1.0754	8.58	.9890	.06
H_2=50	.0008	.9872	.9422	4.50	1.0568	6.96	1.0735	8.63	.9867	.05
Region	.0008	.9872	.9981	1.09	.9973	1.01	.9975	1.03	.9880	.08
5	.00095	.9870	.9975	1.05	.9970	1.00	.9972	1.02	.9878	.08
H_1=1	.0011	.9868	.9972	1.04	.9968	1.00	.9970	1.02	.9876	.08
Region	.0011	--	.9412	--	1.0570	--	1.0757	--	.9860	--
6	.00115	--	.9408	--	1.0553	--	1.0734	--	.9833	--
H_2=50	.0012	--	.9405	--	1.0538	--	1.0715	--	.9812	--

the first region, errors appear in the bulk temperatures for all but the stepwise solution. In general, the low Biot regions H_1, have smaller errors than the high Biot regions H_2, by a factor of 20 to 100 times. This can best be seen by noting the error in converging the bulk temperature at a Biot number jump as seen in Tables 2 and 3. When converging from the H_1 side, the error is much lower than when converging from the H_2 side. This demonstrates the numerical difficulties associated with a step change in Biot number. In reality, the results at a Biot number jump should be identical when converged from either side, as is seen in the bulk temperature results for the connected region technique and stepwise solution.

The zero order approximation, as calculated from Eq. (32) with $\bar{S}_m(\xi) = 0$, represents the easiest and fastest method to determine the temperature transforms, $\bar{\theta}_m(\xi)$. The largest error found in Table 2 using this method is 1.72% which occurs at the beginning of the second region. The error then begins to drop slightly in each region due to the decaying exponential term. These results are within acceptable engineering accuracy.

To hopefully improve upon the zero order approximation, the first order approximation adds in the effects of the first coefficient $A_{m1}(\xi)$ in the determination of the temperature transform, $\bar{\theta}_m(\xi)$, as seen in Eqs. (33) and (34). The error in the H_1 regions is on the average about 20% lower than that for the zero order approximation, while the error in the H_2 regions is about 50% higher. This trend is surprising because the first order approximation is expected to be a better approximation than the zero order. Looking at the numerical values for the bulk

temperature of the zero order approximation, one can see that the H_1 regions overshoot the exact results, while the H_2 regions undershoot the exact results. The addition of the $A_{m1}(\xi)$ coefficient is meant to correct these trends. Yet, where the coefficient improves on the H_1 region, it overcompensates on the H_2 region, creating a larger error.

The second iterative approximation is used to calculate the temperature transforms, $\bar{\theta}_m(\xi)$, from Eq. (41) with $\bar{S}_m(\xi) = 0$. Overall, the results in Table 2 show that the first order and second iterative approximations are essentially similar. The only difference is that the error of the H_2 regions is roughly 10% higher for the second iterative approximation. Both solutions predict values of the bulk temperature greater than 1.0 in the first few regions of constant H_2, which is physically impossible.

The final method studied is the stepwise solution. The transforms, $\bar{\theta}_m(\xi)$, required in Eq. (27b) are available for the stepwise periodic case from Eq. (48) with $\bar{S}_m(\xi) = 0$. The values $\Gamma_m^+(\xi_{ij}^*)$ are obtained from matrix Eq. (59a). The stepwise solution is a formally exact solution, while the others are approximate. However, in order to calculate the coefficients $\Gamma_m^+(\xi_{ij}^*)$ exactly, matrix Eq. (59a) must contain an infinite number of elements. The numerical accuracy of the solution thus depends upon the order of the matrix used for the computations. Table 2 demonstrates that the results are numerically exact for the case $H_2 = 5$ when a matrix size of 100 elements is used.

In Table 3, we see that the level of the high Biot number is increased to $H_2 = 50$. Due to the increased number of terms required for convergence in the connected region technique as shown in Table 1, only

the first five regions are calculated. The main point to be noticed is the marked increase in the level of error associated with all the solution methods. However, the stepwise solution still gives only a negligible error for matrix Eq. (59a) taken with 100 elements.

In conclusion, the zero order approximation provides a computationally fast and easy solution to predict the bulk temperatures with a maximum error of 5.5% for the ratio $H_2/H_1 = 50$. This is within the range of engineering approximation, but is not overall a satisfactory solution. The first order approximation represents a computationally more difficult higher order solution over the zero order approximation. However, this approximation results in greater errors in the H_2 regions with only minor improvement in the H_1 regions. To improve the accuracy, higher order approximations above the first order must be utilized. For a continuously variable heat transfer coefficient, these higher order approximations would not be difficult to implement. However, for a discontinuous stepwise periodic heat transfer coefficient these higher order approximations become computationally extravagant. The second iterative approximation provides the poorest results of the solutions evaluated, and is computationally the most difficult scheme to implement. Further iteration is required for higher accuracy, yet the drastic increase in computational difficulty for higher iterations makes this an undesirable solution method for any variable heat transfer coefficient problem. The stepwise solution is by far the most accurate method and is easier to implement than all but the zero order approximation. The matrix of Eq. (59a) taken with 100 elements provides extremely accurate results, even for the computationally demanding case

with a Biot number ratio of 50 to 1 shown in Table 3. In addition, since the inlet region has the largest rates of heat transfer, errors found here by the stepwise solution are expected to be the largest, while further downstream these errors are expected to diminish. From this point, all results are provided by the stepwise solution for a matirx size of 100 elements.

B. Parameter Study

Presented in this section is a parameter study displaying the effects of the four dimensionless independent variables ξ_1, ξ_2, H_1 and H_2. Again for convenience, the slug plate problem will be used. Due to the similar nature of the essential features and heat transfer characteristics, the trends presented here are characteristic of all the combinations of duct geometry and velocity profile.

Graphical results for the parameter study are presented for the total heat transfer, $Q(\xi)$, given in Eq. (29). The dimensionless quantity $Q(\xi)$ represents the total energy transferred from the fluid up to some axial location, ξ, divided by the total energy transferred at a condition of thermal saturation. Regardless of the axial variation or magnitude of the Biot number, $H(\xi)$, a state of thermal saturation will eventually be reached at sufficiently large ξ as the fluid temperature approaches the external environment temperature. The only exception is the uninteresting case of $H(\xi) = 0$, for which the fluid remains at the inlet temperature. Since the periodic stepwise Biot number serves as a model for a duct fitted with an array of external fins, the quantity $Q(\xi)$ is a meaningful way to display the advantages of heat

transfer enhancement due to finning. The axial parameters for ξ_1 and ξ_2 were chosen of the order $(10)^{-3}$ for graphical presentability.

Figs. 5 through 9 show the total heat transfer, $Q(\xi)$, plotted as a function of axial distance ξ. Note that the discontinuous variation of the external heat transfer coefficient causes the step-like nature shown in Figs. 5-9. The total heat transfer rises at a high rate in regions of large Biot number, and rises at a smaller rate in regions of diminished Biot number. This discontinuous variation, $H(\xi)$, makes purely numerical schemes quite demanding [5] and is one reason that standard analytical techniques fail when applied to this problem. Due to the log-log scale used in these Figures, the axial steps become compressed and thus all curves have been smoothed out for large values of ξ.

Figure 5 displays the results for a constant H_1, along with the effect of heat transfer enhancement due to larger values of H_2. The results are identical until the first change in Biot number is encountered at $\xi = .003$. From this point, the effect of the enhanced heat exchange causes the total heat transfer to rise sharply, with the larger value of H_2 giving the steeper rise. The enhancement is most significant in the inlet region, with effects diminishing downstream as all curves approach thermal saturation.

Figure 6 helps to put these results in perspective. Here is displayed the same results as in Fig. 5, except that all values of the Biot number have been divided by a factor of 5. Although the results of Figs. 5 and 6 are qualitatively similar, the effect of enhanced heat

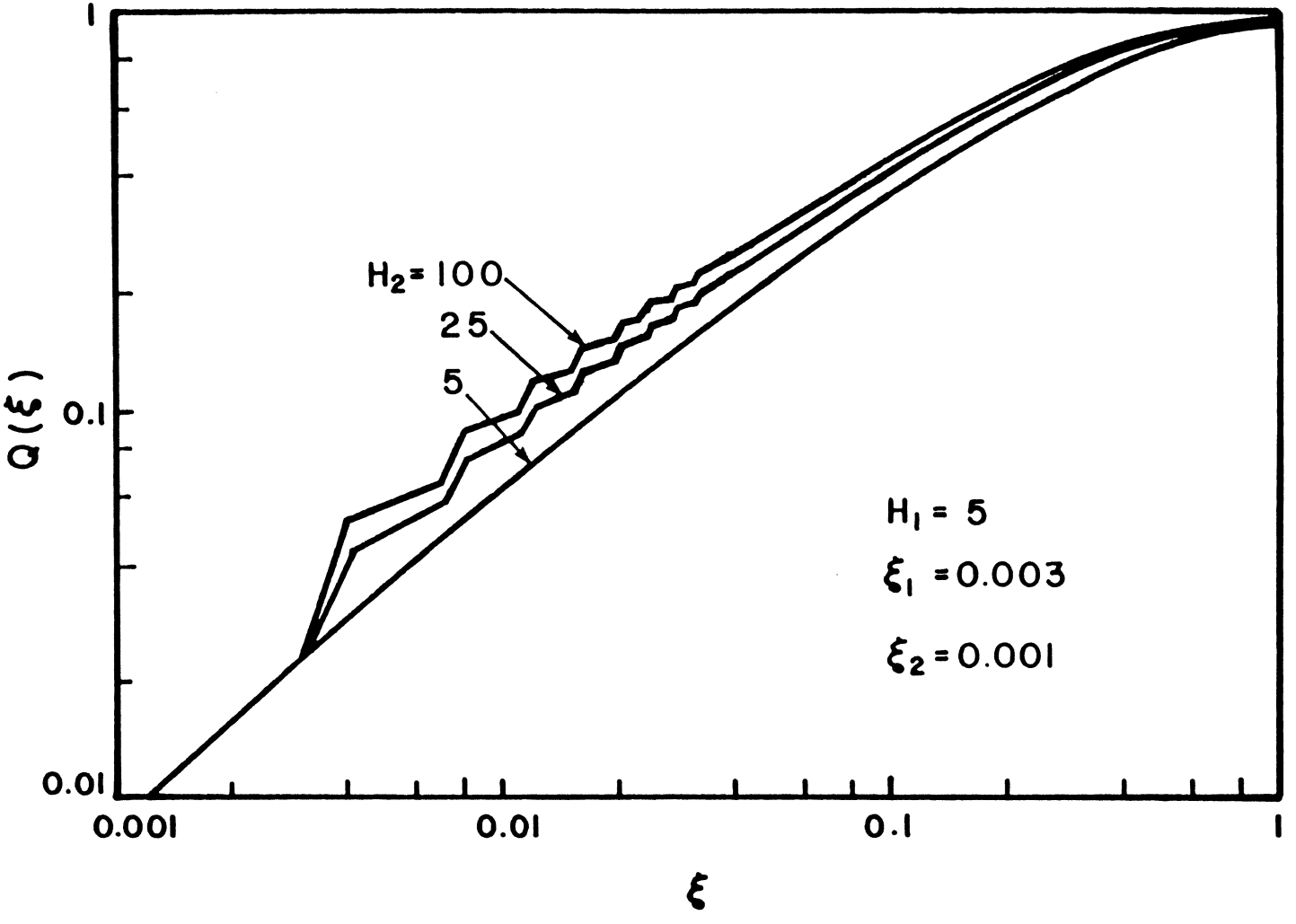

Figure 5 Effect of H_2 on heat transfer (medium value of H_1) for the slug plate problem

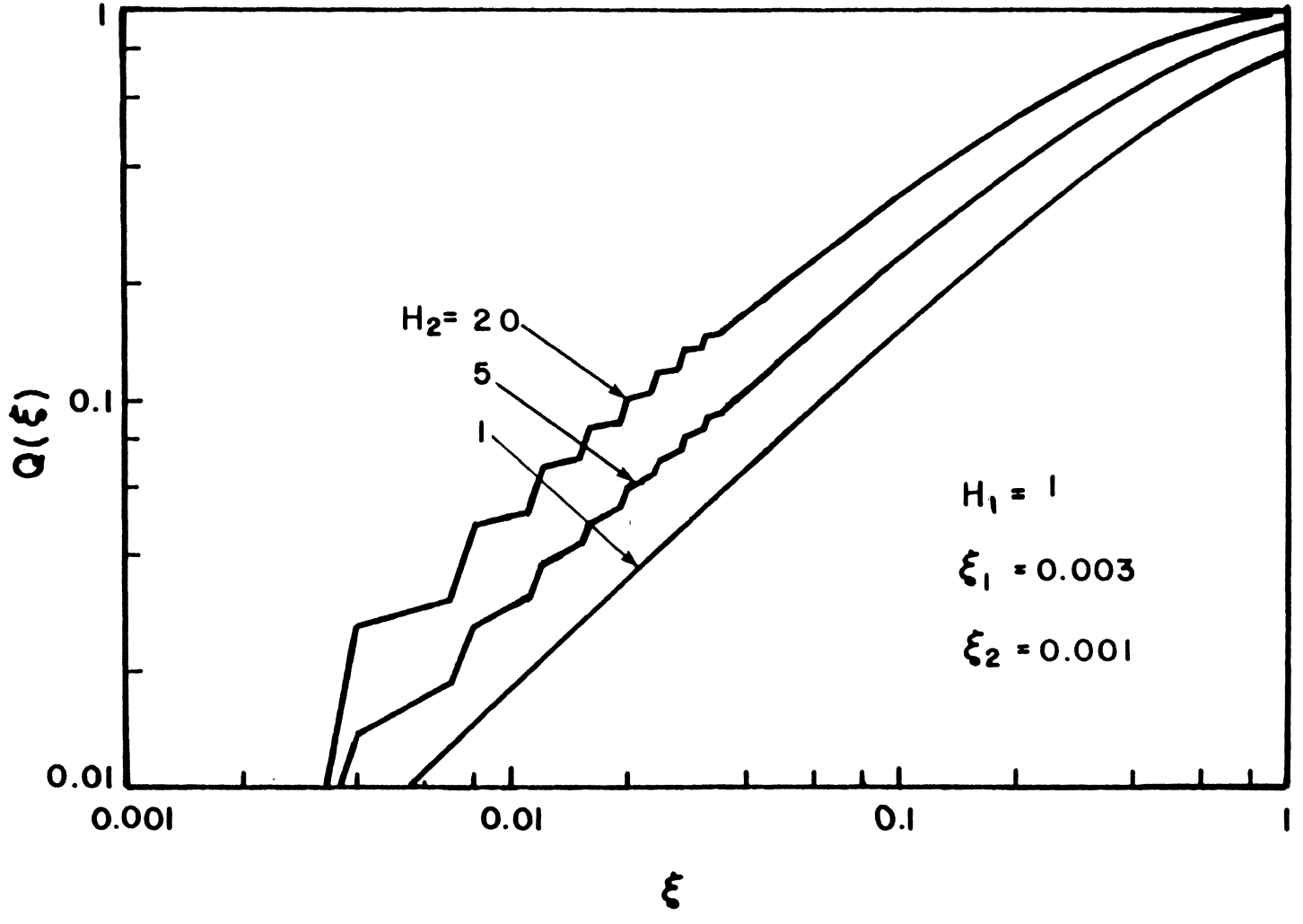

Figure 6 Effect of H_2 on total heat transfer (low value of H_1) of the slug plate problem

transfer is more pronounced when the overall level of the Biot number is decreased, particularly in the inlet region. This effect is further investigated in Fig. 7, where the Biot number ratio is fixed at H_2/H_1 = 10 while the overall level changes. In using a log-log scale, certain subtle points become hidden. The enhancement at ξ = .004 for H_1 = 1 is 18% greater than for H_1 = 25. This means that the lower values of H_1 and H_2 actually provide better heat transfer enhancement than higher values of H_1 and H_2, as long as the ratio H_2/H_1 remains constant. In addition, at ξ = .004 the heat transfer enhancement for the H_1 = 1 curve shown in Fig. 7 is 155% greater than for the corresponding unfinned duct case of $H_1 = H_2 = 1$. However, for the H_1 = 25 curve, the enhancement at ξ = .004 is only 14% greater than for the corresponding unfinned duct case of $H_1 = H_2 = 25$. These results demonstrate that finning is far more efficient for lower values of H_1. The reason for this is because the internal resistance to heat flow is the controlling factor once the external resistance becomes quite low. Therefore, the efficiency of a finned duct is higher in a low heat transfer coefficient environment where enhanced heat transfer becomes important. Thus, an externally finned duct in a high heat transfer environment might not provide appreciable enhancement over an unfinned duct. In such a case, other enhancement methods such as internal finning, may be required.

We now examine the effect of interfin spacing in Fig. 8. Shown here are the results for ξ_1 = .001, 0.005, and ∞ while the other parameters remain constant. The case where $\xi_1 \to \infty$ is equivalent to the constant Biot number case $H_1 = H_2 = 5$. Figure 8 shows that the small values of ξ_1 give the greatest enhancement since the proportion of duct

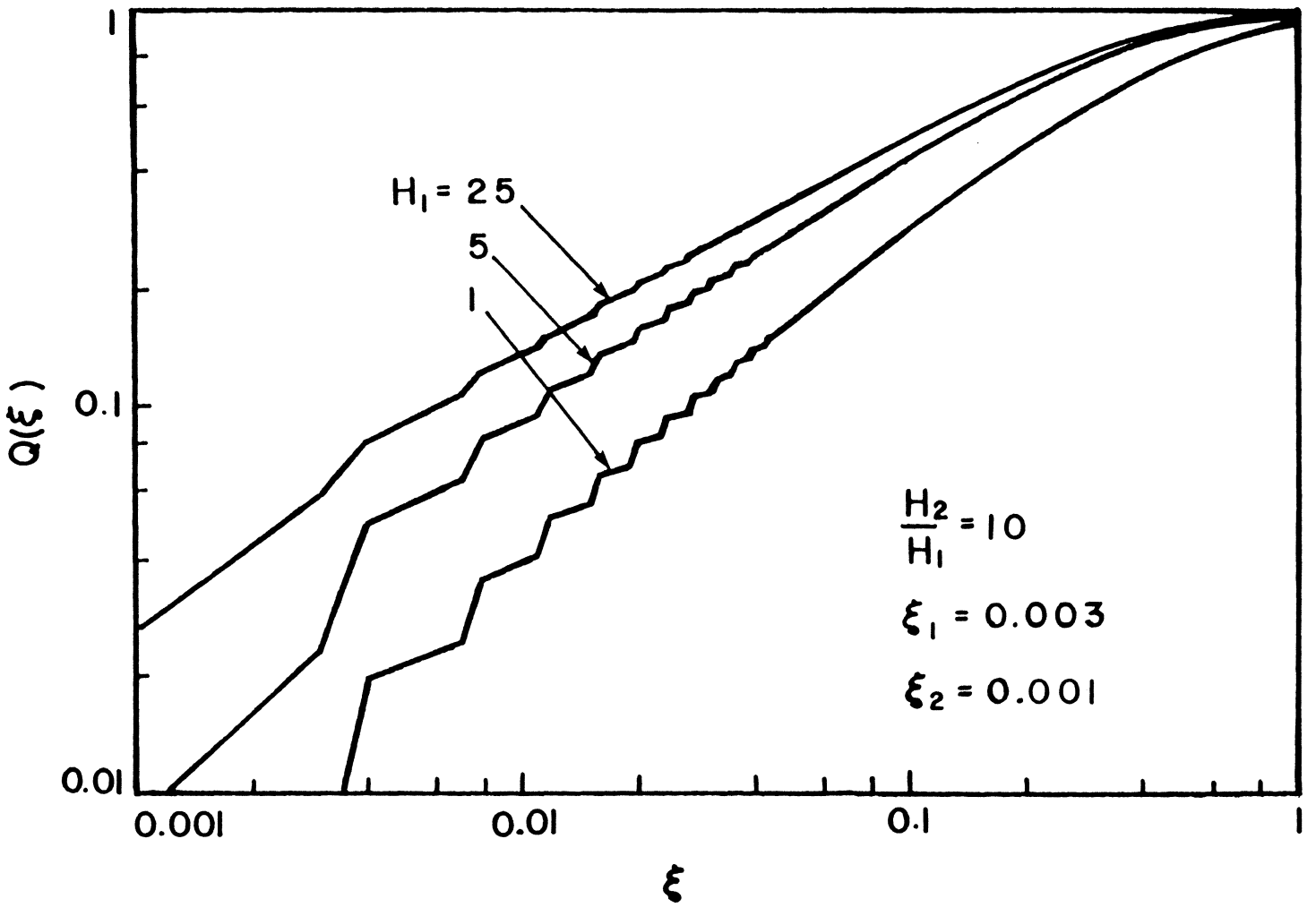

Figure 7 Effect of the overall Biot number level on total heat transfer of the slug plate problem

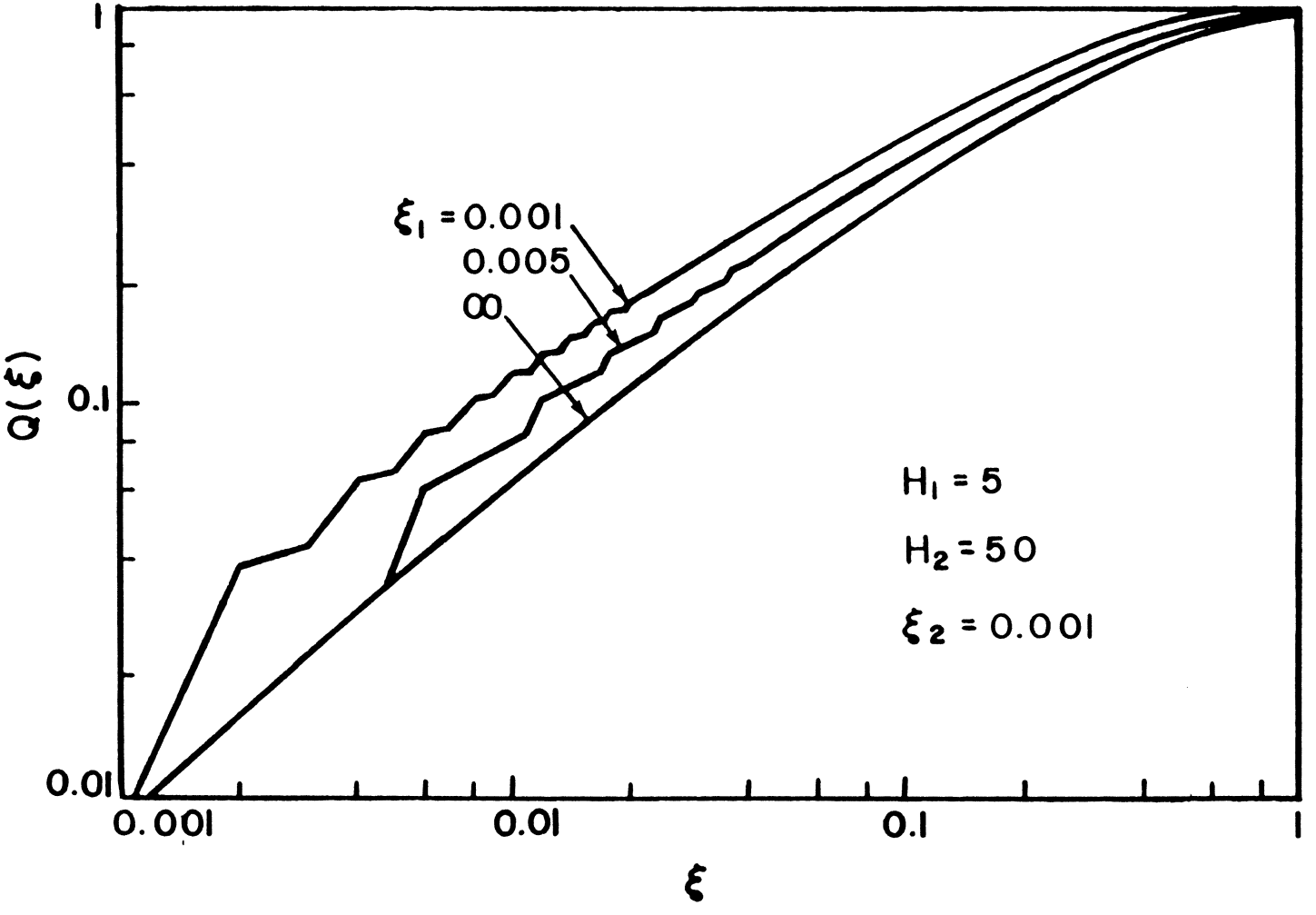

Figure 8 Effect of ξ_1 (interfin spacing) on total heat transfer of the slug plate problem

without fins is reduced. Again, the effects are most pronounced in the duct entrance with all curves approaching thermal saturation further downstream.

Additional insight into geometric effects is gained from Fig. 9. Here the ratio $\xi_1/\xi_2 = 3$ remains fixed while the frequency of low and high Biot number cycles is changed. The case where $\xi_1 = 0.03$ represents a relatively large spacing or low frequency, where a value of $Q = 0.15$ at $\xi = \xi_1 = 0.03$ is reached before any heat transfer augmentation is encountered. The curves for $\xi_1 = 0.003$ and 0.0003 show that a small increase in heat transfer occurs with a higher frequency of fins once the first region of higher Biot number or first fin is encountered. This means that for a constant ratio ξ_1/ξ_2, the frequency of fins can be increased by 10 times, but only a relatively small increase in total heat transfer is gained. However, for small finned and unfinned lengths, much larger heat transfer rates in the duct entrance are initially achieved. In general, whether the heat transfer is enhanced frequently over small intervals or infrequently over longer intervals yields similar heat transfer characteristics at points sufficiently far downstream. A more effective means to increase heat transfer is to make the ratio ξ_1/ξ_2 smaller, as seen in Fig. 8.

To summarize, the most effective fin to unfinned spacing to maximize heat transfer is one where both ξ_1 and ξ_2 are small while maintaining a small ratio ξ_1/ξ_2. In addition, it is desirable to have a high heat transfer coefficient H_2 as shown in Figs. 5 and 6. For heat exchange, a large value for H_1 is preferred, yet as shown in Figs. 5 and 6 a smaller H_1 provides more opportunity for heat transfer enhancement by finning.

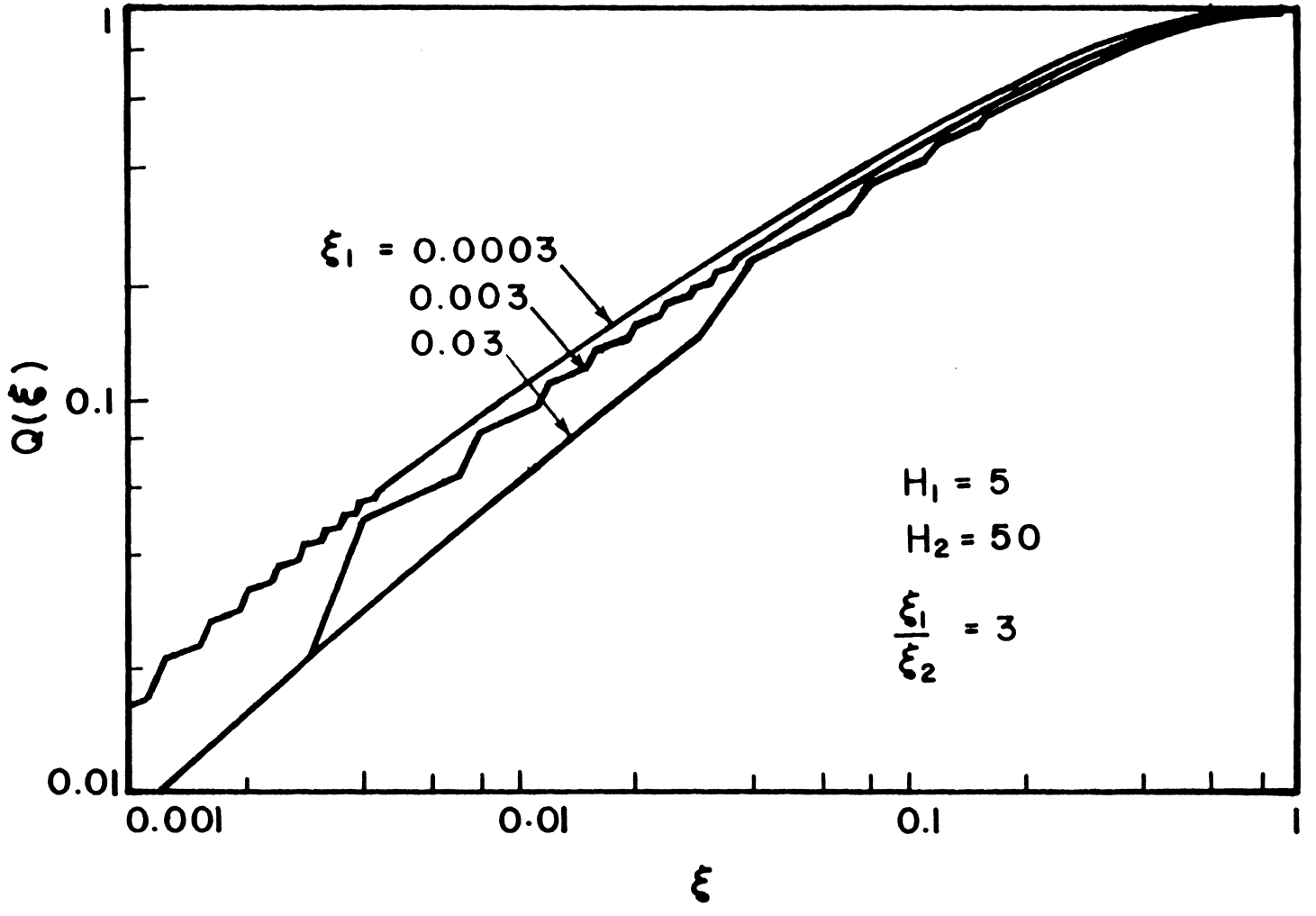

Figure 9 Effect of cycle frequency on total heat transfer of the slug plate problem

C. Influcence of Velocity Profile

This section investigates the influence of the assumed velocity profile on heat transfer by comparing the slug flow in a tube (Bessel problem) with fully developed laminar flow in a tube (Graetz problem). Again all results are obtained using the stepwise solution.

In order to solve Eq. (48) to provide the temperature transforms, $\bar{\theta}_m(\xi)$, required in Eqs. (27b) and (29), one must determine the appropriate eigenvalues and eigenfunctions that satisfy the eigenvalue problem (9), as well as the normalization integral Eq. (12). Table D1 provides the forms of these functions for the cases under study. The calculation of Bessel functions can easily be accomplished by recurance relations such as utilized in the IMSL subroutine MMBSJN. However, the calculation of the Graetz functions is more difficult since no one mathematical relationship will accurately solve for a large number of eigenvalues. Instead, two techniques must be applied. The confluent hypergeometric functions presented in Appendix C, Eqs. (108) and (107), provide exact results for small eigenvalues and eigenfunctions, respectively. Calculation of the normalization integral is performed by numerical integration using Simpson's rule. Only the first 15 eigenvalues are resolvable using confluent hypergeometric functions. Lauwerier's asymptotic solution, presented in Appendix C provides an asymptotic solution that will give accurate results for the larger eigenvalues and eigenfunctions. The normalization integral can be found by using Eq. (112) in Appendix C. Together, these two techniques provide numerically exact values for the Graetz functions over the entire range of eigenvalues required. Appendix E contains the computer program

used to calculate the Graetz functions, eigenvalues and normalization integrals.

The errors resulting from use of the stepwise solution are presented in Table 4 for a computationally difficult case for the Bessel and Graetz problems. The full discussion of error associated with this method has already been discussed. However, it is interesting to note that the error for the Graetz case is much lower than for the Bessel case, even though the Graetz functions are harder to calculate. The primary reason is that the Graetz eigenvalues are larger, which in turn make the decaying exponentials in the temperature transforms smaller. Thus, fewer terms are required to converge the series solution of Eq. (27b) so that the matrix of Eq. (59a) containing 100 elements will be more accurate.

Figures 10-13 compare the heat transfer characteristics for slug and fully developed flow in a tube. In each figure, the dotted line refers to the Bessel problem (slug flow in a tube) and the solid lines to the Graetz problem (fully developed flow in a tube). Note that the step-like nature of the graphs as seen in Figs. 5-9 are smoothed by passing a curve through the $Q(\xi)$ values at the successive midpoints of the unfinned section ξ_1. This is illustrated by the lower Graetz curve in Fig. 10 where a portion of the step-like behavior is shown. From this point, only the smoothed curves will be considered.

Figure 10 displays the results for a fixed H_1, while the value of H_2 varies for both the Bessel and Graetz problems. The enhancement is most significant for a change in H_2 for the Bessel case. The enhancement between the Bessel cases at $\xi = .0011$ is about 62% while the

TABLE 4. Evaluation of Relative Error Between Connected Region Technique and Stepwise Solution for the Bessel and Graetz Problem with Parameters, $\xi_1 = .0003$, $\xi_2 = .0001$, $H_1 = 1$ and $H_2 = 50$.

		Bessel Problem			Graetz Problem		
		Connected Region Technique	Stepwise Solution		Connected Region Technique	Stepwise Solution	
	Axial Position, ξ	$\theta_b(\xi)$	$\theta_b(\xi)$	Relative Error, %	$\theta_b(\xi)$	$\theta_b(\xi)$	Relative Error, %
Region	0	1.0000	1.0000	0	1.0000	1.0000	0
1	.00015	.9994	.9994	0	.9994	.9994	0
H_1=1	.0003	.9988	.9988	0	.9989	.9989	0
Region	.0003	.9988	.9970	.18	.9989	.9986	.03
2	.00035	.9918	.9904	.14	.9955	.9953	.02
H_2=50	.0004	.9863	.9853	.10	.9931	.9930	.01
Region	.0004	.9863	.9877	.14	.9931	.9933	.02
3	.00055	.9858	.9873	.15	.9927	.9929	.02
H_1=1	.0007	.9853	.9868	.15	.9922	.9924	.02
Region	.0007	.9853	.9838	.15	.9922	.9919	.03
4	.00075	.9795	.9781	.14	.9897	.9891	.06
H_2=50	.0008	.9747	.9736	.11	.9875	.9870	.05
Region	.0008	.9747	.9771	.24	.9875	.9876	.01
5	.00095	.9740	.9767	.27	.9868	.9869	.01
H_1=1	.0011	.9736	.9763	.27	.9864	.9867	.03

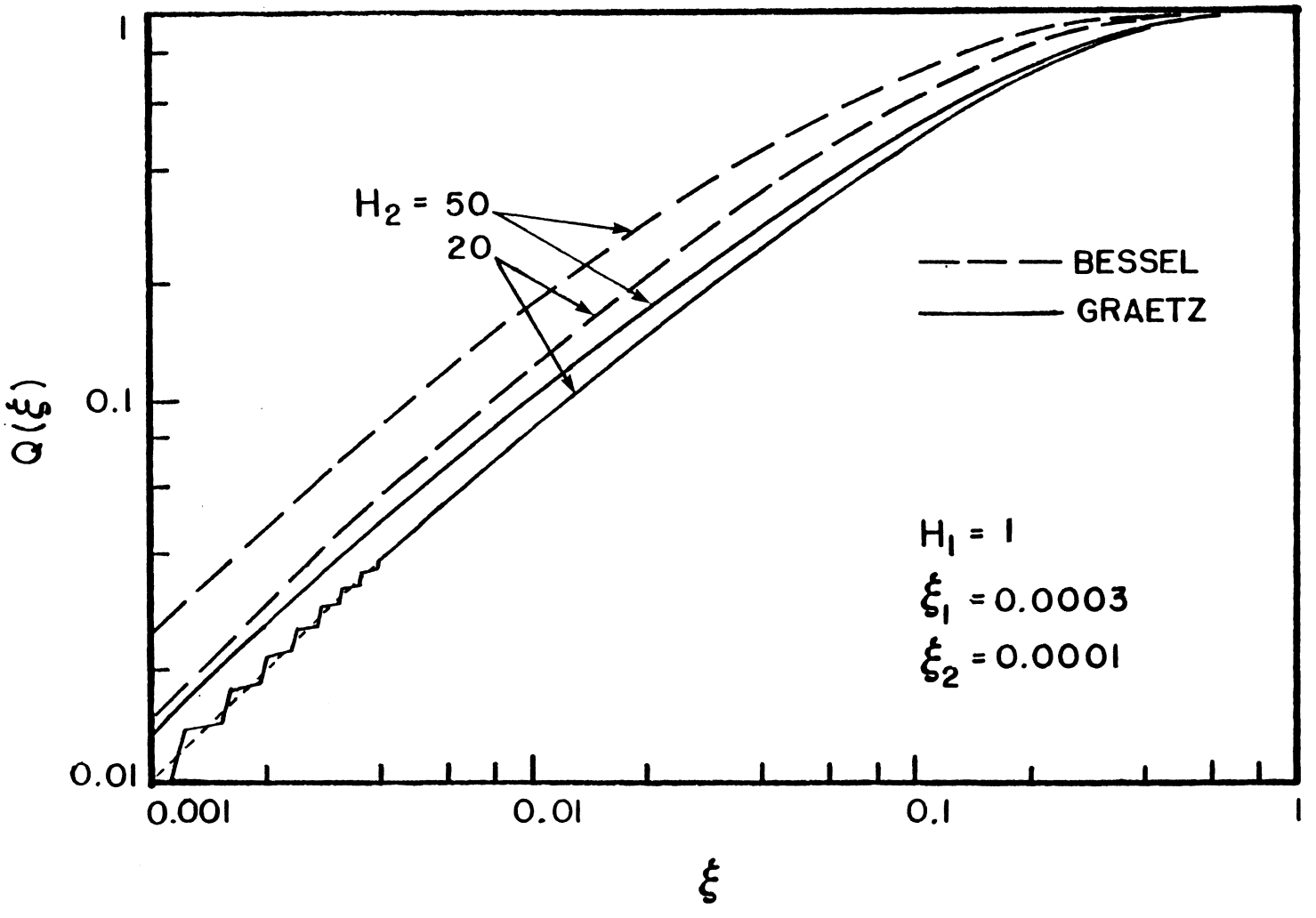

Figure 10 Effect of H_2 on total heat transfer of the Bessel and Graetz problem

enhancement between the Graetz cases at $\xi = .0011$ is about 27%. The greater heat transfer between the Bessel cases as well as the overall increased heat transfer level over the corresponding Graetz cases, is due to the greater velocity near the tube wall. The larger velocity in the region of the tube wall for the Bessel problem effectively lowers the internal resistance to heat flow. As pointed out in the parameter study, as the external resistance becomes quite low, the internal resistance to heat flow becomes the controlling factor. Yet as shown in Fig. 10, by reducing the internal resistance, greater heat transfer can be achieved at both higher and lower external resistances. The two Graetz cases presented in Fig. 10 are cases used by Charmchi and Sparrow [5] and are indistinguishable from the curves show in Ref. [5].

In Fig. 11, the Biot number ratio is fixed at $H_2/H_1 = 10$ while the overall level of the Biot number H_1 is changed. Again notice the pronounced heat transfer enhancement for the Bessel case compared to the Graetz cases. At the low value of $H_1 = 1$, the slope of the Bessel case rises sharper than that of the Graetz case, again due to the lower internal resistance to heat flow associated with the constant velocity profile. Considering the two Bessel curves, the heat transfer in the inlet region increases by a factor of 8 time for the significant jump of $H_1 = 1$ to $H_1 = 25$. For the Graetz curves, this increase is only by a factor of 4.3 times. The milder increase in heat transfer for the Graetz case demonstrates the significance of the tube side (internal) resistance. The results of Figs. 10 and 11 demonstrate that in environments containing a high heat transfer coefficient, finning is more effective for the Bessel case.

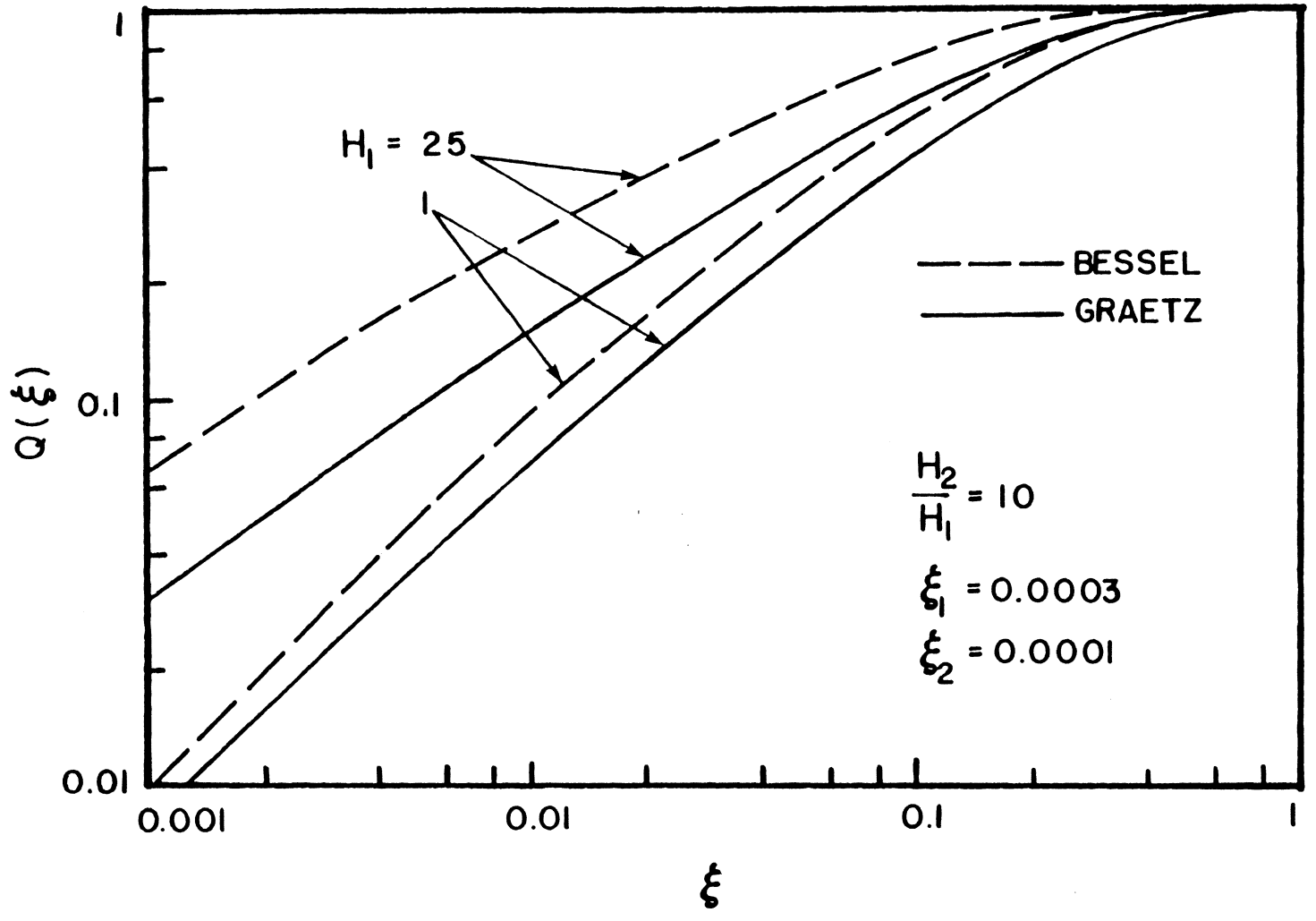

Figure 11 Effect of the overall Biot number level on total heat transfer of the Bessel and Graetz problem

Changes in the geometrical aspects are considered in Figs. 12 and 13. Figure 12 examines the effect of interfin spacing ξ_1, on the total heat transfer for the Bessel and Graetz cases. Here the value for ξ_1 varies while the other parameters remain constant. The slope for the total heat transfer of the Bessel case is greater than that for the Graetz cases, thus signifying better prospects for enhanced heat transfer. This is evident in the cross over at $\xi = .003$ of the upper curve for the Graetz case and of the lower curve for the Bessel case. In the inlet region, the increase in heat transfer between the Bessel cases jumps by a factor of 3.0 times compared to 1.6 times by the Graetz cases. Overall, the Bessel cases can be seen as more responsive to a decrease in interfin spacing. Intuitively any case that offers a lower internal resistance to heat flow would make better use of extra finning.

In Fig. 13 the frequency of low and high Biot cycles is changed as the ratio $\xi_1/\xi_2 = 3$ remains constant. The case $\xi = .003$ represents the case of lower fin frequency. The effect on heat transfer by increasing fin frequency is more pronounced between the Bessel curves than for the Graetz curves. This point is best seen by noticing that the lower Bessel curve rises so drastically as to overcome the upper Graetz curve at $\xi = .005$. Again, the lower internal resistance to heat flow by the Bessel case is the cause of these trends.

Therefore, of the two velocity profiles studied, the largest total heat transfer rate in a tube can be achieved with a constant velocity profile, as would be seen in the flow of a liquid metal. Increasing the overall level of the Biot numbers H_1 and H_2, and decreasing the interfin spacing takes further advantage of the low internal resistance of the Bessel problem in enhancing heat transfer.

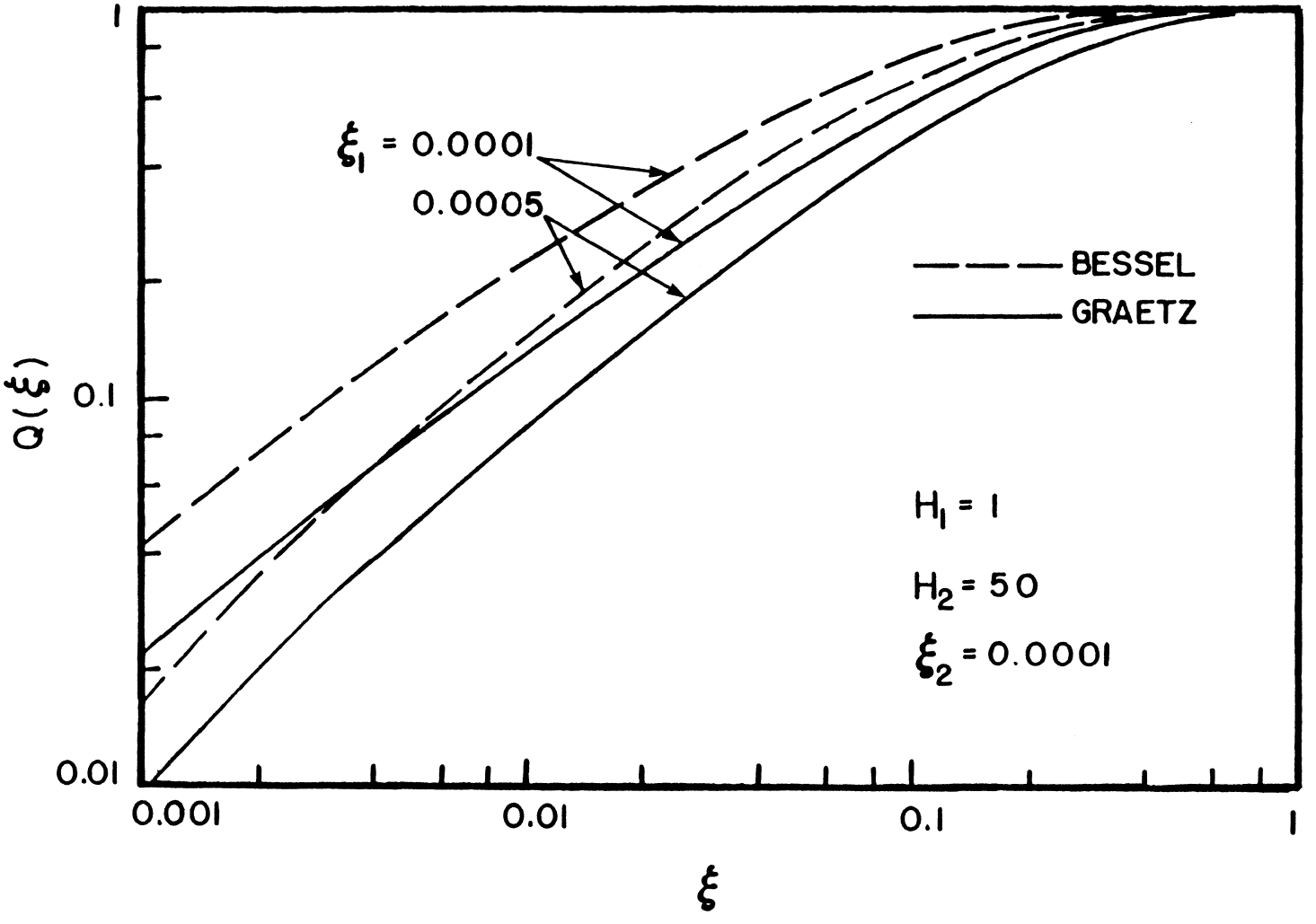

Figure 12 Effect of ξ_1 (interfin spacing) on total heat transfer of the Bessel and Graetz problem

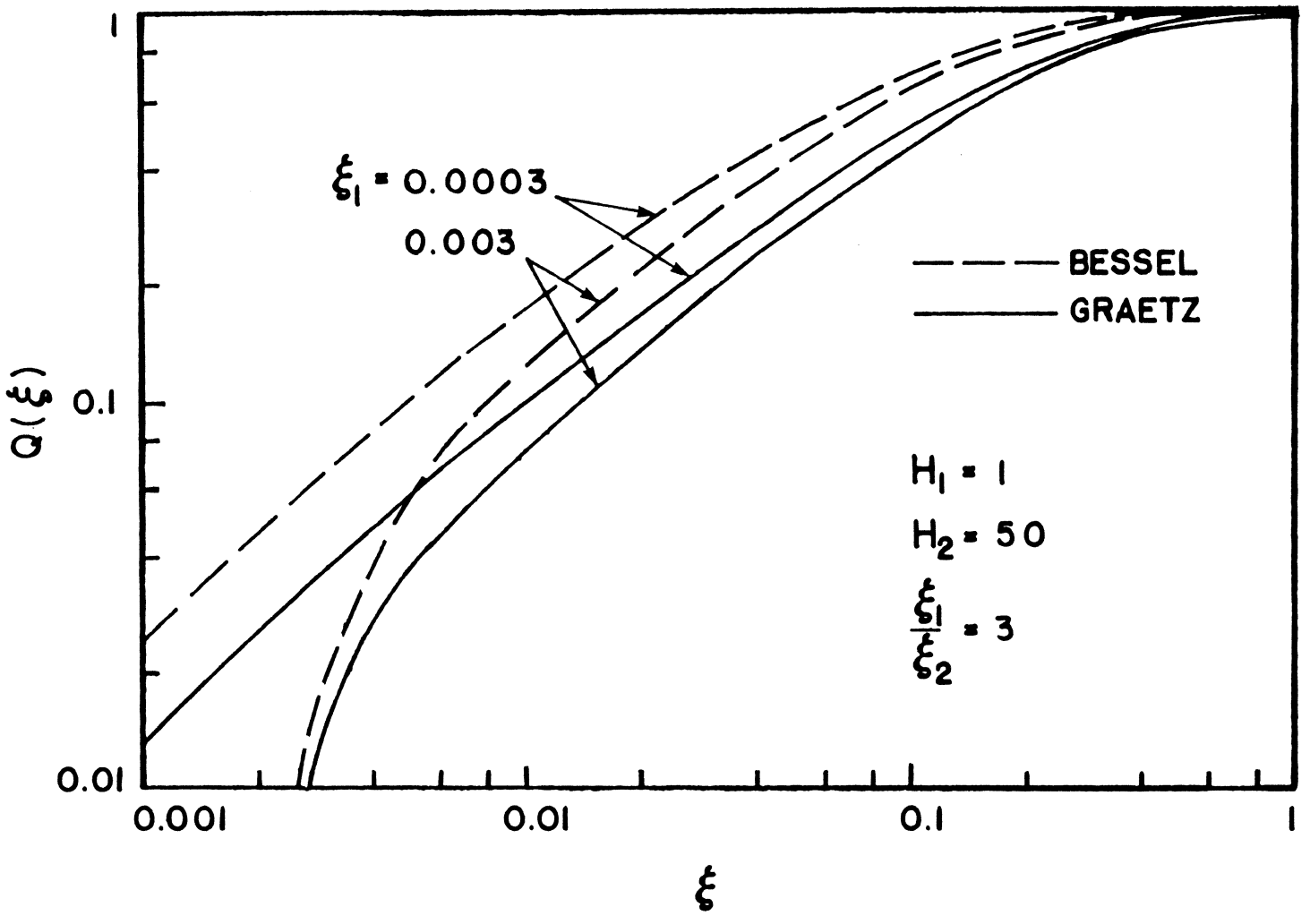

Figure 13 Effect of cycle frequency on total heat transfer of the Bessel and Graetz problem

D. Average Biot Number Approximation

The classical method for analysis of heat transfer rates from a finned duct is to reduce the problem to a corresponding unfinned duct subjected to an average (constant) Biot number [80]. The average Biot number is calculated from the thermal resistances of the unfinned and finned duct sections. In this calculation the finned sections are related to the unfinned sections by a fin effectiveness. This section contains a comparison of the stepwise periodic Biot number solution to the more approximate average Biot number solution for a given duct geometry.

The problem considered is a finned aluminum tube with a 1.59 cm (5/8 in.) diameter and a .099 cm (.039 in.) thickness with radial fins of 3.96 cm (1.56 in.) diameter and .05 cm (.02 in.) thickness. The unfinned to finned ratio is 4.6. Inside the tube, water flows at an average velocity of .03 m/s (.1 ft/s) with a laminar fully developed profile. The comparison between the stepwise periodic Biot number and the approximation using an average Biot number is made for various changes of the internal and external resistance. The stepwise periodic Biot number H_1 and H_2 are calculated from an analysis of the total thermal resistance for the finned and unfinned sections, respectively. The average Biot number is calculated by analyzing the total thermal resistances of the finned and unfinned sections simultaneously.

The comparison of the average Biot number solution to the stepwise periodic Biot number solution is based on total heat transfer, with all errors relative to $Q(\xi) = 1$ as $\xi \to \infty$. The results demonstrate that for a low external and internal heat transfer coefficient (h_e = 57 W/m^2·K (10

BTU/hr•ft^2•F) and h_i = 3408 W/m^2•K (600 BTU/hr•ft^2•F)) the relative accuracy of the average Biot number is within 5% of the stepwise periodic solution. Changing h_e to 568 W/m^2•K (100 BTU/hr•ft^2•F) decreases the maximum difference to 3%. Doubling the internal heat transfer coefficient changes the maximum difference to only 2.8%. In all cases, the difference of the average Biot number solution is smallest in the inlet region and increases to a maximum in the range $Q(\xi)$ = .3 to .6 before decreasing as the flow approaches thermal saturation.

In general, the use of an average Biot number provides a computationally convenient and accurate engineering approximation for heat transfer from a finned duct. The accuracy of the average Biot number is dependent on the axial location for the results, as well as the size of the internal and external heat transfer coefficient. For better accuracy, a stepwise periodic Biot number can be applied.

VII. SUMMARY AND RECOMMENDATIONS

The majority of this work is devoted to the solution of the energy equation for a laminar flow subject to an external stepwise periodic heat transfer coefficient. A variable eigenfunction technique is developed to solve a general class of internal flow problems with variable external heat transfer coefficient, including the effect of viscous dissipation and thermal energy generation. The result is that the energy equation was reduced to the form of an infinite set of linear first order differential equations with variable coefficients.

Three solution methods for the O.D.E.'s from the variable eigenfunction technique are studied; the Nth order approximation method, the iterative method and the stepwise periodic method. The Nth order approximation is well suited for a continuously variable heat transfer coefficient [16], but becomes computationally demanding beyond the first order appoximation for the stepwise periodic heat transfer coefficient. The iterative method becomes restrictive beyond the second iteration for any variation in $H(\xi)$. Neither of these methods provides satisfactory solution accuracy without higher order approximations or iterations. Finally, the stepwise periodic method provides a convenient means for the accurate solution of the stepwise periodic heat transfer coefficient. All graphical results are based on this method for a matrix size of 100 elements, which provides a solution accuracy of at least three decimal places. A comparison of graphical results based on the stepwise periodic method corresponds exactly to those calculated via a finite-difference scheme by Charmchi and Sparrow [5]. A connected region technique is developed to provide exact results for the first six

regions corresponding to the first six stepwise periodic variations of the Biot number. This technique is used to test the validity of the solution methods mentioned above.

The results obtained for the parameter study of the slug plate problem show that heat transfer enhancement is greatest in the entrance region and diminishes downstream. The most effective augmentation occurs when the external resistance is high (H_1 is low). As H_1 increases, the internal resistance becomes dominant and finning provides little extra enhancement. If the interfin spacing is decreased while keeping the ratio ξ_1/ξ_2 small, the enhancement increases, with the extent of the increase affected by the Biot number. Variation of the period of the Biot number causes relatively minor changes in enhancement as long as the ratio ξ_1/ξ_2 remains unchanged. The trends of this parameter study are characteristic for all the combinations of duct geometry and velocity profile.

The effect of the assumed velocity profile on heat transfer shows that the Bessel problem (constant velocity tube flow) has less tube side (internal) resistance to heat flow than the Graetz problem (fully developed tube flow). This lower internal resistance is due to the higher flow velocity near the tube wall for the Bessel problem. As a result, a constant velocity flow provides greater heat transfer rates than a fully developed laminar flow. In addition, the low internal resistance for the Bessel problem makes external finning more efficient than for the Graetz problem.

The average Biot number solution provides accurate results to within 5% of the stepwise periodic Biot number solution for a specified

duct geometry with a laminar fully developed flow. The results included a variation of the external and internal convection coefficient. The accuracy of the average Biot number solution is highest in the inlet region and decreases to a maximum in the range $Q(\xi) = .3$ to .6 before increasing as the flow approaches thermal saturation.

The present investigation of laminar flow with a stepwise periodic heat transfer coefficient in the modeling of finned conduits has a number of logical extensions for future research. This study assumed negligible wall thickness, yet depending upon wall thickness and thermal conductivity, axial conduction in the tube wall would tend to smooth out the abrupt periodic nature shown in Fig. 1b. This smoothing effect can be modeled as a harmonic variation in heat transfer coefficient. However, to fully determine the extent of wall axial conduction would require the simultaneous solution of the heat conduction equation for the wall and fins with the convection energy equation. In addition, the study of a turbulent flow would greatly extend the usefulness of this study. Since both turbulent and constant velocity flows maintain a low internal resistance at the tube wall, a study into the validity of approximating a turbulent flow by modeling it as a constant velocity flow could prove useful. Another extension would be to include three dimensional heat transfer effects. This would be useful in solving problems such as a tube fitted with axial, pin or spiral fins, which presents an angularly as well as an axially dependent heat transfer coefficient.

REFERENCES

1. Kovarik, M., "Optimal Distribution of Heat Conducting Material in the Finned Pipe Solar Collector," Solar Energy, 21, 477-484, (1978).

2. Shah, R. K., "Compact Heat Exchangers," Heat Exchangers - Thermal-Hydraulic Fundamentals and Design, ed. Kakac, S., Bergles, A. E., and Mayinger, F., McGraw-Hill, New York, 111-151, (1981)

3. Hakuraku, Y., and Ogata, H., "Thermal Design and Tests of a Subcooled Superfluid Helium Refrigerator," Cryogenics, 23, 291-297, (1983).

4. Marner, W. J., Bergles, A. E., and Chenoweth, J. M., "On the Presentation of Performance Data for Enhanced Tubes Used in Shell-and-Tube Heat Exchangers," Journal of Heat Transfer, 105, 358-365, (1983).

5. Charmchi, M., and Sparrow, E. M., "Laminar Heat Transfer in an Externally Finned Circular Tube," Journal of Heat Transfer, 102, 605-611, (1980).

6. Reed, J. R., and Mullineux, G., "Quasi-Steady State Solution of Periodically Varying Phenomena," International Journal of Heat and Mass Transfer, 16, 2007-2012, (1973).

7. Mikhailov, M. D., "Quasi-Steady State Temperature Distribution in Finite Regions with Periodically-Varying Boundary Conditions," International Journal of Heat and Mass Transfer, 17, 1475-1478, (1974).

8. Vick, B., and Özisik, M. N., "Quasi-Steady-State Temperature Distribution in Periodically Contacting Finite Regions," Journal of Heat Transfer, 103, 739-744, (1981).

9. Thompson, J. J., and Holy, Z. J., "Axisymmetric Thermal Response Problems for a Spherical Fuel Element with Time Dependent Heat Transfer Coefficients," Nuclear Engineering and Design, 9, 29-44, (1969).

10. Salcudean, M., Bui, T. M., and Lee, Y., "A Three-Dimensional Analysis for the Rewetting Process of Hot Channels," ASME Paper No. 78-WA/HT-27, (1978).

11. Blair, J. M., "An Analytical Solution to a Two-Dimensional Model of the Rewetting of a Hot Dry Rod," Nuclear Engineering and Design, 32, 159-170, (1975).

12. Lemmon, E. C., "Two Dimensional Moving Finite Element Development for Prediction of Rod Thermal Quench," ASME Paper No. 83-WA/HT-31, (1983).

13. Salcudean, M., and Rahman, M., "An Analytical Solution for the Heat Conduction During the Rewetting of Hot Horizontal Channels," Transactions of Canadian Society of Mechanical Engineers, 6, 106-114, (1980-81).

14. Holy, Z. J., "Temperature and Stresses in Reactor Fuel Elements Due to Time- and Space-Dependent Heat Transfer Coefficients," Nuclear Engineering and Design, 18, 145-197, (1972).

15. Ivanov, V. V., and Salomatov, V. V., "On the Calculation of the Temperature Field in Solids with Variable Heat-Transfer Coefficients," Inzhenerno - Fizicheskii Zhurnal, 9, 83-85, (1965).

16. Özisik, M. N., and Murray, R. L., "On the Solution of Linear Diffusion Problems with Variable Boundary Condition Parameters," Journal of Heat Transfer, 96, 48-51, (1974).

17. Yener, Y., and Özisik, M. N., "On the Solution of Unsteady Heat Conduction in Multi-Region Finite Media with Time Dependent Heat Transfer Coefficient," Proceedings of the 5th International Heat Transfer Conference, Tokyo, 9, 188-192, (1969).

18. Özisik, M. N., and Guceri, S. I., "A Variable Eigenvalue Approach to the Solution of Phase-Change Problems," Canadian Journal of Chemical Engineering, 55, 145-148, (1977).

19. Graetz, L., "Uber die Wärmeleitungsfähigheit von Flüssigkeiten," Annalen de Physik und Chemie, 25, 337-357, (1885).

20. Shah, R. K., and London, A. L., Laminar Flow Forced Convection in Ducts, Academic Press, New York, 1978.

21. Burmeister, L. C., Convective Heat Transfer, John Wiley and Sons, New York, 1983, Chapter 6.

22. Özisik, M. N., Heat Conduction, John Wiley and Sons, New York, 1980, Chapters 5 and 13.

23. Javeri, V., "Heat Transfer in Laminar Entrance Region of a Flat Channel for the Temperature Boundary Condition of the Third Kind," Warme-und Stoffubertragung, 10, 137-144, (1977).

24. Hsu, C. J., "Laminar Flow Heat Transfer in Circular or Parallel-Plate Channels with Internal Heat Generation and Boundary Conditions of the Third Kind," Journal of the Chinese Institute of Chemical Engineering, 2, 85-100, (1971).

25. Abramowitz, M., "On the Solution of Differential Equation Occurring in Problem of Heat Convection Laminar Flow in Tube," Journal of Math Physics, 32, 184-187, (1953).

26. Siegel, R., Sparrow, E. M., and Hallman, T. M., "Steady Laminar Heat Transfer in a Circular Tube with Prescribed Wall Heat Flux," Applied Scientific Research, A7, 386-392, (1958).

27. Sellers, J. R., Tribus, M., and Klein, J. S., "Heat Transfer to Laminar Flow in a Round Tube or Flat Conduit - The Graetz Problem Extended," Transactions ASME, 78, 441-448, (1956).

28. Lauwerier, H. A., "The Use of Confluent Hypergeometric Functions in Mathematical Physics and the Solution of an Eigenvalue Problem," Applied Scientific Research, A2, 184-204, (1950).

29. Lauwerier, H. A., "Poiseville Function," Applied Scientific Research, A3, 58-72, (1951).

30. Newman, J., "The Fundamental Principles of Current Distribution and Mass Transport in Electrochemical Cells,: in Electroanalytical Chemistry, Vol. 6, A. J. Bard, ed., Marcel and Dekker, New York, 187-352, (1973).

31. Larkin, B. K., "High-Order Eigenfunctions of the Graetz Problem," AIChE Journal, 7, 530, (1961).

32. Hsu, C. J., "Heat Transfer in a Round Tube with Sinusoidal Wall Heat Flux Distribution," AIChE Journal, 11, 690-695, (1965).

33. Mitchell, J. W., "An Expression for Internal Flow Heat Transfer for Polynomial Wall Temperature Distributions," Journal of Heat Transfer, 91, 175-177, (1969).

34. Bhattacharyya, T. K., and Roy, D. N., "Laminar Heat Transfer in a Round Tube with Variable Circumferential or Arbitrary Wall Heat Flux," International Journal of Heat and Mass Transfer, 13, 1057-1060, (1970).

35. Grigull, U., and Tratz, H., "Thermischer Einlauf in Augsgebildeter Laminarer Rohrstromung," International Journal of Heat and Mass Transfer, 8, 669-678, (1965).

36. Shapovalov, V. V., "Heat Transfer in Laminar Flow of an Incompressible Fluid in a Round Tube," Journal of Engineering Physics (USSR), 12, 363-364, (1967).

37. Zaychik, L. I., "Application of the Laplace Transformation to the Problem of Heat Transfer in a Tube with Variable Boundary Conditions," Heat Transfer Soviet Research, 11, 101-106, (1979).

38. Povarnitsyn, M. S., and Yurlova, E. V., "Calculation of the Temperature Field in a Plane Channel with Nonuniform Heating of Thermally Conducting Walls," Journal of Engineering Physics (USSR), 10, 82-85, (1966).

39. Savkar, S. D., "On a Variational Formulation of a Class of Thermal Entrance Problems," International Journal of Heat and Mass Transfer, 13, 1187-1197, (1970).

40. Chandler, R. D., Panaia, J. N., Stevens, R. B., and Zinsmeister, G. E., "The Solution of Steady State Convection Problems by the Fixed Random Wall Method," Journal of Heat Transfer, 90, 361-363, (1968).

41. Tay, A. O., and De Vahl Davis, G., "Application of the Finite Element Method to Convection Heat Transfer Between Parallel Plates," International Journal of Heat and Mass Transfer, 14, 1057-1069, (1971).

42. Casarella, M. J., Laura, P. A., and Chi, M., "On the Approximate Solution of Flow and Heat Transfer Through Non-circular Conduits with Uniform Wall Temperature," British Journal of Applied Physics, 18, 1327-1335, (1967).

43. Gottifredi, J. C., Quiroga, O. D., and Flores, A. F., "Heat Transfer to Newtonian and Non-Newtonian Fluids Flowing in a Laminar Regime," International Journal of Heat and Mass Transfer, 26, 1215-1220, (1983).

44. Whiteman, I. R., and Drake, W. B., "Heat Transfer to Flow in a Round Tube with Arbitrary Velocity Distribution," Transactions ASME, 80, 728-732 (1958).

45. Kays, W. M., "Numerical Solutions for Laminar-Flow Heat Transfer in Circular Tubes," Transactions ASME, 77, 1265-1274, (1955).

46. Hsu, C. J., "Exact Solution to Entry-Region Laminar Heat Transfer with Axial Conduction and the Boundary Condition of the Third Kind," Chemical Engineering Science, 23, 457-468, (1968).

47. Bayazitoglu, Y., and Özisik, M. N., "On the Solution of Graetz Type Problems with Axial Conduction," International Journal of Heat and Mass Transfer, 23, 1399-1402, (1980).

48. Vick, B., and Özisik, M. N., "Effects of Axial Conduction and Laminar Flow with Convective Boundaries," Journal of the Franklin Institute, 316, 159-173, (1983).

49. Hsu, C. J., "An Exact Mathematical Solution for Entrance-Region Laminar Heat Transfer with Axial Conduction," Applied Scientific Research, 17, 359-376, (1967).

50. Davis, E. J., and Gill, W. N., "The Effects of Axial Conduction in the Wall on Heat Transfer with Laminar Flow," International Journal of Heat and Mass Transfer, 13, 459-470, (1970).

51. Schmidt, F. W., and Zeldin, B., "Laminar Heat Transfer in the Entrance Region of Ducts," Applied Scientific Research, 23, 73-94, (1970).

52. Kader, B. A., "Heat and Mass Transfer in Laminar Flow in the Entrance Section of a Circular Tube," High Temperature (USSR), 9, 1115-1120, (1971).

53. Bergles, A. E., Brown, Jr., G. S., and Snider, W. D., "Heat Transfer Performance of Internally Finned Tubes," ASME Paper No. 71-HT-31, (1971).

54. Bergles, A. E., "Survey and Evaluation of Techniques to Augment Convective Heat and Mass Transfer," in Progress in Heat and Mass Transfer, Vol. 1, ed. Grigull, V., and Hahne, E., Pergamon Press, 331-424, (1969).

55. Murray, W. G., "Heat Dissipation Through an Annular Disk or Fin of Uniform Thickness," Journal of Applied Mechanics, 60, A78-A80, (1938).

56. Gardner, K. A., "Efficiency of Extended Surface," Transactions ASME, 67, 621-631, (1945).

57. Soliman, H. M., and Feingold, A., "Heat Transfer, Pressure Drop, and Performance Evaluation of a Quintuplex Internally Finned Tube," ASME Paper No. 77-HT-46, (1977).

58. Barba, A., Bergeles, G., and Launder, B. E., "The Prediction of Convective Heat Transfer in Viscous Flow Through Spirally Fluted Tubes," ASME Paper 83-WA/HT-37, (1983).

59. Prakash, C., and Patankar, S. V., "Combined Free and Forced Convection in Verticle Tubes with Radial Internal Fins," Journal of Heat Transfer, 103, 566-572, (1981).

60. Hu, M. H., and Chang, Y. P., "Optimization of Finned Tubes for Heat Transfer in Laminar Flow," Journal of Heat Transfer, 95, 332-338, (1973).

61. Harper, D. R., and Brown, W. B., "Mathematical Equations for Heat Conduction in the Fins of Air-Cooled Engines," National Advisory Committee for Aeronautics, Report 158, 1922.

62. Razelos, P., "The Optimum Dimensions of Convective Pin Fins," Journal of Heat Transfer, 105, 411-413, (1983).

63. Kovarik, M., "Optimal Heat Transfer Assemblies with Thin Straight Fins," Journal of Heat Transfer, 105, 203-205, (1983).

64. Razelos, P., and Imre, K., "The Optimum Dimensions of Circular Fins with Variable Thermal Parameters," Journal of Heat Transfer, 102, 420-425, (1980).

65. Poulikakos, D., and Bejan, A., "Fin Geometry for Minimum Entropy Generation in Forced Convection," Journal of Heat Transfer, 104, 616-623, (1982).

66. Güceri, S., and Maday, C. J., "A Least Weight Circular Cooling Fin," Journal of Engineering for Industry, 97, 1190-1193, (1975).

67. Marsh, B. L., and Costello, F. A., "Stochastic Optimization of Convective-Fin Design," Journal of Heat Transfer, 95, 339-343, (1973).

68. Li, C., "Optimum Cylindrical Pin Fin," AiCHE Journal, 29, 1043-1044, (1983).

69. Snider, A. D., and Kraus, A. D., "Recent Developments in the Analysis and Design of Extended Surface," Journal of Heat Transfer, 105, 302-306, (1983).

70. Chu, H. S., Weng, C. I., Chen, C. K., "Transient Response of a Composite Straight Fin," Journal of Heat Transfer, 105, 307-311, (1983).

71. Manzoor, M., Heat Flow Through Extended Surface Heat Exchangers, Springer-Verlag, Berlin, 1984.

72. Manzoor, M., Ingham, D. B., and Heggs, P. J., "The One-Dimensional Analysis of Fin Assembly Heat Transfer," Journal of Heat Transfer, 105, 646-651, (1983).

73. Kraus, A. D., and Snider, A. D., "New Parametrizations for Heat Transfer in Fins and Spines," Journal of Heat Transfer, 102, 415-419, (1980).

74. Kraus, A. D., and Snider, A. D., "The Optimization of an Array of Extended Surface," ASME Paper No. 84-HT-53, (1985).

75. Kraus, A. D., Analysis and Evaluation of Extended Surface Thermal Systems, McGraw-Hill, New York, 1982.

76. Mikhailov, M. D., and Özisik, M. N., "On the Solution of Heat Transfer Through an Array of Extended Surfaces," International Journal of Heat and Mass Transfer, 27, 893-899, (1984).

77. Vick, B., "Heat Transfer in Axially Conducting Flow and Periodically Contacting Solids," Ph.D. Thesis, Department of Mechanical and Aerospace Engineering, North Carolina State University, Raleigh, 1981.

78. Abramowitz, M., and Stegun, I. A., Handbook of Mathematical Functions, Dover Publications, Inc., New York, 1972, Chapter 13.

79. Wolverine Trufin - The Integral Finned Tube, Series I, Wolverine Tube Division, Allen Park, MI, (1963).

80. Threlkeld, J. L., Thermal Environmental Engineering, Prentice-Hall, Inc., Englewood Cliffs, NJ, 1970, Chapter 12.

APPENDIX A

EIGENFUNCTION RELATIONS

Presented is the derivation of the orthogonality condition (10) and the integral relation Eq. (72). Similarly, a representation of the normalization integral defined by Eq.(12) is derived [77].

1. Orthogonality Relation, Eq. (10)

Write the eigenvalue problem (9a) for the normalized eigenfunctions $\psi_m(\eta,\xi)$ and $\psi_p(\eta,\xi)$;

$$\frac{\partial}{\partial\eta}\left(\eta^s \frac{\partial\psi_m}{\partial\eta}\right) + \lambda_m^2(\xi)\ \eta^s \frac{v(\eta)}{2}\ \psi_m(\eta,\xi) = 0 \tag{75}$$

$$\frac{\partial}{\partial\eta}\left(\eta^s \frac{\partial\psi_p}{\partial\eta}\right) + \lambda_p^2(\xi)\ \eta^s \frac{v(\eta)}{2}\ \psi_p(\eta,\xi) = 0 \tag{76}$$

Mulitply Eq. (75) by $\psi_p(\eta,\xi)$ and Eq. (76) by $\psi_m(\eta,\xi)$, then subtract the results and integrate to get

$$\begin{aligned}\left(\lambda_m^2(\xi) - \lambda_p^2(\xi)\right) &\int_{\eta=0}^{1} \eta^s \frac{v(\eta)}{2}\ \psi_m(\eta,\xi)\ \psi_p(\eta,\xi)d\eta \\ &= \int_{\eta=0}^{1} \left[\psi_m(\eta,\xi)\ \frac{\partial}{\partial\eta}\left(\eta^s \frac{\partial\psi_p}{\partial\eta}\right) - \psi_p(\eta,\xi)\ \frac{\partial}{\partial\eta}\left(\eta^s \frac{\partial\psi_m}{\partial\eta}\right)\right]d\eta\end{aligned} \tag{77}$$

Integrate the RHS by parts and apply the homogeneous boundary conditions (9b,c) to obtain

$$\int_{\eta=0}^{1} \eta^s \frac{v(\eta)}{2} \psi_m(\eta,\xi)\ \psi_p(\eta,\xi)d\eta = \begin{cases} 0 \ , & m \neq p \\ 1 \ , & m = p \end{cases} \tag{78}$$

where the case m = p is found by substitution of Eq. (11) into Eq. (12). This relations is valid for all m and p.

2. Integral Relation, Eq. (72)

The procedure to derive the integral relation of Eq. (72) is suggested by the proof of orthogonality just presented. Write eigenvalue problem (9a) for eigenfunctions $\psi_{1m}(\eta)$ and $\psi_{2p}(\eta)$, corresponding to two different Biot numbers, H_1 and H_2

$$\frac{d}{d\eta}\left(\eta^s \frac{d\psi_{1m}}{d\eta}\right) + \lambda_{1m}^2\ \eta^s \frac{v(\eta)}{2}\ \psi_{1m}(\eta) = 0 \tag{79}$$

$$\frac{d}{d\eta}\left(\eta^s \frac{d\psi_{2p}}{d\eta}\right) + \lambda_{2p}^2\ \eta^s \frac{v(\eta)}{2}\ \psi_{2p}(\eta) = 0 \tag{80}$$

Multiply Eq. (79) by $\psi_{2p}(\eta)$ and Eq. (80) by $\psi_{1m}(\eta)$, then substract the results and integrate to get

$$\int_{\eta=0}^{1} \eta^s \frac{v(\eta)}{2}\ \psi_{1m}(\eta)\ \psi_{2p}(\eta)d\eta$$

$$= \frac{1}{\lambda_{1m}^2 - \lambda_{2p}^2} \int_{\eta=0}^{1} \left[\psi_{1m}(\eta) \frac{d}{d\eta}\left(\eta^s \frac{d\psi_{2p}}{d\eta}\right) - \psi_{2p}(\eta) \frac{d}{d\eta}\left(\eta^s \frac{d\psi_{1m}}{d\eta}\right)\right]d\eta \tag{81}$$

Integrate the RHS by parts and apply boundary conditions (9b,c) to obtain

$$\int_{\eta=0}^{1} \eta^s \frac{v(\eta)}{2} \psi_{1m}(\eta)\, \psi_{2p}(\eta) = \frac{H_1 - H_2}{\lambda_{1m}^2 - \lambda_{2p}^2} \left(\psi_{1m}(1)\, \psi_{2p}(1)\right) \tag{82}$$

which is valid over all m and p.

3. Normalization Integral Relation

The normalization integral, $N_m(\xi)$, can be expressed in a more computationally manageable form by further modifying the methodology described above. Write the eigenvalue problem (9a) for the normalized eigenfunction $\psi_m(\eta,\xi)$ and the continuous eigenfunction $\psi(\eta,\xi)$;

$$\frac{\partial}{\partial\eta}\left(\eta^s \frac{\partial\psi_m}{\partial\eta}\right) + \lambda_m^2(\xi)\, \eta^s \frac{v(\eta)}{2}\, \psi_m(\eta,\xi) = 0 \tag{83}$$

$$\frac{\partial}{\partial\eta}\left(\eta^s \frac{\partial\psi}{\partial\eta}\right) + \lambda^2(\xi)\, \eta^s \frac{v(\eta)}{2}\, \psi(\eta,\lambda) = 0 \tag{84}$$

Multiply Eq. (83) by $\psi(\eta,\lambda)$ and Eq. (84) by $\psi_m(\eta,\xi)$, then subtract the results and integrate to get

$$\begin{aligned}
&\int_{\eta=0}^{1} \eta^s \frac{v(\eta)}{2}\, \psi_m(\eta,\xi)\, \psi(\eta,\xi)\,d\eta \\
&= \frac{1}{\lambda_m^2(\xi) - \lambda^2(\xi)} \int_{\eta=0}^{1} \left[\psi_m(\eta,\xi) \frac{\partial}{\partial\eta}\left(\eta^s \frac{\partial\psi}{\partial\eta}\right) - \psi(\eta,\lambda) \frac{\partial}{\partial\eta}\left(\eta^s \frac{\partial\psi_m}{\partial\eta}\right)\right] d\eta \\
&= \frac{1}{\lambda_m^2(\xi) - \lambda^2(\xi)} \left[\psi_m(\eta,\xi) \frac{\partial\psi}{\partial\eta} - \psi(\eta,\xi) \frac{\partial\psi_m}{\partial\eta}\right]_{\eta=1}
\end{aligned} \tag{85}$$

Use L'Hospital's rule on Eq. (85) in the limit as $\lambda(\xi) \to \lambda_m(\xi)$ and apply orthogonality Eq. (10) to obtain

$$N_m(\xi) = \int_{\eta=0}^{1} \eta^s \frac{v(\eta)}{2} R_m^2(\eta,\xi)\,d\eta$$

$$= -\frac{1}{2\lambda_m^2(\xi)} R(1,\xi) \frac{\partial}{\partial\lambda} \left[\frac{\partial R(\eta,\lambda)}{\partial\eta} + H(\xi)\, R(\eta,\xi)\right]_{\substack{\eta=1 \\ \lambda(\xi)=\lambda_m(\xi)}} \tag{86}$$

APPENDIX B

$A_{mp}(\xi)$ RELATIONSHIP

Presented is the derivation of a simplier analytical representation of the $A_{mp}(\xi)$ function of Eq. (24a). Taking the partial derivative of the orthogonality condition (10) with respect to the axial variable, yields

$$\frac{d}{d\xi}\left[\int_{\eta=0}^{1} \eta^s \frac{v(\eta)}{2} \psi_m(\eta,\xi)\ \psi_p(\eta,\xi)d\eta\right]$$

$$= \int_{\eta=0}^{1} \eta^s \frac{v(\eta)}{2} \psi_p(\eta,\xi) \frac{\partial \psi_m}{\partial \xi} d\eta + \int_{\eta=0}^{1} \eta^s \frac{v(\eta)}{2} \psi_m(\eta,\xi) \frac{\partial \psi_p}{\partial \xi} d\eta \qquad (87)$$

$$= 0$$

Applying the definition of the $A_{mp}(\xi)$ function of Eq. (24a) gives

$$A_{pm}(\xi) + A_{mp}(\xi) = 0 \quad , \qquad (88)$$

thus providing the generalized relations

$$A_{mp}(\xi) = -A_{pm}(\xi) \qquad (89a)$$

$$A_{mm}(\xi) = 0 \qquad (89b)$$

which are valid for all m and p.

To determine the $A_{mp}(\xi)$ function, first define a new function

$$\Phi_p(\eta,\xi) = \frac{\partial \psi_p}{\partial \xi} \tag{90}$$

In terms of definition (90), the $A_{mp}(\xi)$ function can be written as

$$A_{mp}(\xi) = \int_{\eta=0}^{1} \eta^s \frac{v(\eta)}{2} \psi_m(\eta,\xi) \Phi_p(\eta,\xi) d\eta \tag{91}$$

Rewrite the eigenvalue problem (9) for the case where m = p and differentiate with respect to the axial variable, ξ .

$$\frac{\partial^2 \Phi_p}{\partial \eta^2} + \lambda_p^2(\xi) \eta^s \frac{v(\eta)}{2} \Phi_p(\eta,\xi) + \eta^s \frac{v(\eta)}{2} \frac{d\lambda_p^2}{d\xi^2} \psi_p(\eta,\xi) = 0 \tag{92a}$$

$$\frac{\partial \Phi_p}{\partial \eta} = 0 \quad , \quad \eta = 0 \tag{92b}$$

$$\left.\frac{\partial \Phi_p}{\partial \eta}\right|_{\eta=1} + H(\xi) \Phi_p(1,\xi) + \frac{dH(\xi)}{d\xi} \psi_p(1,\xi) = 0 \quad , \quad \eta = 1 \tag{92c}$$

Now multiply (92a) by $\psi_m(\eta,\xi)$ and multiply (9a) by $\Phi_p(\eta,\xi)$, substract and integrate to obtain

$$[\lambda_p^2(\xi) - \lambda_m^2(\xi)] \int_{\eta=0}^{1} \eta^s \frac{v(\eta)}{2} \Phi_p(\eta,\xi)\ \psi_m(\eta,\xi)d\eta$$

$$+ \int_{\eta=0}^{1} [\psi_m(\eta,\xi) \frac{\partial^2 \Phi_p}{\partial \eta^2} - \Phi_p(\eta,\xi) \frac{\partial^2 \psi_m}{\partial \eta^2}]d\eta \qquad (93)$$

$$+ \int_{\eta=0}^{1} \eta^s \frac{v(\eta)}{2} \frac{d\lambda_p^2}{d\xi} \psi_p(\eta,\xi)\ \psi_m(\eta,\xi)d\eta = 0$$

To the second integral, integrate by parts and apply boundary conditions (9b,c) and (92b,c) to get

$$\int_{\eta=0}^{1} [\psi_m(\eta,\xi) \frac{\partial^2 \Phi_p}{\partial \eta^2} - \Phi_p(\eta,\xi) \frac{\partial^2 \psi_m}{\partial \eta^2}]d\eta$$

$$= - \frac{dH(\xi)}{d\xi} \psi_m(1,\xi)\ \psi_p(1,\xi) \qquad (94)$$

To the third integral, use orthogonality condition (10) so that

$$\int_{\eta=0}^{1} \eta^s \frac{v(\eta)}{2} \frac{d\lambda_p^2}{d\xi} \psi_p(\eta,\xi)\ \psi_m(\eta,\xi)d\eta = \begin{cases} \frac{d\lambda_p^2}{d\xi}, & m = p \\ 0, & m \neq p \end{cases} \qquad (95)$$

Utilizing relationships (94) and (95) in Eqs. (93) gives

$$A_{mp}(\xi) = \frac{\frac{dH(\xi)}{d\xi}\left[\psi_m(1,\xi)\ \psi_p(1,\xi)\right] - \frac{d\lambda_p^2}{d\xi}\,\delta_{mp}}{\left(\lambda_p^2(\xi) - \lambda_m^2(\xi)\right)} \tag{96}$$

where

$$\delta_{mp} = \begin{cases} 0 \ , & m \neq p \\ 1 \ , & m = p \end{cases}$$

The $A_{mp}(\xi)$ function adds a major complexity in that it is dependent on the first derivative of $H(\xi)$, the space dependent convective coefficient. The $A_{mp}(\xi)$ function is not always in a convenient form for computation and must be further manipulated. For the case of periodic high and low convective coefficients, the eigenvalue properties are not continuous so cannot be directly differentiated. Instead, a different approach is presented.

One can note that Eq. (45) represents the discontinuous nature of the eigenfunction, $\psi_m(\eta,\xi)$, associated with a discontinuous heat transfer coefficient. However, since $\psi_m(\eta,\xi)$ is piecewise continuous for $0 < \xi < \infty$, the Fourier series representation of $\psi_m(\eta,\xi)$ at the discontinuities ξ^*_{2j} and $\xi^*_{1,(j+1)}$ for $j = 0,1,2,\ldots$ will converge to the average value

$$\psi_m(\eta,\xi) = \frac{\left[\psi_{1m}(\eta) + \psi_{2m}(\eta)\right]}{2} \tag{97}$$

By carefully observing the discontinuous behavior of the eigenfunctions, one can conclude that

$$\frac{d\psi_p}{d\eta} = \begin{cases} 0 \ , \ \xi \neq \xi^*_{2,j} \ , \ \xi^*_{1,(j+1)} \\ \lim\limits_{\Delta\xi \to 0} \dfrac{[\psi_{1p}(\eta) - \psi_{2p}(\eta)]}{\Delta\xi} \ , \quad \xi = \xi^*_{2j} \\ \lim\limits_{\Delta\xi \to 0} \dfrac{-[\psi_{1p}(\eta) - \psi_{2p}(\eta)]}{\Delta\xi} \ , \quad \xi = \xi^*_{1,j+1} \end{cases} \tag{98}$$

In terms of a Dirac delta function, δ, Eq. (98) results in

$$\frac{d\psi_p}{d\eta} = [\psi_{2p}(\eta) - \psi_{1p}(\eta)] \sum_{j=1}^{\infty} \delta(\xi - \xi^*_{2j}) - \delta(\xi - \xi^*_{1,j+1}) \tag{99}$$

Substitution of Eqs. (97) and (99) into Eq. (24a) and applying orthogonality relation (10) and the integral relation of Eq. (72) yields

$$A_{mp}(\xi) = a_{mp} \sum_{j=0}^{\infty} \delta(\xi - \xi^*_{2j}) - \delta(\xi - \xi^*_{1,j+1}) \tag{100}$$

where

$$a_{mp} = \frac{(H_2 - H_1)}{2} \left[\frac{\psi_{1m}(1)\ \psi_{2p}(1)}{\lambda^2_{2p} - \lambda^2_{1m}} - \frac{\psi_{2m}(1)\ \psi_{1p}(1)}{\lambda^2_{2m} - \lambda^2_{1p}}\right] \tag{101}$$

Note that for the special case of stepwise periodic heat transfer coefficient, the $A_{mp}(\xi)$ function contributes a delta function whenever a jump is hit, otherwise the function equals zero.

APPENDIX C

SOLUTION TO GRAETZ PROBLEM

Two methods are applied for the calculation of the Graetz functions satisfying the eigenvalue problem (9) for s = 1 and $v(\eta) = 2(1 - \eta^2)$. The first method transforms the original eigenvalue problem into a confluent hypergeometric differential equation and is accurate for smaller eigenvalues. The second method utilizes an asymptotic method and is accurate for larger eigenvalues.

1. Confluent Hypergeometric Solution

To reduce the complexity of the Graetz eigenvalue problem to a convenient form, the following change of variables is implemented [31,77],

$$R_m(\eta) = e^{-x/2}\, W(x) \tag{102}$$

where

$$x = \lambda_m\, \eta^2 \tag{103}$$

Substitution of Eq. (102) into Eq. (9a) and simplifying yields the differential equation governing W(x)

$$x \frac{d^2W}{dx^2} + (b - x) \frac{dW}{dx} - a\, W(x) = 0 \tag{104}$$

where,

$$a = \frac{1}{4} (2 - \lambda_m) \tag{105a}$$

$$b = 1 \tag{105b}$$

Equation (104) is the form of a confluent hypergeometric equation [78] with a series solution given as

$$\begin{aligned} W(x) &= M(a,b,x) \\ &= 1 + \frac{ax}{b} + \frac{(a)_2\, x^2}{(b)_2\, 2!} + \cdots + \frac{(a)_m\, x^m}{(b)_m\, m!} \end{aligned} \tag{106}$$

where

$$(a)_m = a(a+1)(a+2)\cdots(a+m-1) \quad , \quad (a)_o = 1$$

and $M(a,b,x)$ is the confluent hypergeometric function. Rewriting Eq. (102), the eigenfunction can now be expressed as

$$R_m(\eta) = e^{-\lambda_m \frac{\eta^2}{2}}\, M\left[\frac{1}{4}(2 - \lambda_m),\ 1,\ \lambda_m \eta^2\right] \tag{107}$$

Substituting Eq. (107) into the boundary condition (9c) and solving yields the transcendental root equation for the eigenvalues λ_m.

$$\begin{aligned} &\lambda_m \frac{(2 - \lambda_m)}{2}\, M\left[\frac{1}{4}(6 - \lambda_m),\ 2,\ \lambda_m\right] \\ &- (H - \lambda_m)\, M\left[\frac{1}{4}(2 - \lambda_m),\ 1,\ \lambda_m\right] = 0 \end{aligned} \tag{108}$$

2. Lauwerier's Asymptotic Solution

For large eigenvalues, an approximate solution can be obtained. Lauwerier [28] expressed the Graetz eigenfunction, $R_m(\eta)$, in terms of a confluent hypergeometric function and then developed an asymptotic solution at the wall [30] as

$$R_m(1) = \frac{1}{\sqrt{3\pi}} \left(\frac{6}{\lambda_m}\right)^{1/3} \Gamma(1/3) \left\{\cos\left[\left(\frac{\lambda_m}{4} - \frac{1}{6}\right)\pi\right] \sum_{p=0}^{3} \alpha_p \left(\frac{2}{\lambda_m}\right)^{2p} \right.$$
$$\left. + 3^{1/3} \frac{\Gamma(2/3)}{\Gamma(1/3)} \cos\left[\left(\frac{\lambda_m}{4} + \frac{1}{6}\right)\pi\right] \sum_{p=0}^{2} \beta_p \left(\frac{2}{\lambda_m}\right)^{2p+4/3} \right\} \tag{109}$$

A further extension of Lauwerier's method [29,30], yields

$$\left.\frac{dR_m}{d\eta}\right|_{\eta=1} = \frac{2\sqrt{3}}{\pi} \left(\frac{\lambda_m}{6}\right)^{1/3} \Gamma(2/3) \left\{\cos\left[\left(\frac{\lambda_m}{4} + \frac{1}{6}\right)\pi\right] \right.$$
$$\left. \cdot \sum_{p=0}^{3} \gamma_p \left(\frac{2}{\lambda_m}\right)^{2p} + \frac{1}{3^{1/3}} \frac{\Gamma(1/3)}{\Gamma(2/3)} \cos\left[\left(\frac{\lambda_m}{4} - \frac{1}{6}\right)\pi\right] \sum_{p=0}^{2} \delta_p \left(\frac{2}{\lambda_m}\right)^{2p+2/3} \right\} \tag{110}$$

where the coefficients have the values

$$\begin{aligned}
\alpha_0 &= 1 \quad , & \gamma_0 &= 1 \\
\alpha_1 &= -0.01444444444 \quad , & \gamma_1 &= 0.03801587302 \\
\alpha_2 &= 0.009882467268 \quad , & \gamma_2 &= -0.01971517369 \\
\alpha_3 &= -0.02131664753 \quad , & \gamma_3 &= 0.03618529439 \\
\beta_0 &= -0.07857142857 \quad , & \delta_0 &= -0.3 \\
\beta_1 &= 0.02887167277 \quad , & \delta_1 &= 0.02189502164 \\
\beta_2 &= -0.04405535292 \quad , & \delta_2 &= -0.02140401420
\end{aligned} \tag{111}$$

Substitution of Eqs. (109) and (110) into the transcendental Eq. (9c), allows one to solve for the eigenvalues. The normalization integral of Eq. (12) can be obtained by substituting Eqs. (109) and (110) above into the norm relationship (86) and manipulating to the form

$$N_m = -\frac{1}{2\lambda_m}\frac{R_m(1)}{\pi}\left\{H\left|\frac{\Gamma(1/3)}{3^{1/6}}\left[-\frac{\pi}{4}\sin\left(\frac{\lambda}{4}-\frac{1}{6}\right)\pi\right]\right.\right.$$

$$\sum_{p=0}^{3}\alpha_p\left(\frac{2}{\lambda_m}\right)^{2_p+1/3} - \cos\left[\left(\frac{\lambda_m}{4}-\frac{1}{6}\right)\pi\right]\sum_{p=0}^{3}\frac{\alpha_p}{2}\left(2_p+1/3\right)\left(\frac{2}{\lambda_m}\right)^{2_p+4/3}\Bigg]$$

$$+ 3^{1/6}\Gamma(2/3)\left[-\frac{\pi}{4}\sin\left[\left(\frac{\lambda_m}{4}+\frac{1}{6}\right)\pi\right]\sum_{p=0}^{2}\beta_p\left(\frac{2}{\lambda_m}\right)^{2_p+5/3} - \cos\left[\left(\frac{\lambda_m}{4}+\frac{1}{6}\right)\pi\right]\right.$$

$$\left.\sum_{p=0}^{2}\frac{\beta_p}{2}\left(2_p-5/3\right)\left(\frac{2}{\lambda_m}\right)^{2_p+8/3}\Bigg]\right| + \left|2\cdot 3^{1/6}\Gamma(2/3)\left[\left(-\frac{\pi}{4}\sin\left(\frac{\lambda_m}{4}+\frac{1}{6}\right)\pi\right)\right.\right.$$

$$\sum_{p=0}^{3}\gamma_p\left(\frac{2}{\lambda_m}\right)^{2_p-1/3} - \cos\left[\left(\frac{\lambda_m}{4}+\frac{1}{6}\right)\pi\right]\sum_{p=0}^{3}\frac{\gamma_p}{2}\left(2_p-1/3\right)\left(\frac{2}{\lambda_m}\right)^{2_p+2/3}\Bigg]$$

$$+\frac{2}{3^{1/6}}\Gamma(1/3)\left[\left(-\frac{\pi}{4}\sin\left(\frac{\lambda}{4}-\frac{1}{6}\right)\pi\right)\sum_{p=0}^{2}\delta_p\left(\frac{2}{\lambda_m}\right)^{2_p1/3} -\right.$$

$$\left.\left.\cos\left[\left(\frac{\lambda_m}{4}-\frac{1}{6}\right)\pi\right]\sum_{p=0}^{2}\frac{\delta_p}{2}\left(2_p+1/3\right)\left(\frac{2}{\lambda_m}\right)^{2_p+4/3)}\Bigg]\right|\right\} \qquad (112)$$

APPENDIX D

EIGENVALUE PROBLEM SOLUTIONS

The eigenvalue problem (9) and the normalization integral (12) contain the unknowns $R_m(\eta,\xi)$ and $\lambda_m(\xi)$. In order to carry out the solution for the stepwise periodic heat transfer coefficient by any of the solution techniques presented, one must specify the forms of the two unknowns for the cases under study.

Each combination of the geometry specifier, s, and the dimensionless velocity profile $v(\eta)$, results in a different set of eigenfunctions and eigenvalues needed to satisfy the resulting eigenvalue problem (9). Table D1, summarizes the form of the eigenfunction and transcendental root equation for the eigenvalues for the cases under study [22,30]. In addition, the analytical representation of the normalization integral is included. For the Graetz problem, two sets of eigenvalue properties are presented; the first for small eigenvalues and the second for large eigenvalues. Substituting these relations into the appropriate form of a solution technique allows for the calculation of the temperature distribution $\theta(\eta,\xi)$.

TABLE D1. Eigenvalue Problem Solutions

Case	$R_m(\eta,\xi)$	Eigenvalues are Positive Roots of	Normalization Integral
Slug Plate Problem $s = 0$ $v(\eta) = 1$	$\cos\left[\frac{\lambda_m}{\sqrt{2}}(\xi)\eta\right]$	$\cos\left[\frac{\lambda_m}{\sqrt{2}}(\xi)\eta\right]$ $H(\xi) =$ $\sin\left[\frac{\lambda_m}{\sqrt{2}}(\xi)\eta\right]\frac{\lambda_m}{\sqrt{2}}(\xi)$	$\frac{\lambda_m^2(\xi)/2 + H^2(\xi) + H(\xi)}{4\left[\lambda_m^2(\xi)/2 + H(\xi)^2\right]}$
Bessel Problem $s = 1$ $v(\eta) = 1$	$J_o\left[\frac{\lambda_m}{\sqrt{2}}(\xi)\eta\right]$	$J_o\left[\frac{\lambda_m}{\sqrt{2}}(\xi)\eta\right] H(\xi) =$ $J_1\left[\frac{\lambda_m}{\sqrt{2}}(\xi)\eta\right]\frac{\lambda_m}{\sqrt{2}}(\xi)$	$\frac{J_o\left[\frac{\lambda_m}{\sqrt{2}}(\xi)\right]^2\left[H(\xi)^2 + \frac{\lambda_m^2}{2}(\xi)\right]}{2\left(\lambda_m^2(\xi)\right)}$
Graetz Problem $s = 1$ $v(\eta) = 2(1-\eta^2)$	Small $\lambda_m(\xi)$:† Eq. 107 Large $\lambda_m(\xi)$†† Eq. 109*	Small $\lambda_m(\xi)$: Eq. 108 Large $\lambda_m(\xi)$ $\left.\frac{dR_m}{d\eta}\right\|_{\eta=1} + H(\xi)\,R_m(1,\xi) = 0$ Eq. 109, Eq. 110	Small $\lambda_m(\xi)$: Numerical Integration i.e., (Simpson's rule) Large $\lambda_m(\xi)$: Eq. 112

* $\eta = 1$ only
† Confluent hypergeometric solution
†† Lauwerier's asymptotic solution

APPENDIX E

COMPUTER PROGRAMS

This section includes some programming details of the two Graetz programs CRTN and PERSLTN which correspond to the connected region technique and the stepwise periodic solution, respectively. A third program, GCLEF, which calculates the eigenvalues, eigenfunctions, and normalization integrals for use in CRTN and PERSLTN is included.

The two programs, CRTN and PERSLTN, represent general solutions to the connected region technique and stepwise periodic solution valid for all combinations of duct geometry and velocity profile. During operation, both programs require the submission of two data files, one containing the eigenvalues, etc. for the low Biot number value H_1 and the second containing those for the high Biot number value H_2.

The Graetz program GCLEF is included since the calculation of the Graetz eigenfunctions by both confluent hypergeometric functions and Lauwerier's asymptotic formula is rather complex. Once the eigenvalues, eigenfunctions and normalization integrals are calculated, the results are stored in a data file for use in CRTN and PERSLTN. The program GCLEF can readily be converted into a form suitable to find the eigenvalues, etc. for the slug plate and Bessel problem by substitution of the appropriate functional forms from Table D1 in place of the confluent hypergeometric and Lauwerier's asymptotic formulas. The slug plate eigenfunctions are represented by trigonometric functions and easily calculated. The Bessel eigenfunctions are represented by Bessel functions which can be found using the IMSL subroutine MMBSJN.

Further details are commented directly in the programs.

NOMENCLATURE FOR PROGRAM 'GCLEF'

A	Dummy variable
ACCY	Convergence specifier (not solution accuracy)
AL#	Alpha constants
BE#	Beta constants for Eqs. (109), (110) and (112)
DL#	Delta constants
GM#	Gamma constants
B	Dummy constant
Biot	Biot number
CHMAX	Maximum value of CONFLU
CH	Dummy variable
CONFLU	Confluent hypergeometric function
CON#	Constants for NORM function
CTRIG#	Dummy variables
DELR	Function routine for eigenvalue derivative (Lauwerier's method)
DGAMMA	IMSL gamma function routine
E	Eigenvalue
EF	Eigenfunction dummy variable
ETA	Dimensionless radial term
FNEV	Function routine for transcendental root equation
FNR	Function routine for eigenfunction (Lauwerier's method)
INTV	# of radial intervals for Simpson's numerical integration method
JC	Iteration counter for secant solver routine
MLARGE	Maximum number of enginvalues calculated

N	CONFLU term counter
NM	Normalization integral
NORM	Function routine for normalization integral (Lauwerier's method)
PART#	Intermediate dummy variables
PI	
PL , PR	Intermediate dummy variables
POW#	Dummy variables
PSI	Normalized eigenfunction at duct wall (ETA=1.0)
R	Eigenfunction at duct wall (ETA=1.0)
RETA	Eigenfunction at variable ETA
SAL#	Alpha summations
SBE#	Beta summations for Eqs. (109), (110) and (112)
SGM#	Gamma summations
SDL#	Delta summations
STRIG#	Dummy variables
X	Eigenvalue dummy variable
XL	Lower approximation for eigenvalue
XH	Upper approximation for eigenvalue
XNEW	New approximation for eigenvalue

```
//A655RGW JOB 41755,BARD,REGION=1536K,TIME=(4,00)
/*PRIORITY STANDARD
/*JOBPARM LINES=3,CARDS=500
//STEP0001 EXEC FORTVCG,LIB='VPI.IMSL.DP'
//FORT.SYSIN DD *
C
C                          PROGRAM 'GCLEF JCL'
C
C                    EIGENVALUE AND EIGENFUNCTION SOLUTION
C                         GRAETZ SOLUTION, TUBE FLOW
C
C                                 2-6-86
C
C              PROGRAM FOR THE CALCULATION OF THE EIGENVALUES,
C              EIGENFUNCTIONS AND NORMALIZATION INTEGRAL FOR
C              THE GRAETZ CASE.  GRAETZ EIGENFUNCTIONS FOUND
C              USING BOTH CONFLUENT HYPERGEOMETRIC FUNCTIONS
C              AND LAUWERIER'S ASYMPTOTIC SOLUTION.
C
C  ************************  INSTRUCTIONS  ****************************
C
C       EDIT PROGRAM:
C              1. UNDER DIMENSIONLESS INPUT SECTION, SELECT VALUES FOR
C                 ACCY, BIOT, AND MLARGE IN LINES 1-3.
C
C              2. NOTE - ACCY LESS THAN 1.0*10-6 MAY RESULT IN ERRORS
C                 IN CONVERGENCE OF SECANT SOLVER ROUTINE FOUND IN
C                 EIGENVALUES SECTION.
C
C        SUBMIT PROGRAM:
C              3. SUBMIT BY USING SUBMIT COMMAND
C                       SUBMIT GCLEF JCL
C
C  ************************************************************************
C                         PROGRAM INITIALIZATION
C  ************************************************************************
C
       IMPLICIT REAL*8 (A-H,O-Z)
       REAL*8 NM(300),NORM,CONFLU
       DIMENSION R(300),E(300),PSI(300),EV(300)
       COMMON/BLOCK1/N
       COMMON/BLOCK2/PI,DGAM1,DGAM2,M
       COMMON/BLOCK3/AL(3),BE(3)
       COMMON/BLOCK4/GM(3),DL(3)
       COMMON/BLOCK5/CON1,CON2,CON3,CON4,BIOT
C  FUNCTION DEFINITION FOR EIGENFUNCTIONS FOUND USING CONFLUENT
C  HYPERGEOMETRIC FUNCTIONS
       RETA(X,ETA)=DEXP(-X*ETA*ETA/2.D0)*CONFLU((2.0D0-X)/4.0D0,1.0,
     1      X*ETA*ETA)
C
C  ************************************************************************
```

```
C                          DIMENSIONLESS INPUT
C  ***************************************************************************
C
 1      ACCY=1.0D-5
 2      BIOT=5.00D0
 3      MLARGE=200
C    CONSTANTS FOR GAMMA FUNCTIONS AND PI
        DGAM1=DGAMMA(1.0D0/3.0D0)
        DGAM2=DGAMMA(2.0D0/3.0D0)
        PI=3.1415926D0
C    CONSTANTS FOR LAUWERIER'S ASYMPTOTIC SOLUTION
        AL(1)=-.01444444444D0
        AL(2)=0.009882467268D0
        AL(3)=-0.02131664753D0
        BE(1)=-0.07857142857D0
        BE(2)=0.02887167277D0
        BE(3)=-0.044055355292D0
        GM(1)=0.03801587302D0
        GM(2)=-0.01971517369D0
        GM(3)=0.03618529439D0
        DL(1)=-0.3D0
        DL(2)=.02189502164D0
        DL(3)=-.02140401420D0
C
C  ***************************************************************************
C                     CALCULATE EIGENVALUES
C  ***************************************************************************
C
C    SET UP FIRST APPROXIMATION
        XL=1.50D0
        XH=2.70D0
C    TRANSCENDENTAL ROOT EQUATION SOLVED VIA NEWTON'S SECANT METHOD
 20     DO 50 M=1,MLARGE
          JC=0
 25       XNEW=XL-(FNER(XL,BIOT)*(XL-XH)/(FNER(XL,BIOT)-FNER(XH,BIOT)))
          IF(DABS((XNEW-XH)/XNEW).LT.ACCY*.1) GOTO 30
          XH=XNEW
          JC=JC+1
          IF(JC.GE.150)GOTO 500
          GOTO 25
 30       E(M)=XNEW
C   SET UP APPROXIMATIONS FOR NEXT EIGENVALUE
          XL=XL+4.0D0
          XH=XNEW+4.0D0
          XNEW=0
 50    CONTINUE
C
C  ***************************************************************************
C                          BASIC CALCULATIONS
C  ***************************************************************************
C
```

```
 90     INTV=20
        DO 110 M=1,7
C  CALCULATE EIGENFUNCTION USING CONFLUENT HYPERGEOMETRIC FUNCTIONS
C  UP TO THE 7TH EIGENVALUE
           R(M)=RETA(E(M),1.0)
C
C  CALCULATE NORM USING SIMPSON'S ONE THIRD METHOD
C
           INTV=INTV+10
           NM(M)=0.0D0
C     -CALC ODD INTERVALS OVER ETA=0 TO 1
           DO 105 K=1,INTV,2
             ETA=DFLOAT(K)/DFLOAT(INTV)
             NM(M)=NM(M)+4.D0*ETA*(1.0D0-ETA**2)*RETA(E(M),ETA)**2
 105       CONTINUE
C     -CALC EVEN INTERVALS OVER ETA=0 TO 1
           DO 107 K=2,INTV,2
             ETA=DFLOAT(K)/DFLOAT(INTV)
             NM(M)=NM(M)+2.D0*ETA*(1.0D0-ETA**2)*RETA(E(M),ETA)**2
 107       CONTINUE
           NM(M)=NM(M)/(3.0D0*DFLOAT(INTV))
 110       CONTINUE
C
C  CALCULATE EIGENFUNCTION AND NORM USING LAUWERIER'S SOLUTION
C
C    CONSTANTS USED IN NORM FUNCTION ROUTINE
           CON1=DGAM1/3.0D0**(1./6.)
           CON2=DGAM2*3.0D0**(1./6.)
           CON3=DGAM2*2.0D0*3.0D0**(1./6.)
           CON4=DGAM1*2.0D0/3.0D0**(1./6.)
           DO 111 M=8,MLARGE
              R(M)=FNR(E(M))
              NM(M)=NORM(E(M),R(M))
 111       CONTINUE
C  STORE EIGENVALUE PROPERTIES IN A DATA FILE
           WRITE(3,112)MLARGE,BIOT
 112       FORMAT(5X,I3,4X,F9.4)
           DO 114 M=1,MLARGE
              PSI(M)=R(M)/DSQRT(NM(M))
              WRITE(3,113)E(M),NM(M),PSI(M)
  113         FORMAT(3X,E17.11,2X,E17.11,2X,E17.11)
  114       CONTINUE
C   PRINT EIGENVALUE PROPERTIES
           WRITE(6,115)
  115      FORMAT(35X,'LAUWERIER-CONFLUENT SOLUTION')
           WRITE(6,116)
  116      FORMAT(27X,'GRAETZ FUNCTIONS FOR TUBE - CONFLUENT TILL M=7')
           WRITE(6,117)
  117      FORMAT(/,35X,'EIGENFUNCTIONS AND EIGENVALUES'/)
           WRITE(6,119)BIOT,ACCY
  119      FORMAT(34X,'BIOT=',F6.2,4X,'ACCURACY=',E8.2/)
```

```
      WRITE(6,120)
  120 FORMAT(16X,'M',14X,'E',13X,'R',14X,'NM',12X,
     1   'PSI1')
      WRITE(6,130)(M,E(M),R(M),NM(M),PSI(M),M=1,40)
  130 FORMAT(15X,I3,7X,F10.6,5X,F9.6,6X,F9.6,6X,F9.6)
      GOTO 1000
C   ERROR STATEMENT
  500 WRITE(6,600)
  600 FORMAT(4X,'ERROR IN CONVERGENCE OF SECANT SOLVER ROUTINE')
 1000 STOP
      END
C
C   ***********************************************************************
C                          SUBROUTINES
C   ***********************************************************************
C
C       EIGENVALUE ROOT EQUATION
C
      DOUBLE PRECISION FUNCTION FNER(X,BIOT)
      IMPLICIT REAL*8 (A-H,O-Z)
      COMMON/BLOCK2/PI,DGAM1,DGAM2,M
      IF(M.GE.8) GOTO 5
C     EIGENVALUES VIA CONFLUENT GEOMETRIC FUNCTIONS
      A=(2.0D0-X)/4.0D0
      FNER=X*2.0D0*A*CONFLU(A+1.D0,2.D0,X)+(BIOT-X)*CONFLU(A,1.D0,X)
      RETURN
C     EIGENVALUES VIA LAUWERIER'S SOLUTION
 5    FNER=DELR(X)+BIOT*FNR(X)
      RETURN
      END
C
C   EIGENFUNCTIONS VIA LAUWERIER'S SOLUTION
C
      DOUBLE PRECISION FUNCTION FNR(X)
      IMPLICIT REAL*8 (A-H,O-Z)
      COMMON/BLOCK2/PI,DGAM1,DGAM2,M
      COMMON/BLOCK3/AL(3),BE(3)
      SAL=1.0
      SBE=0.0
      DO 10 N=1,3
        POW1=2*N
        POW2=2.0*DFLOAT(N-1)+4.0/3.0
        SAL=SAL+AL(N)*(2.0/X)**POW1
        SBE=SBE+BE(N)*(2.0/X)**POW2
 10   CONTINUE
          PL=DCOS(X*PI/4.D0-1.D0*PI/6.D0)*(6.D0/X)**(1./3.)*DGAM1/
     1      (DSQRT(3.0D0)*PI)
          PR=DCOS(X*PI/4.D0+1.D0*PI/6.D0)*(6.0D0/X)**(1./3.)*DGAM2/
     1      (3.0D0**(1./6.)*PI)
          FNR=PL*SAL+PR*SBE
          RETURN
```

```
            END
C
C   EIGENFUNCTION DERIVATE VIA LAUWERIER'S SOLUTION
C
      DOUBLE PRECISION FUNCTION DELR(X)
      IMPLICIT REAL*8 (A-H,O-Z)
      COMMON/BLOCK2/PI,DGAM1,DGAM2,M
      COMMON/BLOCK4/GM(3),DL(3)
      SGM=1.0
      SDL=0.0
      DO 10 N=1,3
        SGM=SGM+GM(N)*(2.0/X)**(2*N)
        SDL=SDL+DL(N)*(2.0/X)**(2.0*DFLOAT(N-1)+2.0/3.0)
 10   CONTINUE
           PL=DCOS(X*PI/4.D0+1.D0*PI/6.D0)*(X/6.0D0)**(1./3.)*DGAM2*
     1       2.0*DSQRT(3.0D0)/PI
           PR=DCOS(X*PI/4.D0-1.D0*PI/6.D0)*3.0D0**(1./6.)*2.0D0*DGAM1*
     1       (X/6.0D0)**(1./3.)/PI
           DELR=PL*SGM+PR*SDL
           RETURN
           END
C
C   NORM SOLVED USING LAUWERIER'S ASYMPTOTIC VALUES
C
      DOUBLE PRECISION FUNCTION NORM(X,R)
      IMPLICIT REAL*8 (A-H,O-Z)
      COMMON/BLOCK2/PI,DGAM1,DGAM2,M
      COMMON/BLOCK3/AL(3),BE(3)
      COMMON/BLOCK4/GM(3),DL(3)
      COMMON/BLOCK5/CON1,CON2,CON3,CON4,BIOT
      CTRIG1=DCOS(X*PI/4.0D0-1.0D0*PI/6.0D0)
      CTRIG2=DCOS(X*PI/4.0D0+1.0D0*PI/6.0D0)
      STRIG1=DSIN(X*PI/4.0D0-1.0D0*PI/6.0D0)*PI/4.0D0
      STRIG2=DSIN(X*PI/4.0D0+1.0D0*PI/6.0D0)*PI/4.0D0
      SAL1=(2.0D0/X)**(1.0/3.0)
      SAL2=(2.0D0/X)**(4.0D0/3.0D0)/6.0D0
      SGM1=(2.0D0/X)**(-1.0/3.0)
      SGM2=-1.0*(2.0D0/X)**(2.0/3.0)/6.0D0
      SBE1=0.0D0
      SBE2=0.0D0
      SDL1=0.0D0
      SDL2=0.0D0
      DO 10 N=1,3
         POW1=2.0*FLOAT(N)+1.0/3.0
         POW2=2.0*FLOAT(N)+4.0/3.0
         POW3=2.0*FLOAT(N-1)+5.0/3.0
         POW4=2.0*FLOAT(N-1)+8.0/3.0
         POW5=2.0*FLOAT(N)-1.0/3.0
         POW6=2.0*FLOAT(N)+2.0/3.0
         POW7=2.0*FLOAT(N-1)+1.0/3.0
         POW8=2.0*FLOAT(N-1)+4.0/3.0
```

```
            SAL1=SAL1+AL(N)*(2.0D0/X)**POW1
            SAL2=SAL2+AL(N)*(2.0/X)**POW2*POW1/2.0D0
            SBE1=SBE1+BE(N)*(2.0/X)**POW3
            SBE2=SBE2+BE(N)*(2.0/X)**POW4*POW3/2.0D0
            SGM1=SGM1+GM(N)*(2.0D0/X)**POW5
            SGM2=SGM2+GM(N)*(2.0D0/X)**POW6*POW5/2.0D0
            SDL1=SDL1+DL(N)*(2.0D0/X)**POW7
            SDL2=SDL2+DL(N)*(2.0D0/X)**POW8*POW7/2.0D0
 10     CONTINUE
        PART1=CON1*(-SAL1*STRIG1-SAL2*CTRIG1)
        PART2=CON2*(-SBE1*STRIG2-SBE2*CTRIG2)
        PART3=CON3*(-SGM1*STRIG2-SGM2*CTRIG2)
        PART4=CON4*(-SDL1*STRIG1-SDL2*CTRIG1)
        NORM=-1.0D0*R*(BIOT*(PART1+PART2)+PART3+PART4)/(2.0D0*X*PI)
        RETURN
        END
C
C   CONFLUENT HYPERGEOMETRIC SERIES
C
         DOUBLE PRECISION FUNCTION CONFLU(A,B,X)
         IMPLICIT REAL*8 (A-H,O-Z)
         CONFLU=1.0D0
         ACCY=1.0D-8
         N=1
         CH=A*X/B
         CHMAX=1.0D16
 10      CONFLU=CONFLU+CH
         IF(DABS(CH).LE.ACCY)RETURN
         CH=CH*(A+DFLOAT(N))*X/((B+DFLOAT(N))*(DFLOAT(N)+1.0D0))
         IF(DABS(CH).GT.CHMAX)GOTO 60
         N=N+1
         GOTO 10
C  ERROR STATEMENT
 60      WRITE(6,65)CH,CONFLU
 65      FORMAT(5X,'NEXT TERM IS TO LARGE',E20.10,' CONFLU=',E20.10)
         STOP
         END
/*
//GO.FT03F001 DD SYSOUT=B
```

NOMENCLATURE FOR PROGRAMS 'CRTN' AND 'PERSLTN'

ACCY	Convergence specifier (not solution accuracy)
AINV1	Inverse of AMP1
AMP1	Coefficent Matrix defined by Eq. (60a)
BIOT1	Biot number of unfinned region
BIOT2	Biot number of finned region
BM	Inlet condition
BT	TBULK array
CHKZ1	Index for unfinned (BIOT1) region
CHKZ2	Index for finned (BIOT2) region
DGVP	Flow problem constant = 2.0 slug plate problem = 4.0 Bessel and Graetz problem
DTBULK	Single term of bulk temperature summation
DTWALL	Single term of wall temperature summation
E1	Eigenvalues for unfinned (BIOT1) region
E2	Eigenvalue for finned (BIOT2) region
GAMMA	Dummy variable
GAMMIN	Gamma transforms before a biot jump
GAMPLS	Gamma transforms after a biot jump
HT	HTOT array
HTOT	Dimensionless total heat transfer up to a specified axial distance
HWALL	Dimensionless heat transfer at a specified axial position
ICC	Iteration counter
ICOUNT	Number of axial positions results printed for

IDGT	Decimal places of accuracy in calculation of AINV1 via IMSL subroutine LINV2F
IER	Error code for IMSL subroutine LINV2F
IPRT	Print/no print specifier for eigenvalues, eigenfunctions and norm
JCYC	Number of full BIOT1-BIOT2 cycles transversed
K	Number of step changes in Biot number since results last printed
KCYC	Total number of step changes in Biot number encountered
KP#	Number of step changes in Biot number between printed results
LINV2F	IMSL matrix inversion subroutine
MDATA1	Number of eigenvalues in first data file
MDATA2	Number of eigenvalues in second data file
MLARGE	Maximum number of eigenvalues
MMULT	Matrix multiplier subroutine
NM1	Normalization integral for unfinned (BIOT1) region
NM2	Normalization integral for finned (BIOT2) region
OGAMMN	Old value of GAMMIN
PEL , PER	Dummy variables
PSI1	Normalized eigenfunction at duct wall for unfinned (BIOT1) region
PSI2	Normalized eigenfunction at duct wall for finned (BIOT2) region
PZ#	Axial location when a new value for KP# is defined
S1	Square of eigenvalue E1
S2	Square of eigenvalue E2
SPSI1	Square of normalized eigenfunction PSI1
SPSI2	Square of normalized eigenfunction PSI2

TBULK	Dimensionless bulk temperature at a specified axial position
TRANS	Decaying exponential term
TWALL	Dimensionless wall temperature at a specified axial position
TZ	Old value of ZSTEP
WKAREA	Work area for subroutine LINV2F
WRONG	Number of failures to converge results to specified ACCY
Z	Dimensionless axial position
Z1	Dimensionless interfin spacing
Z2	Dimensionless fin thickness
ZMAX	Maximum dimensionless axial position at which program ends
ZSTEP	Axial increment step size

```
//A655RGW JOB 41755,BARD,REGION=1536K,TIME=(40,00)
/*PRIORITY STANDARD
/*JOBPARM LINES=1,CARDS=500
//STEP0001 EXEC FORTVCG,PARM.FORT='NOSOURCE,NOSRCFLG'
//FORT.SYSIN DD *
C
C                              PROGRAM 'CNTN JCL'
C
C                  STEPWISE PERIODIC HEAT TRANSFER COEFFICENT
C                     -----CONNECTED REGION TECHNIQUE-----
C                                GENERAL FORM
C
C                                   2-6-86
C
C            GENERAL PROGRAM FOR THE CALCULATION OF TEMPERATURE
C            AND HEAT TRANSFER RESULTS FOR A INTERNAL FLOW SUBJECTED
C            TO A PERIODIC HEAT TRANSFER COEFFICENT USING THE
C            CONNECTED REGION TECHNIQUE.  RESULTS CAN BE CALCULATED
C            AT ANY AXIAL POINT IN THE FIRST SIX CONSTANT BIOT
C            REGIONS.
C
C            ALL CALCULATIONS AND RESULTS IN DIMENSIONLESS FORM
C                  SEE SOLUTION DERIVATIONS FOR DETAILS
C
C  ************************  INSTRUCTIONS  ****************************
C       EDIT PROGRAM:
C               1. UNDER DIMENSIONLESS INPUT SECTION, SELECT VALUES FOR
C                  ACCW, Z1, Z2, ZMAX, ZSTEP, AND MLARGE IN LINES 1-6.
C
C               2. IN LINE 7 SET CONSTANT FOR THE CORRECT FLOW PROBLEM
C
C        SUBMIT PROGRAM:
C               3. USE MULTSUB COMMAND AND SUBMIT
C                        CRTN JCL
C                        <DATA FILE>
C                        <DATA FILE>
C                        END JCL
C                  WHERE DATA FILES CONTAIN THE APPROPRIATE EIGENVALUE,
C                  EIGENFUNCTION AND NORMALIZATION INTEGRALS FOR THE
C                  FLOW CASE UNDER STUDY.  THESE DATA FILES HAVE BEEN
C                  CREATED BY AN EIGENVALUE SOLUTION PROGRAM (I.E. FOR
C                  GRAETZ CASE FILES CREATED FROM 'GCLEF JCL')
C
C               4. THE DATA FILES SUBMITTED IN 3 ABOVE CAN NOT BE
C                  THE SAME.  THIS PROGRAM WILL NOT CALCULATE A CONSTANT
C                  BIOT CASE. SEE PROGRAM PERSLTN JCL FOR CONSTANT CASE.
C  ******************************************************************
C                       PROGRAM INITIALIZATION
C  ******************************************************************
C
       IMPLICIT REAL*8(A-B,D-H,O-Z)
```

```
      INTEGER Q,WRONG,Q1,Q2,Q3
      REAL*8 NM1(300),NM2(300)
      DIMENSION BM(200),S1(200),S2(200),SPSI1(200),SPSI2(200),
     1   E2(200),E1(200),PSI1(200),PSI2(200)
C  EXPONENTIAL UNDERFLOW TRAPPING ROUTINE
      CALL ERRSET(208,256,-1,0,0)
C
C  ***************************************************************************
C                            DIMENSIONLESS INPUT
C  ***************************************************************************
C
 1      ACCW=1.0D-7
 2      ZSTEP=.00005
 3      Z1=.0003D0
 4      Z2=.0001D0
 5      ZMAX=.020D0
 6      MLARGE=90
        WRONG=0
C   SET DGVP CONSTANT FOR DESIRED FLOW PROBLEM.  SLUG PLATE = 2.0,
C   BESSEL AND GRAETZ = 4.0
        DGVP=4.0
C  READ EIGENVALUE AND EIGENFUNCTION DATA FROM FILE
C  -FIRST DATA FILE
       READ(5,*)MDATA1,BIOT1
       DO 10 M=1,MDATA1
 10       READ(5,*)E1(M),NM1(M),PSI1(M)
       READ(5,*)MDATA2,BIOT2
C  -SECOND DATA FILE
       DO 15 M=1,MDATA2
 15       READ(5,*)E2(M),NM2(M),PSI2(M)
       IF(MDATA2.LT.MDATA1) MDATA1=MDATA2
       IF(MDATA1.LT.MLARGE) GOTO 1050
C
C  ***************************************************************************
C                  SET UP VARIABLES AND  PRINT HEADING
C  ***************************************************************************
C
          DO 40 M=1,MLARGE
             SPSI1(M)=PSI1(M)*PSI1(M)
             SPSI2(M)=PSI2(M)*PSI2(M)
             S1(M)=E1(M)*E1(M)
             S2(M)=E2(M)*E2(M)
C  CALCULATE INITIAL CONDITION
             BM(M)=BIOT1*PSI1(M)/S1(M)
 40       CONTINUE
C  TITLE HEADING FOR RESULTS
 141      WRITE(6,142)
 142      FORMAT(41X,'CONNECTED REGION SOLUTION - LAMINAR FLOW IN TUBE')
          WRITE(6,144)Z1,BIOT1
 144      FORMAT(/,45X,'UNFINNED WIDTH=',F6.4,7X,'BIOT 1=',F5.2)
          WRITE(6,148)Z2,BIOT2
```

```
 148      FORMAT(45X,'FINNED WIDTH=',F8.4,7X,'BIOT 2=',F6.2)
          WRITE(6,149)ACCW,MLARGE
 149      FORMAT(45X,'CONV ACCY=',E8.3,10X,'SUMMATION LIMIT=',I3)
          WRITE(6,154)
 154      FORMAT(4X,120(1H-),/,8X,'AXIAL',8X,'WALL',8X,'CONV ',6X,'BULK'
     1     ,8X,'CONV',3X,'JCYC',3X,'CHKZ',6X,'WALL HEAT',5X,'TOTAL WALL',
     2     7X,'NUSSELT',/,7X,'LOCATION',6X,'TEMP',19X,'TEMP',22X,'1  2',
     3     8X,'FLUX',8X,'HEAT FLUX',8X,'NUMBER',/,4X,120(1H-))
C
C  ***********************************************************************
C                          AXIAL LOOP CALC
C  ***********************************************************************
C
C   INITIALIZE AXIAL LOOP
 200  Z=0.0D0
C   AXIAL INCREMENT LOOP
 210  Z=ZSTEP+Z
      KCYC=0
C   DETERMINE NUMBER OF FULL PERIODIC BIOT CYCLES TRANSVERSED
      JCYC=IDINT((Z-1.0D-06)/(Z1+Z2))
      Z=DFLOAT(IDINT(Z*1.0D6+.5D0))/1.0D6
      Z3=DABS(Z-DFLOAT(JCYC)*(Z1+Z2))
C   DETERMINE NUMBER OF BIOT REGIONS ENCOUNTERED
      KCYC=JCYC*2+1
      IF((Z3-1.0D-6).GT.Z1) KCYC=KCYC+1
      IF(KCYC.EQ.5) ACCW=1.D-8
C
C  ***********************************************************************
C             TEMPERATURE AND HEAT TRANSFER CALCULATION
C  ***********************************************************************
C    THIS SECTION CALCULATES THE WALL TEMPERATURE, BULK TEMPERATURE AND
C    OTHER HEAT TRANSFER RESULTS FOR THE FIRST SIX CONSTANT BIOT REGIONS
C
 300      ICC=0
          K=0
 310      TWALL=0.0D0
          TBULK=0.0D0
 312      DO 700 Q3=1,MLARGE
 315      DO 650 M3=1,MLARGE
 320      DO 600 Q2=1,MLARGE
 340         DO 550 M2=1,MLARGE
 360            DO 500 Q1=1,MLARGE
 380               DO 450 M1=1,MLARGE
                      ICC=ICC+1
                      GO TO(410,420,430,435,437,440),KCYC
                      IF(KCYC.EQ.7) GO TO 1010
C                  -------------------------
C                  FIRST REGION
 410                   TRANS=DEXP(-Z3*S1(M1))
                       DTWALL=SPSI1(M1)*BIOT1*TRANS/S1(M1)
                       DTBULK=DGVP*DTWALL*BIOT1/S1(M1)
```

```
                    GO TO 444
C                  -------------------------
C                  SECOND REGION
 420                TRANS=DEXP(-(Z3-Z1)*S2(Q1)-Z1*S1(M1))
                    DTWALL=BIOT1*(BIOT1-BIOT2)*SPSI1(M1)*TRANS*
     1                SPSI2(Q1)/(S1(M1)*(S1(M1)-S2(Q1)))
                    DTBULK=DGVP*DTWALL*BIOT2/S2(Q1)
                    GO TO 444
C                  -------------------------
C                  THIRD REGION
 430                TRANS=DEXP(-Z2*S2(Q1)-Z1*S1(M1)-Z3*S1(M2))
                    DTWALL=BIOT1*((BIOT1-BIOT2)**2)*SPSI1(M1)*TRANS*
     1                SPSI2(Q1)*SPSI1(M2)/(S1(M1)*(S1(M1)-S2(Q1))
     2                *(S1(M2)-S2(Q1)))
                    DTBULK=DGVP*DTWALL*BIOT1/S1(M2)
                    GO TO 444
C                  -------------------------
C                  FOURTH REGION
 435                TRANS=DEXP(-Z2*S2(Q1)-Z1*S1(M1)-Z1*S1(M2)
     1                -(Z3-Z1)*S2(Q2))
                    DTWALL=BIOT1*((BIOT1-BIOT2)**3)*SPSI1(M1)*TRANS
     1                *SPSI2(Q1)*SPSI1(M2)*SPSI2(Q2)/(S1(M1)*
     2                (S1(M1)-S2(Q1))*(S1(M2)-S2(Q1))*(S1(M2)-S2(Q2)))
                    DTBULK=DGVP*DTWALL*BIOT2/S2(Q2)
                    GO TO 444
C                  -------------------------
C                  FIFTH REGION
 437                TRANS=DEXP(-Z2*S2(Q1)-Z1*S1(M1)-Z1*S1(M2)-Z2*S2(Q2)
     1                -Z3*S1(M3))
                    DTWALL=BIOT1*((BIOT1-BIOT2)**4)*SPSI1(M1)*TRANS*
     1                SPSI2(Q1)*SPSI1(M2)*SPSI2(Q2)*SPSI1(M3)
     2                /(S1(M1)*(S1(M1)-S2(Q1))*(S1(M2)-S2(Q1))
     3                *(S1(M2)-S2(Q2))*(S1(M3)-S2(Q2)))
                    DTBULK=DGVP*DTWALL*BIOT1/S1(M3)
                    GO TO 444
C                   -------------------------
C                   SIXTH REGION
 440                 TRANS=DEXP(-Z2*S2(Q1)-Z1*S1(M1)-Z1*S1(M2)
     1                 -Z2*S2(Q2)-Z1*S1(M3)-(Z3-Z1)*S2(Q3))
                     DTWALL=BIOT1*((BIOT1-BIOT2)**5)*SPSI1(M1)*TRANS*
     1                 *SPSI2(Q1)*SPSI1(M2)*SPSI2(Q2)*SPSI1(M3)*
     2                 SPSI2(Q3)/(S1(M1)*(S1(M1)-S2(Q1))*(S1(M2)-S2(Q1))
     3                 *(S1(M2)-S2(Q2))*(S1(M3)-S2(Q2))*(S1(M3)-S2(Q3)))
                    DTBULK=DGVP*DTWALL*BIOT2/S2(Q3)
                    GO TO 444
C                  ---------------------------------------------
 444                TBULK=TBULK+DTBULK
 445                TWALL=TWALL+DTWALL
                    IF (DABS(DTWALL).LT.ACCW) GO TO 460
 450                CONTINUE
                    WRONG=WRONG+1
```

```
 460                IF(M1.EQ.1) GO TO 510
                    IF(KCYC.EQ.1) GO TO 900
 500              CONTINUE
                  WRONG=WRONG+1
 510              IF(Q1.EQ.1) GO TO 560
                  IF(KCYC.EQ.2) GO TO 900
 550           CONTINUE
               WRONG=WRONG+1
 560           IF(M2.EQ.1) GO TO 610
               IF(KCYC.EQ.3) GO TO 900
 600       CONTINUE
           WRONG=WRONG+1
 610       IF(Q2.EQ.1) GO TO 660
           IF(KCYC.EQ.4) GO TO 900
 650       CONTINUE
           WRONG=WRONG+1
 660       IF(M3.EQ.1) GO TO 900
           IF(KCYC.EQ.5) GO TO 900
 700       CONTINUE
           WRONG=WRONG+1
C  CALCULATE REST OF PROPERTIES UNDER STUDY
 900       CHKZ1=1.0D0
           IF(MOD(KCYC,2).EQ.0) CHKZ2=0.0D0
 920       HWALL=BIOT1*TWALL*CHKZ1+BIOT2*CHKZ2*TWALL
           HTOT=1.0D0-TBULK
C
C     ***************************************************************************
C                               PRINT SECTION
C     ***************************************************************************
C
 925       WRITE(6,930) Z,TWALL,ICC,TBULK,ICC,KCYC,JCYC,HWALL,HTOT
 930       FORMAT(14X,F8.6,5X,F8.6,3X,I7,6X,F8.6,4X,I6,4X,I3,4X,I3,6X,F9.6
     1      ,6X,F9.6)
 1000      IF(TBULK.GT..1) GO TO 210
C  END OF PROGRAM SUMMARY
 1010      WRITE(6,1011)WRONG
 1011      FORMAT(//,45X,'CONVERGENCE ERRORS=',I2,/,4X,120(1H-))
           WRITE(6,1040)
 1040      FORMAT(2X,///,45X,'  --- END ---',///)
           GOTO 1060
C  ERROR STATEMENTS
 1050      WRITE(6,1055)
 1055      FORMAT(3X,'MLARGE EXCEEDS DATA FILE ELEMENTS - PROGRAM ABORTED')
 1060      STOP
           END
/*
//GO.SYSIN DD *
```

```
//A655RGW JOB 41755,BARD,REGION=1536K,TIME=(12,00)
/*PRIORITY STANDARD
/*JOBPARM LINES=3,CARDS=500
//STEP0001 EXEC FORTVCG,LIB='VPI.IMSL.DP',PARM.FORT='NOSOURCE,NOSRCFLG'
//FORT.SYSIN DD *
C
C                          PROGRAM 'PERSLTN JCL'
C
C                 STEPWISE PERIODIC HEAT TRANSFER COEFFICENT
C                     -----EXACT PERIODIC SOLUTION-----
C                               GENERAL FORM
C                                 2-6-86
C
C            GENERAL PROGRAM FOR THE CALCULATION OF TEMPERATURE
C            AND HEAT TRANSFER RESULTS FOR A FLOW SUBJECTED TO
C            A PERIODIC HEAT TRANSFER COEFFICENT USING THE EXACT
C            PERIODIC SOLUTION METHOD.  RESULTS ARE FOUND AT
C            POINTS IMMEDIATELY AFTER A JUMP IN BIOT NUMBER ONLY.
C
C            ALL CALCULATIONS AND RESULTS IN DIMENSIONLESS FORM
C                  SEE SOLUTION DERIVATIONS FOR DETAILS
C
C  ************************** INSTRUCTIONS ******************************
C
C       EDIT PROGRAM:
C               1. UNDER PROGRAM INITIALIZATION SECTION, SET AMP1(MLARGE,
C                  MLARGE), AINV1(MLARGE,MLARGE) AND WKAREA(MLARGE**2+
C                  3*MLARGE) IN LINES 1-2 WHERE MLARGE IS TO BE
C                  SUBSTITUTED BY THE VALUE IN LINE 7 (DIMENSIONLESS
C                  INPUT SECTION)
C
C               2. UNDER DIMENSIONLESS INPUT SECTION, SELECT VALUES FOR
C                  ACCW, Z1, Z2, ZMAX, AND MLARGE IN LINES 3-7.
C
C               3. IN LINE 8, SET CONSTANT FOR THE CORRECT FLOW PROBLEM
C
C               4. SET PRINT CYCLE KP'S AND PRINT CYCLE AXIAL SPECIFIERS
C                  PZ'S IN LINES 9-15. KP DETERMINES NUMBER OF CONSTANT
C                  BIOT REGIONS BETWEEN PRINTED RESULTS.  PZ'S SPECIFY
C                  AT WHAT AXIAL LOCATION A NEW VALUE FOR KP WILL BE
C                  USED.  NOTE: KP'S MUST BE ODD AND >=1.
C
C               5. TO PRINT EIGENVALUE PROPERTIES SET IPRT=0 IN LINE 16
C
C               6. IN SUBROUTINE SECTION UNDER MATRIX MULTIPLIER, SET
C                  AINV1(MLARGE,MLARGE) IN THE COMMON STATEMENT AS PER
C                  2 ABOVE.
C
C        SUBMIT PROGRAM:
C               7. USE MULTSUB COMMAND AND SUBMIT
C                        PERSLTN JCL
```

```
C                        <DATA FILE>
C                        <DATA FILE>
C                        END JCL
C                   WHERE DATA FILES CONTAIN THE APPROPRIATE EIGENVALUE,
C                   EIGENFUNCTION AND NORMALIZATION INTEGRALS FOR THE
C                   FLOW CASE UNDER STUDY.  THESE DATA FILES HAVE BEEN
C                   CREATED FROM AN EIGENVALUE SOLUTION PROGRAM (i.e. FOR
C                   THE GRAETZ CASE FILES CREATED FROM 'GCLEF JCL')
C
C               8. THE DATA FILES SUBMITTED IN 7 ABOVE CAN BE THE
C                  SAME IN ORDER TO CALCULATE A CONSTANT BIOT CASE.
C
C  ***********************************************************************
C                        PROGRAM INITIALIZATION
C  ***********************************************************************
C
      IMPLICIT REAL*8(A-B,D-H,O-Z)
      INTEGER Q,WRONG
      REAL*8 NM1(300),NM2(300)
 1    DIMENSION BM(300),GAMMIN(300),OGAMMN(300),PSI1(300),PSI2(300),
     1  GAMPLS(300),E2(300),E1(300),AMP1(100,100),WKAREA(45000),
     2  BT(300),HT(300),ZT(300),S1(300),S2(300)
      COMMON/BLOCK1/MLARGE
 2    COMMON/BLOCK2/AINV1(100,100)
C   EXPONENTIAL UNDERFLOW TRAPPING ROUTINE
      CALL ERRSET(208,256,-1,0,0)
C
C  ***********************************************************************
C              DIMENSIONLESS INPUT AND VARIABLE INITIALIZATION
C  ***********************************************************************
C
 3    ACCW=1.0D-5
 4    Z1=.0003D0
 5    Z2=.0001D0
 6    ZMAX=.95D0
 7    MLARGE=100
      IDGT=4
      WRONG=0
C   SET DGVP CONSTANT FOR DESIRED FLOW PROBLEM.  SLUG PLATE=2.0,
C   BESSEL AND GRAETZ = 4.0
      DGVP=4.0
C   CALCULATE AND PRINT THE HEAT TRANSFER RESULTS EVERY KP NUMBER OF
C   BIOT JUMPS.  KP MUST BE ODD AND >=1.  PZ'S SPECIFY AXIAL
C   LOCATIONS FOR CHANGE IN KP VALUE AND MUST BE INCREASING IN VALUE FROM
C   PZ2 TO PZ4.
 9    KP=1
 10   PZ2=.005D0
 11   KP2=11
 12   PZ3=.01D0
 13   KP3=51
 14   PZ4=.80D0
```

```
 15    KP4=131
C   PRINT EIGENVALUE PROPERTIES, 0=YES, 1=NO
 16    IPRT=1
C   READ EIGENVALUE PARAMETERS FROM DATA FILE
C   -FIRST DATA FILE
      READ(5,*)MDATA1,BIOT1
      DO 19 M=1,MDATA1
 19      READ(5,*)E1(M),NM1(M),PSI1(M)
      READ(5,*)MDATA2,BIOT2
C   -SECOND DATA FILE
      DO 20 M=1,MDATA2
 20      READ(5,*)E2(M),NM2(M),PSI2(M)
      IF(MDATA2.LT.MDATA1) MDATA1=MDATA2
      IF(MDATA1.LT.MLARGE) GOTO 1050
C
C  ***********************************************************************
C                    SET UP VARIABLES AND PRINT HEADINGS
C  ***********************************************************************
C
      DO 100 M=1,MLARGE
        S1(M)=E1(M)*E1(M)
        S2(M)=E2(M)*E2(M)
        BM(M)=BIOT1*PSI1(M)/S1(M)
        GAMPLS(M)=BM(M)
 100  CONTINUE
C  PRINT EIGENVALUE PARAMETERS
        IF(IPRT.EQ.1) GOTO 141
        WRITE(6,115)
 115    FORMAT(40X,'LAUWERIER-CONFLUENT SOLUTION')
        WRITE(6,116)
 116    FORMAT(32X,'GRAETZ FUNCTIONS FOR TUBE - CONFLUENT TILL M=7')
        WRITE(6,117)
 117    FORMAT(/,40X,'EIGENFUNCTIONS AND EIGENVALUES'/)
        WRITE(6,119)BIOT1,BIOT2,ACCW
 119    FORMAT(32X,'BIOT1=',F6.2,4X,'BIOT2=',F6.2,4X,'ACCURACY=',E8.2/)
        WRITE(6,120)
 120    FORMAT(8X,'M',13X,'E1',12X,'NM1',13X,'PSI1',13X,'E2',12X,'NM2',
     1    14X,'PSI2')
        WRITE(6,130)(M,E1(M),NM1(M),PSI1(M),E2(M),NM2(M),PSI2(M),M=1,40)
 130    FORMAT(7X,I3,7X,F10.6,5X,E11.5,5X,F9.6,6X,F10.6,6X,E11.6,
     1    6X,F9.6)
C  TITLE HEADING FOR RESULTS PRINTOUT
 141    WRITE(6,142)
 142    FORMAT(///,41X,'EXACT PERIODIC SOLUTION - LAMINAR FLOW IN TUBE')
        WRITE(6,144)Z1,BIOT1
 144    FORMAT(/,45X,'UNFINNED WIDTH=',F6.4,7X,'BIOT 1=',F5.2)
        WRITE(6,148)Z2,BIOT2
 148    FORMAT(45X,'FINNED WIDTH=',F8.4,7X,'BIOT 2=',F6.2)
        WRITE(6,149)ACCW,MLARGE
 149    FORMAT(45X,'CONV ACCY=',E8.3,10X,'SUMMATION LIMIT=',I3)
        WRITE(6,152)IDGT
```

```
 152    FORMAT(45X,'IDGT=',I2,21X,'LINV2F'/)
        WRITE(6,154)
 154    FORMAT(4X,120(1H-),/,16X,'AXIAL',8X,'WALL',8X,'CONV ',6X,'BULK'
     1    ,8X,'CONV',3X,'JCYC',3X,'CHKZ',6X,'WALL HEAT',5X,'TOTAL WALL',
     2    7X,/,15X,'LOCATION',6X,'TEMP',19X,'TEMP',22X,'1  2',
     3    8X,'FLUX',8X,'HEAT FLUX',8X,/,4X,120(1H-))
C
C  ***********************************************************************
C                      AMP COEFFICENT MATRIX
C  ***********************************************************************
C   SET UP Amp COEFFICENT MATRIX OF Eq. (60a)
C
      IF(BIOT1.EQ.BIOT2) GOTO 201
      DO 190 M=1,M LARGE
         DO 190 Q=1,MLARGE
            IF(M.NE.Q) GOTO 185
            AMP1(M,Q)=2.0
            GOTO 190
 185        PDUM1=PSI1(M)*PSI2(Q)/(S2(Q)-S1(M))
            PDUM2=PSI2(M)*PSI1(Q)/(S2(M)-S1(Q))
            AMP1(M,Q)=.5*(BIOT2-BIOT1)*(PDUM1-PDUM2)
 190  CONTINUE
C  NOTE: AMP2 IS THE NEGATIVE OF AMP1 (EXCEPT FOR THE DIAGONAL WHICH
C        REMAINS POSITIVE).  THIS RELATIONSHIP WILL BE UTILIZED IN
C        LIEU OF CALCULATING A SEPARATE AMP2 MATRIX.
C
C  ***********************************************************************
C                      AMP MATRIX INVERTER
C  ***********************************************************************
C   MATRIX INVERSION BY IMSL SUBROUTINE PACKAGE (LINV2F).  SEE IMSL
C   MANUAL FOR EXPLANATION OF SUBROUTINE AND VARIABLES.
C
       IA=MLARGE
       L=MLARGE
C   INVERT AMP1 MATRIX
       CALL LINV2F(AMP1,L,IA,AINV1,IDGT,WKAREA,IER)
C  NOTE:  THE TRANSPOSE OF AINV1 IS THE INVERSE OF THE AMP2 MATRIX. THIS
C         RELATIONSHIP WILL BE USED IN LIEU OF CALCULATING A SEPARATE
C         AINV2 MATRIX.
C
C  ***********************************************************************
C                        AXIAL LOOP CALC
C  ***********************************************************************
C
C   INITIALIZE VALUES FOR AXIAL LOOP
 201  Z=0.0D0
      K=KP
      CHK2=0.0
      ZSTEP=Z1
      TZ=0.0D0
      ICOUNT=0
```

```
      CHKZ1=0.0
      WRONG=0
C   AXIAL INCREMENT LOOP
 210  Z=ZSTEP+Z
 220  TWALL=0.0D0
      TBULK=0.0D0
      IF(BIOT1.EQ.BIOT2) GOTO 2000
      K=K+1
C   DETERMINE # OF PERIODIC BIOT CYCLES TRANSVERSED
      JCYC=IDINT((Z-1.0D-06)/(Z1+Z2))
      Z=DFLOAT(IDINT(Z*1.0D06+.5D0))/1.0D06
C   DETERMINE BIOT REGION AND SET INDEXES
      TZ=ZSTEP
 230  IF(CHKZ1.EQ.0.0) GOTO 240
C    -HIGH BIOT REGION
 235     ZSTEP=Z1
         CHKZ1=0.0
         CHKZ2=1.0
         GOTO 300
C    -LOW BIOT REGION
 240     ZSTEP=Z2
         CHKZ1=1.0
         CHKZ2=0.0
C
C  ***********************************************************************
C            GAMMA PLUS AND TEMP CALC AT BIOT DISCONTINUITY
C  ***********************************************************************
C   THIS SECTION UPDATES GAMPLS VALUES EVERY TIME A STEP CHANGE IN BIOT
C   IS ENCOUNTERED AND DETERMINES WHETHER TO CALCULATE AND PRINT RESULTS
C   OR ADVANCE TO THE NEXT BIOT JUMP POINT.
C
 300   DO 325 M=1,MLARGE
          TRANS=DEXP(-1.0D0*(S1(M)*Z1*CHKZ1+S2(M)*Z2*CHKZ2))
          OGAMMN(M)=GAMPLS(M)*TRANS
 325   CONTINUE
       DO 350 M=1,MLARGE
          GAMMIN(M)=0.0D0
          DO 340 Q=1,MLARGE
C  FOR M EQUALS Q
             IF(M.NE.Q)GOTO 328
               GAMMA=2.0D0*OGAMMN(M)
               GOTO 330
C  FOR M NOT EQUAL Q
 328         GAMMA=-AMP1(M,Q)*OGAMMN(Q)*CHKZ1+AMP1(M,Q)*OGAMMN(Q)*CHKZ2
 330         GAMMIN(M)=GAMMIN(M)+GAMMA
 340      CONTINUE
 350   CONTINUE
C   MULTIPLY MATRICES AINV*GAMMIN TO FIND NEW GAMPLS
       CALL MMULT(GAMMIN,GAMPLS,CHKZ1,CHKZ2)
C   DETERMINE IF CALCULATE RESULTS OR ADVANCE TO THE NEXT REGION
       IF(K.LT.KP) GOTO 210
```

```
      K=0
C   CALCULATE TEMP IMMEDIATELY AFTER A BIOT CHANGE
      TWALL=0.0D0
      TBULK=0.0D0
      DO 370 M=1,MLARGE
        DTWALL=GAMPLS(M)*(PSI1(M)*CHKZ2+PSI2(M)*CHKZ1)
        DTBULK=DGVP*DTWALL*(BIOT1*CHKZ2/S1(M)+BIOT2*CHKZ1/S2(M))
           TWALL=TWALL+DTWALL
           TBULK=DTBULK+TBULK
 360       IF(DABS(DTWALL).LT.ACCW)GOTO 380
 370  CONTINUE
      WRONG=WRONG+1
 380  HWALL=TWALL*(BIOT1*CHKZ2+BIOT2*CHKZ1)
      HTOT=1.0D0-TBULK
C
C  ***********************************************************************
C                          PRINT RESULTS
C  ***********************************************************************
C
 900  IF(CHKZ2.NE.1.0) GOTO 910
C  AXIAL PRINT CHECK
      IF(Z.LT.PZ2) GOTO 905
        KP=KP2
 905  IF(Z.LT.PZ3) GOTO 907
        KP=KP3
 907  IF(Z.LT.PZ4) GOTO 910
        KP=KP4
C   HT, BT AND ZT SET UP SPECIFIED VALUES OF HTOT, TBULK AND Z IN A
C   A MATRIX TO BE STORED IN A DATA FILE
 910  ICOUNT=ICOUNT+1
      BT(ICOUNT)=TBULK
      HT(ICOUNT)=HTOT
      ZT(ICOUNT)=Z
C   DATA PRINT STATEMENT
 920  ICHKZ1=INT(CHKZ1)
      ICHKZ2=INT(CHKZ2)
      WRITE(6,930)Z,TWALL,M,TBULK,M,JCYC,ICHKZ1,ICHKZ2,HWALL,HTOT
 930  FORMAT(14X,F8.6,5X,F8.6,4X,I5,6X,F8.6,4X,I5,3X,I4,4X,I1,2X,I1,5X,
     1  F9.6,5X,F9.6)
C   CHECK FOR CONTINUATION OF AXIAL INCREMENTING
      IF(Z.GT.ZMAX)GOTO 950
      IF(TBULK.GT..02)GOTO 210
C   DATA FILE STORAGE ROUTINE
 950  WRITE(3,960)ICOUNT
 960  FORMAT(5X,I3)
      DO 970 I=1,ICOUNT
        WRITE(3,965)BT(I),HT(I),ZT(I)
 965    FORMAT(3X,F8.5,F8.5,F9.6)
 970  CONTINUE
C   PRINT END OF PROGRAM SUMMARY
      WRITE(6,1012)WRONG,IER
```

```
 1012  FORMAT(//,30X,'CONVERGENCE ERRORS=',I2,10X,'INVERSION ERROR=',I3
     1   ,/,4X,120(1H-))
       WRITE(6,1040)
 1040  FORMAT(2X,//,45X,'  ---END---',/)
       GOTO 2050
C  ERROR STAEMENTS
 1050  WRITE(6,1055)
 1055  FORMAT(3X,'MLARGE LESS THAN DATA ELEMENTS IN DATA FILES',3X,
     1  '---  PROGRAM ABORTED')
       GOTO 2050
C
C   ***********************************************************************
C                    SPECIAL CASE BIOT1 = BIOT2
C   ***********************************************************************
C
 2000  CHKZ1=1.0
       DO 2010 M=1,MLARGE
         TRANS=DEXP(-1.0D0*Z*S1(M))
         DTWALL=TRANS*PSI1(M)*BM(M)
         DTBULK=DGVP*DTWALL*BIOT1/S1(M)
            TWALL=TWALL+DTWALL
            TBULK=DTBULK+TBULK
         IF(DABS(DTWALL).LT.ACCW)GOTO 2020
 2010  CONTINUE
       WRONG=WRONG+1
 2020  HWALL=TWALL*BIOT1*CHKZ1
       HTOT=1.0D0-TBULK
       IF(Z.GE..01) ZSTEP=.01D0
       IF(Z.GE..1) ZSTEP=.1D0
       GOTO 910
 2050  STOP
       END
C
C   ***********************************************************************
C                         SUBROUTINES
C   ***********************************************************************
C
C           MATRIX MULTIPLIER SUBROUTINE
        SUBROUTINE MMULT(GAMMIN,GAMPLS,CHKZ1,CHKZ2)
        INTEGER Q
        REAL*8 GAMMIN(MLARGE),GAMPLS(MLARGE),AINV1
        COMMON/BLOCK1/MLARGE
 10     COMMON/BLOCK2/AINV1(100,100)
        DO 50 M=1,MLARGE
           GAMPLS(M)=0.0D0
           DO 40 Q=1,MLARGE
              SUM=GAMMIN(Q)*(AINV1(M,Q)*CHKZ1+AINV1(Q,M)*CHKZ2)
              GAMPLS(M)=GAMPLS(M)+SUM
 40        CONTINUE
 50     CONTINUE
        RETURN
```

```
        END
/*
//GO.FT03F001 DD SYSOUT=B




C
C                       PROGRAM 'END JCL'
C
/*
//
```

The vita has been removed
from the scanned document